Delft University of Technology

Modelling the influence of vegetation on the morphodynamics of the river Allier

Graduation committee

Prof. dr. ir. H.J. de Vriend
Dr. ir. M.J. Baptist
Dr. ir. C.J. Sloff
Dr. H. Middelkoop

M.Sc. Thesis in Civil Engineering
Final Report

Jelle de Jong
1021524
Delft, September 2005

Preface

This report presents the findings of the final examination thesis before receiving the Master's degree in Civil Engineering at the Delft University of Technology. This thesis hopes to contribute to the ongoing research on the riverdynamics. Thereto the influence of vegetation on morphodynamics is studied by modelling a part of the natural meandering river Allier in France. In doing so it increases the knowledge concerning the modelling of morphodynamics and gives useful recommendations for further research. This report is especially useful for researchers who want to model free meandering rivers with the software program Delft3D from WL|Delft Hydraulics.

I enjoyed doing this study very much. This was not only a result of the interesting subject, the books and papers I could read, the software I could use, the things I learned and the time I was able to spend during this period to follow other courses at the University and to be a member of some committees at my fraternity. I believe that the people I was able to work with have also been very important for the good memories I keep. To start with the period I have the most fierce memories about. The field survey. This were 5 weeks in which I tried to learn to speak and think like an Utrecht student of Geographical Sciences. I did not succeed. To me a river remains something that ought to be modelled and normalized between dikes and groins immediately. A shrub can be represented by vertical rods, and if the things I see do not have numbers attached to them, I don't see them. Of course this is highly exaggerated, but it was wonderful to notice that the students from Utrecht do actually interpret and look different at a free meandering river than a student from Delft, like me. Nevertheless, they accepted me (I believe), and we all did like spare time and a good meal (although most of them didn't drink coffee). I also want to thank them all for the levelling measurements they carried out. None of them could use this data, nevertheless they used two full days two measure the main channel for me. Information without which my modelling would have become very difficult. Their names are: Véronique Maronier, Roel Rink, André Chaigneau, Marije Hoevers, Dirkjan Douma and Deon Slagter.

Besides the students from Utrecht, I want to thank Sander Vos and Jurgen de Kramer. On a completely voluntary basis, as far as I know, they visit the river Allier field survey almost every year. Especially their knowledge about respectively the RTK-DGPS and the river Allier was unsurpassed by anyone present. So, besides the enjoyment I had of their presence, their knowledge was also very welcome.

Another person I want to thank sincerely is Bert Jagers from WL|Delft Hydraulics. He implemented the Reduction factor approach in Delft3D-flow, he answered all my questions

about Delft3D fast and thorough and he allowed me to call him Bert instead of mister Jagers. All this was granted to me although I never met him in person, I do not pay him and he has nothing to do with my thesis. I can only hope to meet more people in my live who, like him, give good advice happily and for free.

I also want to thank the members of my graduation committee. First of all, prof. dr. ir. H.J. de Vriend. Although his time for M.Sc. students is limited, his comments during meetings were remarkably to the point and the corrections I received on my report made very clear he understood what I meant, even better than I did myself. I also want to thank dr. H. Middelkoop. What I said about the Utrecht students, looking from a different perspective on the river Allier, also goes for him, even stronger. This was especially clear in the comments I received from him on my report. He gave me a lot of extra work, but I honestly believe this led to a better end product. I also want to thank Cees Sloff. Who started of just like Bert Jagers. Answering my questions and helping me to set up my model for free, but he ended in my graduation committee.

Of course, the biggest 'thank you' goes to Martin Baptist. He was my most direct supervisor and he spent much more time helping me than he was technically and socially obliged to do. He finished his Phd. study during my thesis research. But even when his own promotion date got closer and closer, I was allowed to annoy him with all kind of questions which did not seem to annoy him. He helped me finding useful information, even if I was not looking for it myself, he showed interest, also in subjects I thought uninteresting, it was very pleasant to work with him and of course, I would not have been able to test his Reduction factor approach if he had not come up with it in the first place.

Delft, 12 September 2005
J.F. de Jong

Graduation committee

Prof. dr. ir. H.J. de Vriend	TU Delft, Faculty of Civil Engineering and Geosciences, Hydraulic Engineering section H.J.deVriend@CiTG.TUDelft.NL
Dr. ir. M.J. Baptist	TU Delft, Faculty of Civil Engineering and Geosciences, Water Resources section M.J.Baptist@CiTG.TUDelft.NL
Dr. ir. C.J. Sloff	TU Delft, Faculty of Civil Engineering and Geosciences, Hydraulic Engineering section C.J.Sloff@CiTG.TUDelft.NL
Dr. H. Middelkoop	University Utrecht, Faculty of Geographical Sciences, Department of Physical Geography H.Middelkoop@geog.uu.nl

Table of contents

List of symbols

A	[L^2]	wet surface
A_s	[L^2]	conveying cross-sectional area
B	[L]	(river) width
c	[ML^{-3}]	mass concentration
C	[$L^{1/2}T^{-1}$]	Chézy-coefficient
C'	[$L^{1/2}T^{-1}$]	grain related Chézy-coefficient according to Van Rijn
$C_{g,\,90}$	[$L^{1/2}T^{-1}$]	grain related Chézy-coefficient according to Meyer-Peter and Müller
D	[L]	particle diameter
D	[L^2T^{-1}]	eddy diffusivity
D_{50}	[L]	50% mass sieve diameter
D_{90}	[L]	90% mass sieve diameter
Fr	[-]	Froude number
g	[LT^{-2}]	acceleration due to gravity
h	[L]	mean depth of flow
i	[-]	mean slope of energy line
i_b	[-]	bed slope
k_n	[L]	Nikuradse roughness height
O	[L]	wet perimeter
q	[LT^{-1}]	magnitude of the flow velocity
q_s	[L^2T^{-1}]	rate of lateral sediment inflow per unit channel length
Q	[L^3T^{-1}]	discharge
R	[L]	hydraulic radius
s	[L^2T^{-1}]	sediment load per unit width
S	[L^3T^{-1}]	sediment load
u	[LT^{-1}]	time-averaged flow velocity component in x-direction
u*	[LT^{-1}]	shear flow velocity component in x-direction (U-ū)
U	[LT^{-1}]	flow velocity component in x-direction; cross-sectional mean flow velocity in x-direction (Q/As)
ū	[LT^{-1}]	depth-averaged flow velocity in x-direction
v	[LT^{-1}]	time-averaged flow velocity component in y-direction
z	[L]	vertical coordinate; level
z_0	[L]	zero-velocity level (u=0 at $z=z_0$)
Δ	[-]	relative density $(\rho_s-\rho)/\rho$

ε	[-]	porosity
θ	[-]	Shields mobility parameter
θ_{cr}	[-]	critical mobility parameter (=0.047)
κ	[-]	Von Kármán's constant
μ	[-]	ripple factor or efficiency factor according to Meyer-Peter and Müller
μ_c	[-]	ripple factor or efficiency factor according to Van Rijn
ν	$[L^2T^{-1}]$	kinematic viscosity
ρ	$[ML^{-3}]$	density of water
ρ_s	$[ML^{-3}]$	density of sediment
τ	$[ML^{-1}T^{-2}]$	shear stress
τ_b	$[ML^{-1}T^{-2}]$	bed shear stress
τ_{bc}	$[ML^{-1}T^{-2}]$	bed shear stress according to Van Rijn
τ_{bcr}	$[ML^{-1}T^{-2}]$	critical bed shear stress according to Shields
ξ_c	[L]	reference level (bed-load layer thickness) or roughness height
ζ	[L]	water level above some horizontal plane of reference

Summary

Modelling of water systems is getting more and more important in planning and decision-making. The possibilities and reliability of these models are therefore continually studied and improved.

This master thesis attributes to these developments by investigating the numerical modelling of a part of the free meandering natural river Allier in France. The model is build to simulate the hydrodynamical and morphodynamical response of the river to a major flood event.

One of the difficulties in modelling natural rivers concerns the influence of vegetation on the morphodynamics. The Ph.D. thesis by Baptist (2005), 'Modelling floodplain biogemorphology', addresses this problem. It states that the commonly used method increase the Nikuradse roughness height yields erroneous results with respect to the bottom shear stress and the sediment transport capacity. Baptist (2005) proposes some methods to tackle these problems. One of these methods, the 'Reduction factor approach' for bed shear stress in combination with the Rodríguez Uthurbu (2004) roughness formulation for the Chézy-coefficient, is studied in this thesis.

Before the modelling could start a field survey had to be carried out in order to acquire the needed data. This field survey took about five weeks of measuring and two months of processing. It was used to determine:

- the bathymetry of the study area;
- the vegetation characteristics of floodplain grassland, herbaceous vegetation, floodplain forest and open floodplain shrub;
- the vegetation distribution.

The field survey showed that the flood of December 2003 had lead to some major changes in the bathymetry of the study area. Cliff erosion was measured of up to 60 meters and about 200,000 m^3 of sediment was carried out of the study area. The point bars showed numerous chute channels and chute bars with widths of up to 15 m and depths of up to 2 m. It appeared that some of the obstructions, like trees, on the point-bars had a very strong impact on the formation of the chute and cut off channels.

The floodplain between the main channel and the abandoned channel on point-bar Chateau de Lys was completely eroded. Almost halfway along the length of this abandoned channel sedimentation had occurred of nearly 1.5 m in height along ¾ of the width of the channel.

The construction of the digital elevation map showed at first major errors with respect to the main channel. This was mainly due to the fact that the density of the measured points is far lower in the main channel than on the point-bars. Most of the inaccuracies could be eradicated

through the separate interpolation of the main channel and the point-bars. It remains however advisable to measure more points in the main channel.

In the model the vegetation is characterised by vertical rods with a certain density, diameter and height. It showed that the deviance between the measured spots of floodplain grassland showed no significant impact on the model's behaviour. It is therefore not necessary to refine the available vegetation type measurements by doing more investigations on the same vegetation type. The model, however, showed great sensitivity to the presence of vegetation. Therefore the location of the vegetated and non-vegetated parts must be accurately known.

The next field survey should focus on the following aspects:

- The characteristics of the unknown vegetation types;
- the location of the vegetation types;
- the bathymetry of the main channel.

With the data accumulated in the last and previous field survey a model of the study area was built using the software package Delft3D by WL | Delft Hydraulics. The total absence of water level and flow velocity measurements in the study area rendered the calibrating and validating of the flow model impossible. The morphological model could theoretically be calibrated on the basis of the bathymetry measurements. This was not accomplished because of, among other things, the lack of a calibrated hydrodynamic model. The model was calculated on a 20m grid. Because of the scale of the river Allier, the main channel for example is in most places only 60 m width, this is too coarse to account for many important features, like secondary flow, cliff erosion and the growth of chute channels.

The model showed to be able to predict some features with a reasonable accuracy:

- the flow direction on the point-bars;
- the appearance of channel cut-offs;
- the strong influence of major obstructions, like trees, on the flow and morphology;
- the chute-bar like movement of sediment over the point-bars.

The most remarkable errors are:

- the erosion of the main channel;
- no erosion of the cliffs;
- not enough morphological activity on the vegetated parts of the point-bars;
- the sedimentation on the banks on both sides of the main channel.

The incapability of the model to justly simulate the cliff erosion is thought to strongly influence many of the other residual errors of the model. Because of the major influence the cliff erosion seems to have on the morphological behaviour of the river Allier it is strongly advised to investigate the modelling of this feature.

Another important source for the difference between the model results and field measurements, residual errors, is ascribed to the sediment. The simulations used only one sediment fraction, while the field survey showed a major difference in the diameter of the sediment in the vegetated areas, the bare point-bars and the main-channel. The model affirms that the sediment diameter has a major impact on the morphodynamics. A good way forward would therefore be to account for several sediment fractions.

The last feature that is thought responsible for the errors is the secondary flow. In reality this flow is of major influence on the formation of the typical features of a natural meandering

river. The simulations however do not show any of the secondary flow induced morphodynamics, for example the build up of a point-bar on the inside of a river bend.

The Reduction factor approach seems to simulate more reliable bed shear stresses than the Increased Nikuradse roughness height method. With respect to the sediment transport capacity it was found that the effect of the Reduction factor approach is relatively small if the Van Rijn (1984) transport formula is used. If the Engelund and Hansen (1967) or the Meyer-Peter and Müller (1948) transport formula is used, the differences between the 'common' approach and the approach proposed by Baptist (2005) are much larger. But due to the residual errors in the simulation runs, it was not possible to say anything conclussive about the correctness of the Reduction factor approach (Baptist, 2005) concerning the sediment transport capacity. But the much more physical convincing simulated bed shear stresses and more accurate physics underlying this theory, indicate strongly that the Reduction factor approach is superior to the Increased Nikuradse roughness height method.

1 Introduction

1.1 Problem definition

In planning and decision-making, the use of models is very helpful in predicting future development and the impact of different strategies. Within the field of river engineering the reliability and predictive capability of these models is growing rapidly. This is due to ongoing research, but also to an increasing computational capacity.

Particularly, numerical models have proven their capacity to predict hydrodynamics with quite some accuracy. The modelling of river morphodynamics, however, showed to be of greater difficulty. In the case of meandering rivers, especially with respect to:

- Cliff erosion; the erosion and collapse of steep cohesive banks;
- graded sediment and armouring;
- the presence of vegetation in the flow.

In qualitative terms it is possible to describe, to some extent, the above-mentioned phenomena. But the need for quantitative predictions is increasing because of the following trends:

1. A decreasing public acceptance of floods, economic damage and other drawbacks of living close to rivers.
2. An increasing water resources utilization.

In order to meet these high demands on the water resources, good management practice is necessary. In order to accomplish this, good models can be very helpful, almost mandatory. Since the impact of vegetation has shown to be considerable, more insight and predictive capability will be needed to enhance the current models.

Another reason why better insight is needed in the impact of vegetation on flow and morphology is:

3. An increasing awareness of the need to establish a sustainable environment and to preserve ecosystems. Which, in the case of rivers, often leads to vegetation and nature development in the floodplain.

1.2 Objectives

The objective of this M.Sc. thesis is the last of the three major difficulties mentioned above: the presence of vegetation in the flow. More specifically, to investigate the Reduction factor approach. A method to model the influence of vegetation on flow and morphodynamics, proposed by Baptist (2005) in his doctoral thesis.

1.3 Research approach

The Reduction factor approach, was tested on a part of the free meandering river Allier in France, of approximately 5 km length near Moulins. The model was constructed with the modelling program Delft3D in which the Reduction factor approach was implemented. A sensitivity analyses was then carried out on the constructed model. In doing so recommendations concerning the research were made that should lead to the possibility of constructing models capable of producing morphodynamic predictions. It was beyond the scope of this study to make a calibrated and validated model of the river Allier.

To compare model results with the actual field situation, obviously two things are necessary. Firstly, model results. Secondly, elaborated field data (i) to use as input for the model and (ii) to compare the model results with. In the year 1995 the University of Utrecht started doing field research on the river Allier. In later years the Delft University of Technology and the Radboud University Nijmegen joined. In the year 2003 the Russian Academy of Sciences, Moscow, participated as well. Usually these surveys take place in the months July and August. This thesis relies heavily on the data retrieved in these previous field surveys.

Based on the objectives and the models used, it was decided what field data would be absolutely necessary and what helpful. Once this was clear, a list was made of data actually available and data still to be retrieved.

After this analyses the fieldwork was carried out during a four and a half week field trip. The bathymetry of the floodplains was measured with a RTK-DGPS device. The main channel was measured with a levelling instrument. More detailed information of the vegetation was acquired using a measuring rod, a slide caliber and a photo camera.

Once the raw data was collected, it was processed in order to make it suitable for model input. The data also was organized and presented in a clear and understandable format to make a comparison with model results possible.

Following the processing of the data the models could be set up. First a hydraulic model simulating the largest flood of the studied period was constructed. In this first modelling phase the field data was corrected if necessary and other parameters were calibrated to yield velocities, water depths and bed shear stresses that showed no major abnormalities or instabilities.

After the construction of the hydraulic model the morphological model was build. On this model a sensitivity analyses was carried out, using the Reduction factor approach or the often used approach of the Increased Nikuradse roughness height.

Eventually conclusions and recommendations are drawn on the basis of the fieldwork and the application and results of the models.

1.4 Outline of the report

In Chapter 2, 'Biogeomorphology of meandering rivers', some background information is given on the processes governing the hydraulic and morphological behaviour of a meandering river such as the river Allier. Within this chapter special attention is given to the influence of vegetation on the hydraulics and morphodynamics.

Next, Chapter 3 gives an outline of the river Allier, to get a general overview of the modelled river and to be able to interpret the results.

With the background information presented in Chapter 2 and 3, one should be able to interpret the remainder of this research.

Chapter 4, 'Field survey', elaborates on the fieldwork and the processing of the raw data to prepare for the model input and to make it suitable for interpretation. In the following Chapter 5, these field survey results will be interpreted, discussed and summarized.

Subsequently, Chapter 6, 'Modelling the river Allier' describes the construction of the hydrodynamic and the morphodynamic models.

In Chapter 7, the results of the sensitivity analysis are presented.

Than, in Chapter 8, the model results are discussed and conclusions on the general behaviour are presented with a clear focus on the morphodynamics.

This report will close with Chapter 9, in which conclusions will be drawn about the performance of the different models. Recommendations will be made on the necessary fieldwork and on a sensible approach for ongoing research concerning the modelling of biogeomorphology.

2 Biogeomorphology of meandering rivers – a review

2.1 Introduction

Biogeomorphology is a discipline that combines ecology and geomorphology. The term was first used in the 1980s (Viles, 1988). Geomorphology is the study of landforms and their formation. Ecology is the study of the relationships between biota and their environment. The environment is defined as factors that affect biota. These factors can be abiotic (physical, chemical), biotic (organisms), or anthropogenic (humans). Abiotic geomorphological processes may affect biota and biota may in turn affect geomorphological processes. The interaction between the two defines the interdiscipline of biogeomorphology. Biogeomorphology is thus the study of the interaction between geomorphological factors and biota (Baptist, 2005).

In this chapter the theory of aspects of biogeomorphology of interest for this study are discussed. This means that the information will focus on the influence of vegetation on flow and morphodynamics. This chapter will not present theories about the development of vegetation and the influence of flow and morphodynamics on vegetation succession because this is outside the scope of this research. For information on vegetation development and rejuvenation in alluvial rivers, see Baptist (2005).

It would be ideal if there were a universal law governing the time-space relation of water and sediment. If it exists, at all, it has not yet been formulated. Instead one has to do with a number of equations, each of which has particular schematizations for the description of a particular phenomenon. As a result each equation is an approximation of physical reality and it is important to know the limits of applicability and the accuracy of the calculations.

Starting from the basic conservation equations for mass and momentum, several cases of water movement can be schematized and made accessible for analytical or numerical solutions.

Assuming that all elements of these equations are exactly known, this description of the water motion is essentially deterministic.

The same goes for the description of the sediment movement: all sediment transport formulae are based on essentially similar assumptions about the actions of forces on particles.

Yet, it appears that the movement of a water or a sediment particle cannot be described in this manner, since there is a degree of uncertainty as to the action of the forces on the particle and as to the movement of the particle as a result of these forces. Such a process is called stochastic instead of deterministic. This stochastic character is also apparent on a much larger scale in morphological features such as meanders that cannot, with certainty, be predicted to appear in a specific shape at a specific place at a specific time. The stochastic nature of morphological processes gives another meaning to the afore mentioned aspect of accuracy.

The process of averaging is an important facet of river engineering. In many instances it is used to remove the stochastic element from the water and sediment movement equations. The fact that water and sediment theories use averaged values underlines the importance of time- and space-scales, see also Section '2.3 River morphology' (Jansen, 1994).

The outline of this chapter is in accordance with the schematization of biogeomorphology by Tsujimoto (1999); see Figure 2-1. Each separate block is discussed in a separate section. The figure shows the interrelations that exist between the different sections.

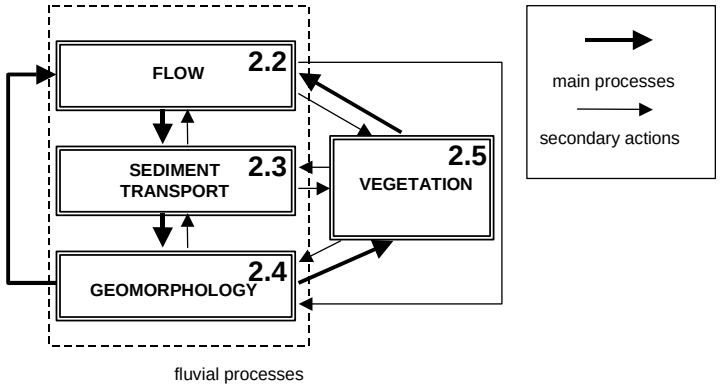

Figure 2-1, The influence of vegetation on fluvial processes, modified after Tsujimoto, 1999 (Baptist, 2005). With section numbers.

The water movement is the driving force behind sediment transport. Gradients in sediment transport determine whether erosion or sedimentation will occur. Sedimentation and erosion, in turn, shape the morphological behaviour and thus the geomorphology. The vegetation influences, and is influenced by all three of these fluvial processes. The section that discusses the vegetation (section 2.4) will present the Reduction factor approach by Baptist (2005).

2.2 Flow

Flow is the driving force behind erosion and sediment transport. Therefore, it is of great importance to have insight into the flow characteristics if one wants to make morphological predictions.

Channel flow is mainly determined by the discharge, topography of the riverbed and the floodplains, the slope of the bed, the imposed water depth at the downstream end - or at certain points along the river - and the resistance the flowing water experiences from the bed and

floodplains. The mean flow velocity (u) is therefore a function of the hydraulic radius (R), the slope (i) and a certain roughness coefficient representing the amount of flow resistance. The most common roughness parameters for open channel flow are the Chézy-coefficient, the Manning coefficient, the Nikuradse roughness height and the Darcy-Weisbach friction factor.

The simplicity of these expressions makes them easy to use, which have made them well-known to hydraulic designers and researchers throughout the world. They were all designed in an empirical way, they represent the same phenomenon and can be easily converted into each other [Chang, 1988)]

The empirical roughness coefficient C, after Chézy, is widely used in the Netherlands. The Chézy equation to calculate the mean flow velocity is expressed as:

$$u = C\sqrt{Ri} \qquad [m/s] \qquad (2\text{-}1)$$

in which:

u	time-averaged flow velocity component in x-direction	[m·s^{-1}]
C	Chézy-coefficient	[m$^{1/2}$·s^{-1}]
R	hydraulic radius = A·O^{-1}	[m]
i	energy slope of the river	[-]
A	wet surface	[m^2]
O	wet perimeter	[m]

In a channel in which the width B is much larger than the depth, the hydraulic radius can be taken equal to the water depth h.

According to Meyer-Peter and Müller (1948) ,the Chézy-coefficient, used in equation (2-1), can be divided in two parts. This is a division into 'grain roughness' and 'form roughness'. The first would be present without bedforms, the second is due to bedforms (see Figure 2-2). The grain roughness can be easily approximated by the White-Colebrook formulation:

$$C = 18\log\left(\frac{12R}{k_n}\right) \qquad [m] \qquad (2\text{-}2)$$

in which k_n is the equivalent geometrical roughness of Nikuradse (1933):

$$k = k_n = \text{Nikuradse roughness height} = 3 \cdot D_{90} \qquad [m^{1/2}\cdot s^{-1}] \qquad (2\text{-}3)$$

The bedform roughness is much harder to determine. Therefore the Chézy-value is usually used as a calibration parameter.

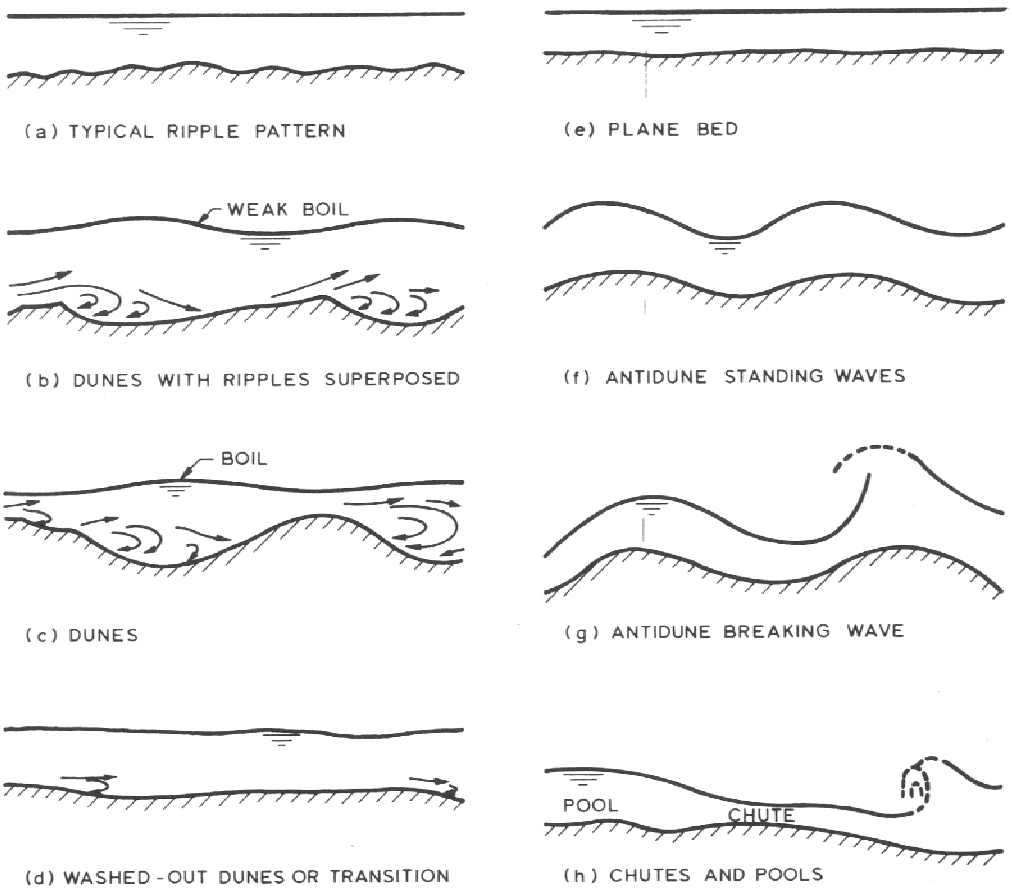

Figure 2-2, Bedforms (after Simons and Richardson, 1961)

2.2.1 Vertical flow profile

The following text is largely based on Van Rijn (1990).

This section will present some general characteristics of the velocity distribution over the vertical in a non-vegetated area. The changes that occur in the case of flow over a vegetated area will be discussed in Section 2.4.

Shear stress is of great importance in the understanding of the vertical velocity profile and erosion. The horizontal shear stress in the water column determines the friction and thus the momentum transport between one 'layer' and the other and thus the velocity distribution. A clear understanding of shear stress is also of value to comprehend the sedimentation and erosion processes, because the shear stress at the bottom is the driving force behind these processes.

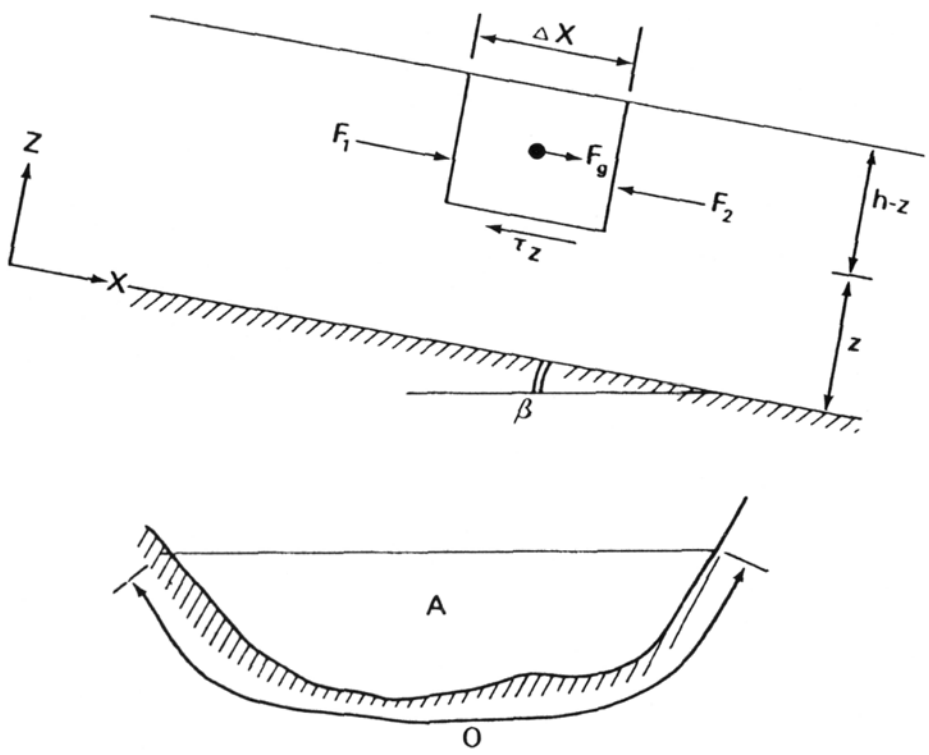

Figure 2-3, Fluid forces (Van Rijn, 1990)

In Figure 2-3, the forces per unit width on a fluid element Δx of a steady uniform flow are given. F_1 and F_2 represent the hydrostatic pressure forces and are equal to each other. F_g symbolizes gravity component in x-direction. Equilibrium of forces in x-direction yields for the shear stress:

$$\tau_z = \rho g i (h - z) \qquad [N \cdot m^{-2}] \qquad (2\text{-}4)$$

In which:

ρ	density of fluid	[kg·m^{-3}]
g	gravitational constant = 9.81	[m·s^{-2}]
i	bed slope = energy gradient	[-]
h	water depth	[m]
z	height above bedlevel	[m]

Formula (2-4) gives a theoretical distribution of the shear stress from the water level to the bottom. Measurements, however, indicate that the shear stress near the bed is approximately constant (≈ τ_b) in a layer with a thickness of about 0,1·h.

This shear stress, τ_z, is a summation of the viscous shear stress, τ_v, and the turbulent shear stress, τ_t. Based on the type of shear stress that is dominant, the vertical velocity profile can be divided in several layers, see Figure 2-4.

The viscous shear stress is dominant in the viscous sublayer. In this layer the flow is laminar. In laminar flow the fluid particles move horizontally without the turbulent fluctuations, i.e. the

laminar flow can be visualised as layers that slide smoothly over each other. The layers closer to the bottom have slower velocity and therefore there is a shear stress between the different 'layers' since the upper layer moves faster than the layer below.

In the transition layer viscosity and turbulence are both important. In the turbulent logarithmic and turbulent outer layer, the turbulent shear stress is dominant. In turbulent flow the particles move irregularly causing continuous exchange of momentum from one portion of fluid to another and this momentum exchange is the reason for the turbulent shear stress, which is also called the Reynolds stress (Van Rijn, 1990).

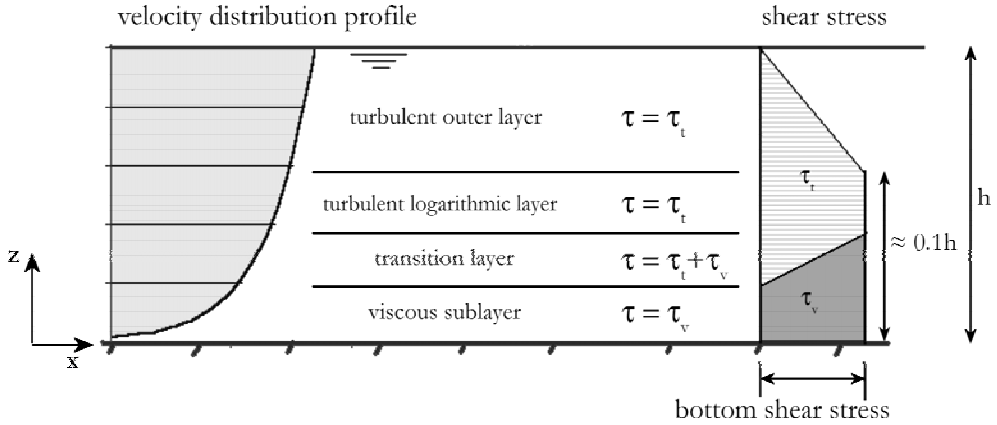

Figure 2-4, Viscous and turbulent sublayers for a smooth bottom (modified after Van Rijn, 1990)

In natural rivers the flow can be characterized as hydraulically rough, which means that the viscous sublayer does not exist. In that case, based on formula (2-4) and the mixing length theorem of Prandtl, the following logarithmic equation for the velocity distribution over the vertical in non-vegetated areas can be formulated.

$$u = \frac{u_*}{\kappa} \ln\left(\frac{z}{z_0}\right) \qquad [\text{m s}^{-1}] \qquad (2\text{-}5)$$

in which:

u_*	shear velocity	[m s^{-1}]

defined as

$$u_* = \sqrt{\frac{\tau_b}{\rho}} \qquad [\text{m s}^{-1}] \qquad (2\text{-}6)$$

with

z	height above bedlevel	[m]
z_0	zero-intercept level (u = 0 at z = z_0)	[m]

A typical phenomenon of the turbulent outer layer is that the velocities are almost constant, which is caused by the presence of large eddies that produce a strong mixing of the flow. Measurements in open channels show that the maximum flow velocity does not occur at the surface (z=h), as would follow from formula (2-5), but at a small distance below the surface (z=0.9h). This is probably due to a non-linear stress distribution and/or by friction effects at the interface of the fluid and the air.

2.2.2 Overbank flow

In a meandering river, with a main channel and floodplains, overbank flow takes place during high discharges. Overbank flow takes place from the main channel onto the floodplains and back. A factor of paramount importance is the floodplain roughness, which is determined by the presence and type of vegetation. It is expected that with an increase of vegetation on the floodplains, the overbank flow will be reduced and inbank flow will be enhanced.

2.2.3 Flow in bends

Bends in a river, such as the Allier, give rise to curvature-induced secondary flow. Secondary flow is the flow diverting from primary flow, which is the depth-averaged flow with a vertical distribution profile (e.g. logarithmic). Secondary flow consists of a component in the direction of the flow, which exists due to downstream accelerations and decelerations, and a component in the direction normal to the flow, due to the centripetal acceleration. The combination of the latter with the main flow is called spiral flow or helical flow (Jansen, 1994).

In a bend, water is forced towards the outer bank because of the centrifugal force ($F=m \cdot u^2/r$). This causes the water surface at the outer bank to be elevated with respect to that at the inner bank. This cross-stream gradient causes an inward directed pressure gradient. The resulting inward directed pressure force is distributed equally over the vertical. The centrifugal force, however, is quadratic proportional to the flow velocity, which is much greater at the water surface than at the bottom, see Figure 2-5. Therefore the water flows to the outer bank at the surface and to the inner bank at the bottom. This leads to a 3D pattern of helical flow (spiral flow), see Figure 2-6.

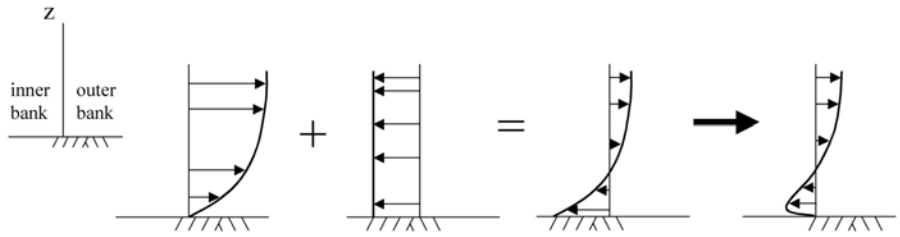

Figure 2-5, Forces on the water at a river bend, and the resulting secondary velocity.

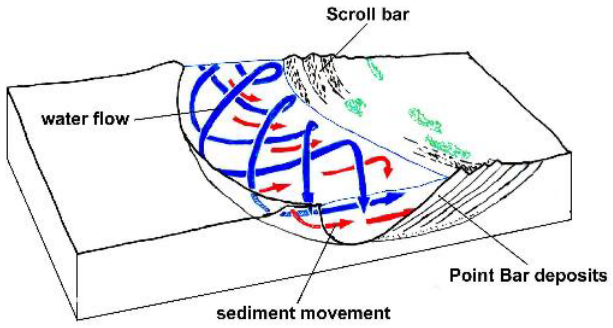

Figure 2-6, Cross-section of a meandering stream.

In a straight channel, the primary flow velocities are greatest in the centre of the channel. This is because the water at the channel centre is least slowed down by friction. In a channel bend

the maximum depth averaged flow velocity shifts to the outer bank, see Figure 2-7. This can be explained in two ways:

- The secondary flow brings the fast water particles at the water surface to the outer bank, and the slow water particles at the bed to the inner bank (Dietrich et al., 1979).
- The development of the cross-stream gradient in a bend causes, in the first half of the bend, the along stream gradient to get smaller at the outer bank and greater at the inner bank. Due to the smaller gradient the flow at the outer bank has to slow down, while the flow at the inner bank can accelerate due to the greater gradient. This causes the maximum flow velocity to shift to the inner bank. After the apex of the bend the cross-stream gradient gets less and the process is reversed. The along-stream gradient at the outer bank gets greater, and the along-stream gradient at the inner bank gets smaller. This results in the shifting of the maximum flow velocity to the outer bank (Terwindt & Van den Berg, 1997).

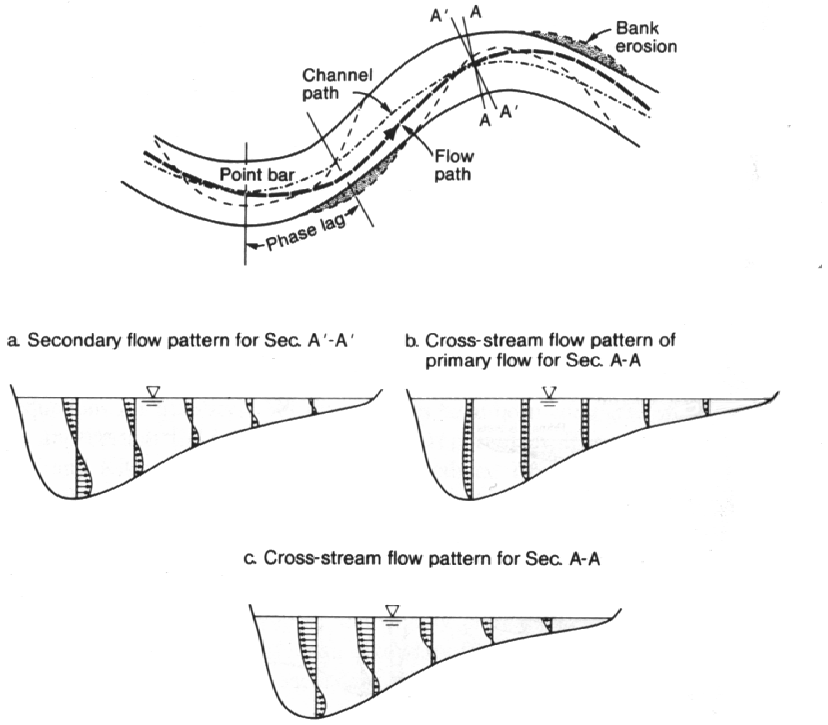

Figure 2-7, Schematics of meander bend showing channel path (channel centerline), flow path (discharge centerline), and flow patterns (Chang, 1988).

2.2.4 General

In rivers, complex phenomena of interrelated water movement and sediment movement occur. For a basic understanding of these morphological processes in rivers knowledge of sediment transport is essential.

Therefore this chapter forms a logical link between Section 2.2, and Section 2.3. On the one hand, it provides the necessary information (notably on bed roughness) to be used for the computation of the water movement; on the other hand it gives the necessary insight into the mechanism of loose boundary hydraulics and river morphology.

Both cohesive (clay) and non-cohesive (sand and gravel) sediments take part in morphological processes. For the cohesive sediments the physical-chemical interaction between particles plays a significant role. In comparison with non-cohesive sediment, the knowledge concerning cohesive sediment is still very limited. In this thesis only non-cohesive sediment will be accounted for.

The following non-cohesive particle properties are of interest when studying sediment transport, erosion and sedimentation:

- size,
- shape,
- density,
- fall velocity (Jansen, 1994).

2.2.5 Initiation of motion

The stability of a non-cohesive particle on the bed of a channel depends on the forces acting on it, such as the submerged weight, drag forces and lift forces. The two latter forces are due to the flow around the particle causing pressure differences and shear stresses on the particle surface. Their magnitude will depend on particle dimension and shape, roughness of the bed, local mean velocities and velocity fluctuations (see Figure 2-8).

$$Fb = Ga$$

or

$$C_F \frac{1}{2} \rho U_b^{\,2} \frac{\pi}{4} D^2 b = \frac{\pi}{6} D^3 \left(\rho_s - \rho\right) g a$$

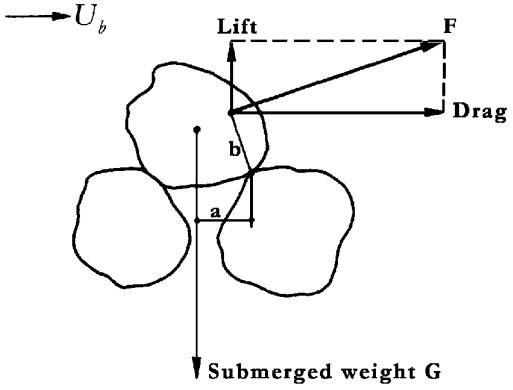

Figure 2-8, Forces acting on a non-cohesive particle on the bed (Jansen, 1994)

As can be concluded from the equilibrium shown in Figure 2-8, major variables that affect the incipient motion of uniform sediment on a level bed include τ_b, D, ρ, ρ_s, g and ν. The drag and lift force being a function of τ_b, D and ν; the submerged weight a function of D, g, ρ and ρ_s. From dimensional analysis, they may be grouped into the following dimensionless parameters

$$F\left[\frac{\tau_b}{(\rho_s-\rho)gD},\frac{\left(\frac{\tau_b}{\rho}\right)^{\frac{1}{2}}D}{\nu}\right]=0 \qquad [-] \qquad (2\text{-}7)$$

that is,

$$\frac{\tau_b}{(\rho_s-\rho)gD}=F\left(\frac{u_*D}{\nu}\right) \qquad [-] \qquad (2\text{-}8)$$

in which:

$$\tau_b=\rho u_*^2 \qquad [\mathrm{m\,s^{-1}}] \qquad (2\text{-}9)$$

u_* is the friction velocity. The left-hand side of this equation is the dimensionless shear stress, Ψ. The right-hand side is called the boundary Reynolds number and is denoted by Re_* (Chang, 1988).

Shields (1936) demonstrated experimentally that the parameter Re_* is sufficient to characterize the flow pattern near the particle. He has given an empirical relation between the dimensionless parameters Ψ and Re_* at which the sediment starts to move. If the dimensionless stress exceeds the critical dimensionless shear stress, Ψ_c, the sediment starts to move. This relation is given in Figure 2-9.

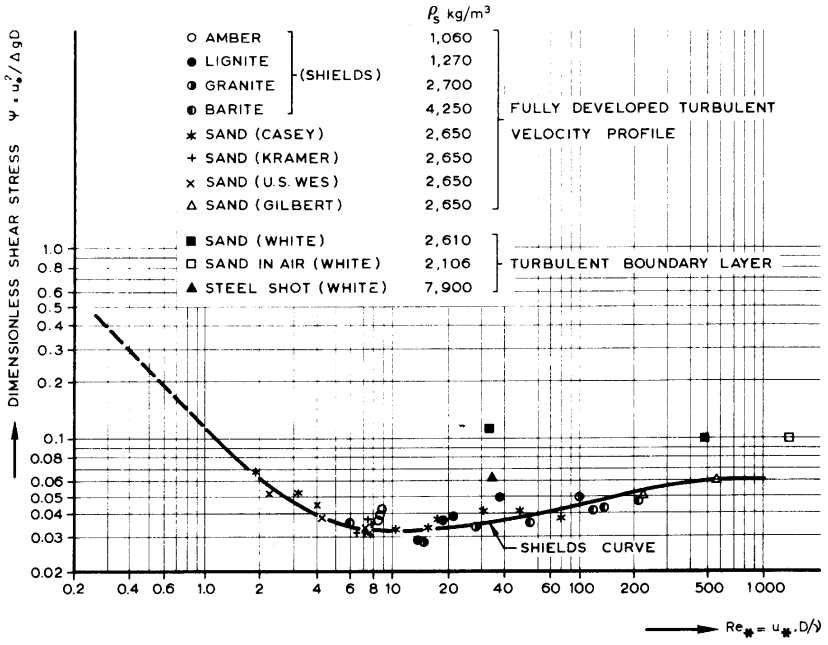

Figure 2-9, Shields' diagram with data added (Jansen, 1994)

Shields (1936) found that gradation (distribution of particle size in the sediment) is only important under extreme conditions ($D_{95}/D_{50}>5$). The critical shear stress for a mixture is roughly equal to the critical shear stress corresponding to the median diameter.

The influence of particle shape on initiation of motion is generally small: only flattened shapes give larger values for the critical bed shear stress.

Another aspect of influence is the slope of the bed. For a bank the bed can only deliver a reaction force G ·cos(α) ·tan(ø) in which ø is the angle of repose of the bed material. This reduces the critical shear stress (Jansen, 1994, 89).

2.2.6 Transport of sediment

When flow conditions reach the critical stage, the loose bed material starts moving. While observing increasing flow velocity on a sand bed in a laboratory flume, the following picture is seen. Above a certain flow velocity individual particles start moving along the bed: rolling, sliding or making small jumps. At higher velocities more particles move at increasing speeds. For fine sediment some grains are carried away from the bed because of turbulent velocity fluctuations and they remain suspended for some time. Depending on the characteristics of the bed material and on flow velocity and depths, a typical bedform can develop (such as ripples, dunes, etc.).

The sediment transport can be classified according to origin and mechanism as in the following scheme (see Figure 2-10). Bed load (transport) is defined as the transport of bed material by rolling and sliding. Suspended load (transport) is defined as the transport of sediment, which is suspended in the fluid for some time. According to mechanism of suspension the suspended sediment may belong to the bed material load and the wash load. Wash load is defined as the transport of material finer than the bed material. It has no relation to the transporting capacity of the stream: the rate is determined by the amount that becomes available by erosion in the catchment area upstream (Jansen, 1994, 90).

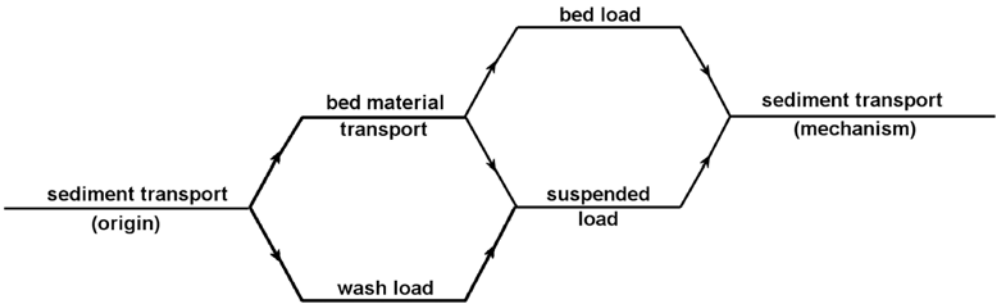

Figure 2-10, Classification of sediment transport (Jansen, 1994)

2.2.7 Bedform and alluvial roughness

The prediction of bedform and bed roughness employs, besides theoretical considerations, a great deal of empiricism. Moreover the prediction methods apply to homogeneous conditions both in time and space. Very little information is available on the variation of the bedform in time due to varying discharges. These non-steady conditions are probably responsible for the scatter of data obtained from nature when compared with laboratory data obtained under (controlled) steady conditions.

Water flowing over a loose bed can produce different bedforms and hence the resultant hydraulic roughness may vary considerably. From the Chézy equation the relation between shear stress τ and Chézy roughness C can be found to be

$$\tau = \frac{\rho g}{C^2} u^2 \qquad [\mathrm{N \cdot m^{-2}}] \qquad (2\text{-}10)$$

In principle this is a parabolic relation between τ and u for a constant C. For a mobile bed, however, C changes and this leads to a relation as sketched in Figure 2-11. For relatively low flow velocities this is a unique relation between τ and u. However, for high flow velocities it is no longer unique. For this upper range Vanoni and Brooks (1957) conclude that shear stress or shear velocity are not good parameters for expressing sediment transport in terms of flow conditions (Jansen, 1994, 91).

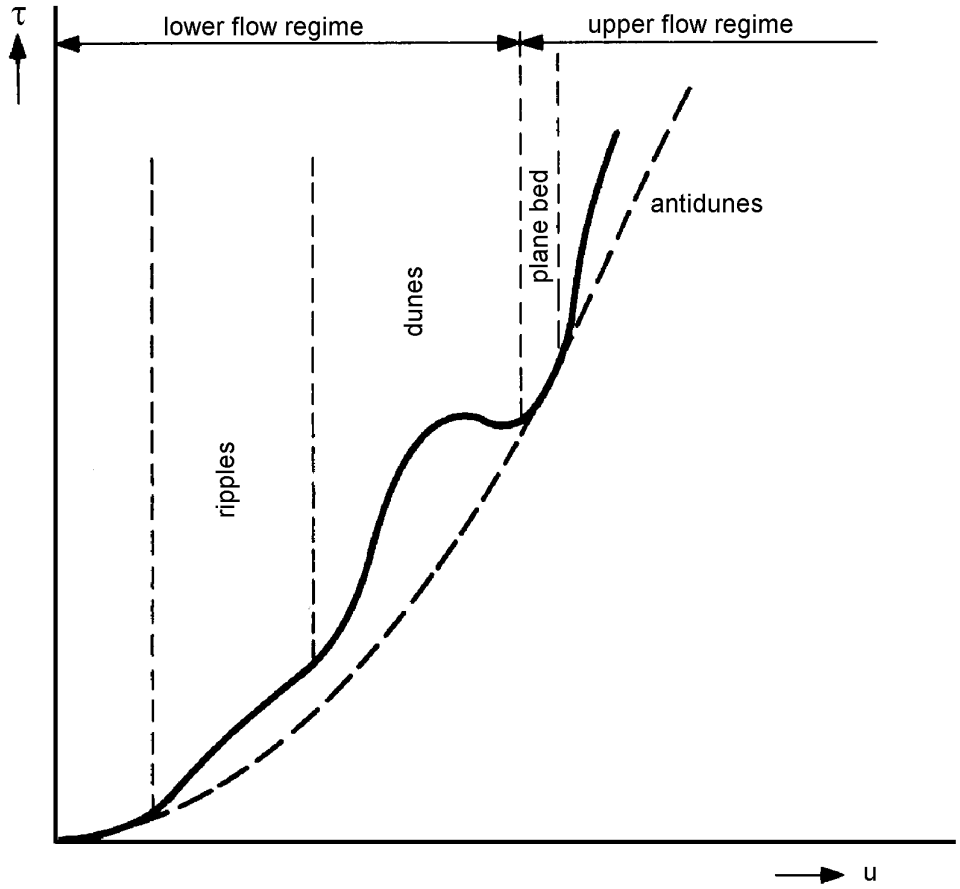

Figure 2-11, The relation τ=f(u) (Jansen, 1994)

It is customary to follow Meyer-Peter and Müller (1948) in dividing the shear stress τ acting on the riverbed into two parts:

1. the shear stress τ' that would be present without bed forms, caused by the grains only;
2. the shear stress τ" due to the bedform.

This is a division into 'skin roughness' and 'form roughness'. Hence

$$\tau = \tau' + \tau'' \qquad [\mathrm{N \cdot m^{-2}}] \qquad (2\text{-}11)$$

Because of formula (2-4)

$$hi = (hi)' + (hi)'' \qquad [-] \qquad (2\text{-}12)$$

with formula (2-1) this yields

$$C^{-2} = (C')^{-2} + (C'')^{-2} \qquad [\mathrm{m^{1/2} \cdot s^{-1}}] \qquad (2\text{-}13)$$

(Jansen, 1994)

2.2.8 Transport formulae

Whilst the physical-mathematical descriptions of flowing water are reasonably successful, those of sediment transport in suspension do not always show fair agreement with measurements. Concerning bed load or cohesive-sediment there are no physical-mathematical descriptions whatsoever that have led to formulae suitable for practical use. For the description of non-cohesive bed load movement, only experimental formulae exist, tested in a statistical manner. When applying these formulae one should take great care not to overstep their applicability (Jansen, 1994). So usually it is necessary to apply and calibrate different formulae on a given river reach. After which the most suitable formula can be used.

Since the bed material transport is – unlike washload – linked to the hydraulic properties of the stream, there are only formulae for this type of transport. The bed material load is divided into bed load and suspended load. Based on this division the formulae can be distinguished into three categories:

- formulae for bed load,
- formulae for suspended load,
- formulae for total load.

All formulae consider sediment transport as a function of gravity (g), fluid characteristics (ρ, υ), sediment characteristics (ρ_s, D) and one or more parameters to characterize the flow (τ_b), e.g.:

$$s = f(g, \rho, \upsilon, \rho_s, D, \tau_b) \qquad [m^3 s^{-1} m^{-1}] \qquad (2\text{-}14)$$

When considering the different transport formulae it is important to note that the way in which they are expressed differ widely from publication to publication. Even when examining the same formulae.

Another point of attention is which sediment characteristic is used as a representative grain size. Some formula use the mean grainsize while others us the median grain size (D_{50}).

Finally, also the unit in which sediment transport is expressed differs. Some use mass transport, others volume. The volume transport is sometimes considered including the porosity and sometimes excluding the porosity. In this theses the transport *s* will be defined as the net volume transported per unit of width and time (e.g. pores excluded).

A dimension analysis of formula (2-14) leads to two dimensionless parameters that are used in many of the available transport formulae.

The transport parameter:

$$\Phi = \frac{s}{\sqrt{g \Delta D^3}} \qquad [-] \qquad (2\text{-}15)$$

In which:

s	sediment load per unit width	$[m^2 \cdot s^{-1}]$
g	acceleration due to gravity	$[m \cdot s^{-2}]$
Δ	relative density = $(\rho_s - \rho)/\rho$	[-]
ρ_s	density of sediment	$[kg \cdot m^{-3}]$
ρ	density of water	$[kg \cdot m^{-3}]$
D	characteristic grain-size	[m]

The flow parameter:

$$\Psi = \frac{\mu \tau_b}{\rho g \Delta D} = \mu \frac{hi}{\Delta D} \quad [-] \quad (2\text{-}16)$$

In which:

τ_b	bed shear stress	[N·m^{-2}]
h	depth of flow; mean depth of flow	[m]
i	mean slope of energy line	[-]

The ripple factor μ allows for the fact that only the grain induced shear stress and not the bedform-induced shear stress is used for transport. This results in a division of τ similar to the one used in formula (2-11). Therefore a logical choice would be

$$\mu = \frac{(hi)'}{hi} = \left(\frac{C}{C'} \right)^2 \quad (2\text{-}17)$$

However, as μ also acts as a correction factor to adapt the basic formula to transport measurements, different expressions are found. Most expressions for μ are a function of the form

$$\mu = f\left(\frac{C}{C_{90}} \right) \quad [-] \quad (2\text{-}18)$$

In which:

$$C_{90} = 18 \log\left(\frac{12h}{D_{90}} \right) \quad [-] \quad (2\text{-}19)$$

A few transport formulae are summarised below:

Meyer-Peter and Müller (1948)

This formula is purely experimental and applies only to the bedload. As an indication it can be said that this formula is only applicable if D ≥ 0.4 mm and the suspended load can be neglected. For the river Allier, this is possible because the coarse sediment of the river Allier is mostly transported as bed load (Van den Berg, 2004).

The formula has been extensively tested and used for rivers with coarse bed material.

$$\frac{w_s}{u_*} > 1 \quad [-] \quad (2\text{-}20)$$

In which:

w_s	settling velocity	[m·s^{-1}]

Expressed in the transport and flow parameter, Meyer-Peter and Müller becomes for bulk volume transport

Basic form

$$\Phi = 8(\Psi - 0{,}047)^{3/2} \quad [-] \quad (2\text{-}21)$$

Ripple factor

$$\mu = \left(\frac{C}{C_{90}} \right)^{\frac{3}{2}} \quad [-] \quad (2\text{-}22)$$

Characteristic grain-size (mean grain-size)

$$D = \overline{D} = \sum^{i} (p_i D_i) \quad [\text{m}] \quad (2\text{-}23)$$

In which:

D_i	mean size of the i^{th} fraction of bed material	[m]
p_i	portion of total by weight of i^{th} fraction	[-]

Engelund and Hansen (1967)

In contrast with Meyer-Peter and Müller this is a total transport formula. The formula is of a semi-empirical nature. It has shown particularly useful in fine sandy rivers with substantial suspended load.

Basic form

$$\Phi = 0,05\Psi^{\frac{5}{2}} \quad [-] \quad (2\text{-}24)$$

Ripple factor

$$\mu = \left(\frac{C^2}{g}\right)^{\frac{2}{5}} \quad [-] \quad (2\text{-}25)$$

Characteristic grain size D_{50}.

Van Rijn (1984)

This formula has been calibrated on a total of 130 flume experiments with particle diameters (d50) ranging from 200 to 2000 μm, waterdepths larger than 0,1 m and a Froude number smaller than 0,9.

Van Rijn (1984) distinguishes between bed load (s_b) and suspended load (s_s).

$$s = s_b + s_s \quad [\text{m}^2 \cdot \text{s}^{-1}] \quad (2\text{-}26)$$

This formula doesn't use the parameters **Φ** and **Ψ**. Instead it defines the dimensionless parameters

Bed shear stress parameter

$$T = \frac{\tau_b' - \tau_{b\,cr}}{\tau_{b\,cr}} \quad [-] \quad (2\text{-}27)$$

In which:

τ'_b bed shear stress related to the grains

$$\tau_b' = \left(\frac{C}{C_{90}}\right)^2 \tau_b \quad [\text{N} \cdot \text{m}^{-2}] \quad (2\text{-}28)$$

$\tau_{b\,cr}$ critical bed shear stress according to shields [N ·m^{-2}]

Grain-size parameter

$$D_* = D_{50}\left(\frac{\Delta g}{\nu^2}\right)^{\frac{1}{3}} \quad [-] \quad (2\text{-}29)$$

Concerning the bed load transport

$$\Phi_b = 0,053\frac{T^{2,1}}{D_*^{0,3}} \text{ for } T<3 \quad [-] \quad (2\text{-}30)$$

$$\Phi_b = 0,1\frac{T^{1,5}}{D_*^{0,3}} \text{ for } T\geq 3 \quad [-] \quad (2\text{-}31)$$

In which:

$$\Phi_b = \frac{s_b}{\sqrt{g\Delta D_{50}{}^3}} \quad [-] \qquad (2\text{-}32)$$

In which:

s_b bed load including pores $[m^2 \cdot s^{-1}]$

For a description of the formula for suspended load one is referred to Van Rijn (1993).

2.3 River morphology

River flow is an open-channel flow because of the free surface. A rigid channel has only one free surface, but an alluvial river that is unconstrained in developing its own geometry has all its boundaries as free surfaces. The self-formed geometry of the alluvial river encompasses many variables. The abundance of variables has made river morphology and river mechanics a complex subject that has attracted the attention of many engineers and scientists. As an initial step in searching for an adequate understanding of river channel formation and changes, the variables and their interconnected relationships involved in the fluvial processes need to be identified (Chang, 1988, p. 4).

Within this thesis special attention is given to the influence of vegetation on the fluvial processes. Figure 2-1 presents a schematic overview of the interactions. The many arrows back and forth between the different sub-systems clearly show the beauty and complexity of the river system. The flow is affected by bed morphology and vegetation. The flow in turn, drives the sediment transport to cause bed deformation (geomorphology) including surface-layer sorting. The violent change of bed morphology during floods causes the removal or burying of vegetation, and the bed morphology controls vegetation growth. The vegetation has a strong influence on the stream profile (flow) and the erodibility of the soil (geomorphology). This sums up to every sub-system influencing other sub-systems, while this sub-system at the same time is being influenced by these sub-systems. The fine arrows indicate, secondary actions, such as break of vegetation by flood or debris, effect of bed morphology on sediment transport, effect of sediment concentration on the turbulent structure, abrasion of structures by debris and so on (Tsujimoto, 1999).

Variables for the alluvial river are classified as control and effect variables. Those that are imposed upon the river by any source are control variables, whereas those that result are effect variables (Kennedy and Brooks, 1963). The river has no control of the control variables, but instead is controlled by such variables (Chang, 1988).

It is necessary to take the time- and space scales into account to be able to decide upon which variables are to be regarded as control and effect variables. On a certain scale the time- and space scales of a higher level can be considered steady, thus control, while the phenomena of a lower level should ideally be considered effects.

Table 2-1, Time scales for several hydro- and morphodynamic phenomena

Phenomena	Time scales
floods	a few days – one week
cross-profile	one to a few years
longitudinal profile	decades to a century
alignment	centuries
branching pattern	millennia
river basin	geological timescales

Geomorphological processes occur on time scales ranging from microseconds, relevant to turbulence, up to hundreds of millions of years for geological processes. The spatial scale range is similarly wide, from micrometers for capillary flows in sediments up to continental and global scales (Baptist, 2005). Table 2-1 presents a usable division in time scales of several hydro- and morphodynamic phenomena. Kirkby (1990) presents an example for the wide variety in scales for river systems, see Figure 2-12. He presents a measure for the response rate of systems, defined as a diffusive transport rate, i.e. the ratio of the squared spatial dimension (m^2) over the temporal dimension (y). However, when attempting to attribute specific scale levels to certain classes of phenomena, this turns out to depend not only on the river, but also even on the river reach. This means that it is not possible to state with certainty in advance which variables will lead over which others. Figure 2-12 shows that in general morphodynamics is leading over vegetation dynamics, but the reverse may be true in small, vegetation-dominated streams.

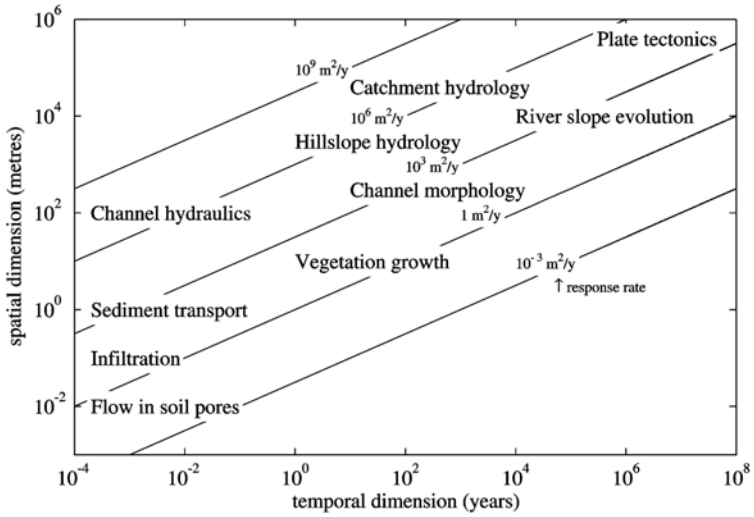

Figure 2-12, Temporal and spatial scales for geomorphological processes. The response rate indicates the evolution rate of the processes. Modified after Kirkby (1990) (Baptist, 2005).

The division between dependent and independent variables is of particular importance in modelling geomorphology.

When a straight river reach is left to itself the mentioned interrelations between flow, sediment transport, bed morphology and vegetation (see Figure 2-1) give rise to natural instability. Therefore most alluvial rivers have a tendency to meander or to braid. A single channel and a mild bottom slope mostly characterize meandering channels, whereas braided rivers have a number of channels and a steep bottom slope. With increasing sediment transport capacity the likelihood that a braided river will develop also increases (Van den Berg, 2000).

The morphology of a channel is related to the flow conditions. At places of high flow velocity, the shear stress is greater, and the channel bed erodes. Therefore the greatest water depth at the straight reaches can be found at the channel centre, and the greatest water depth at the bends can be found at the outer bank. The channel gets much deeper at the bend than at the straight reaches because of the downward flowing water at the outer bank and the inward directed flow at the bed. The downward flowing water causes the shear stress, and thus sediment transport to get greater. The inward directed flow transports sediment to the inner bank, causing the typical asymmetrical cross-section of a bend to develop, see Figure 2-7. This process of erosion and sedimentation results in the typical migration phenomenon of meanders. This meandering is composed of downstream translation and lateral extension.

Figure 2-13 shows the nomenclature of the characteristics of a meandering river. Typically one can distinguish, the already mentioned, point bar and pool. But aside from these two most specific features a meandering river typically contains: scrollbars, floodplains, riffles, abandoned channels (or oxbow lake) and the main channel. The main channel is the part of the river system that discharges the bulk of the water during mean flow.

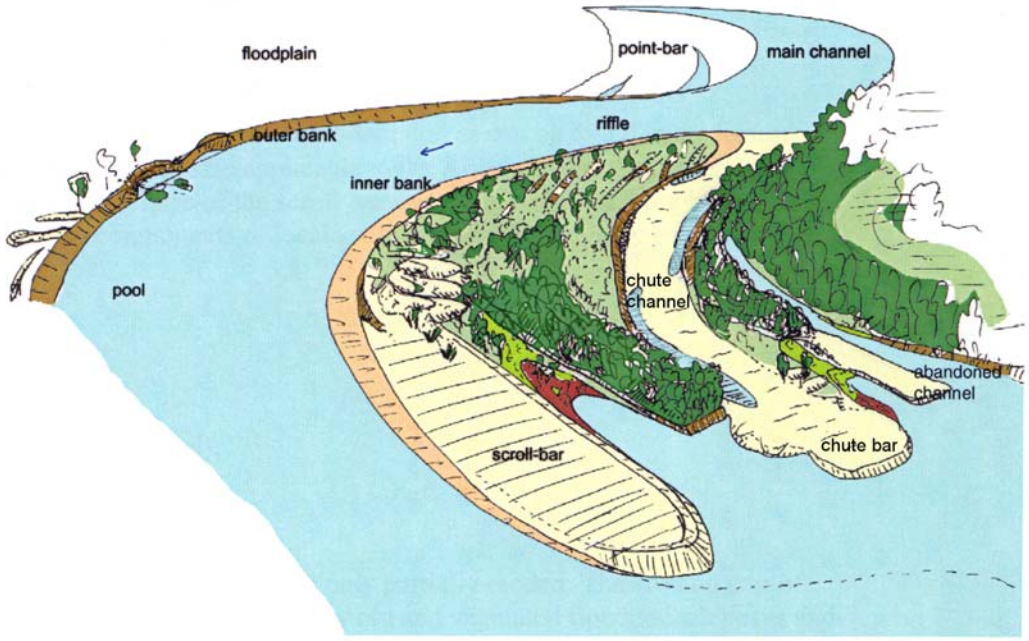

Figure 2-13, River section with nomenclature (De Kramer, 2003)

2.3.1 Point-bars and scroll-bars

The sparsely vegetated area at the inner bend is indicated with the term point bar. The densely vegetated part at the inner bend is called the floodplain. This floodplain is relatively stable and because of the vegetation and lower flooding frequency only small particles are deposited here.

Figure 2-14, Scroll bar in the river Allier near Chateau de Lys, Augustus 2004

Figure 2-14 shows a sickle shaped bank at the sharpest part of the expanding inner bend. This bank is called the *scroll-bar*. These scroll-bars develop to compensate for the increase of the cross-section, which occurs as a result of the erosion of the outer bend. Eventually these scroll-bars develop into an extension of the point-bars (De Kramer, 2000).

2.3.2 Pools and riffles

In between the scrollbar en de outer bank the river is quite deep, as well with respect to the inner bank as with respect to the parts upstream and downstream of the scrollbar. This deepest part can be found right under the outer bank. These deep segments are the 'pools', the shallower areas up- and downstream are called 'riffles'. Riffles are located on the transition section from one bend to another and connect the corresponding point-bars with each other, see Figure 2-15.

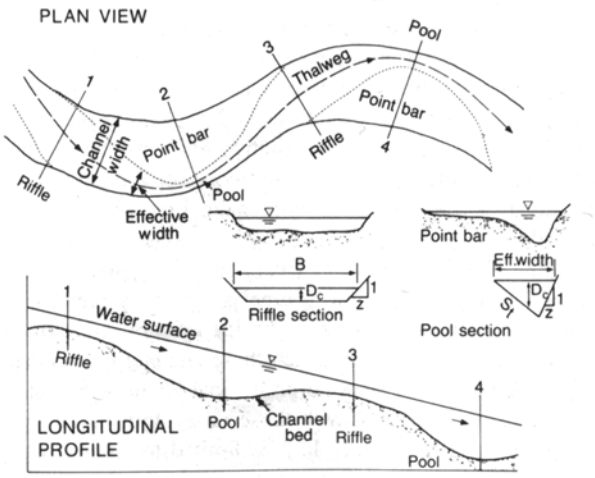

Figure 2-15, Schematic of sinuous point-bar river (Chang, 1988).

On basis of the appearance of pools and riffles one can distinguish individual bends and complex bends. An individual bend consists of one pool confined on both sides by a riffle. A complex bend consists of a multitude of pools and riffles.

It is found that the space between the middle of two pools or riffles is more or less constant and can be approximated by 2π times the main channel width. In the case of the river Allier the meander arc length is somewhere between 570 and 630 metres.

The erodability and the possibility of the outer bank to migrate are of great influence on the development of the riffles. If for some reason (parts of) the outer bend are relatively hard to erode, the riffles will be more pronounced. The same is the case if the outer bank cannot migrate because of limited migration possibility of up- or downstream bends. In some cases this can even lead to drying of the riffles during low flow (De Kramer, 2000).

2.3.3 Abandoned channels

In some studies abandoned channels are called oxbow lakes or oxbow channels. It constitutes those parts of the riverbed that are no longer, or only in a limited way connected with the main channel. Usually they come into existence because a meander bend becomes inactive (see Figure 2-16). These channels are ecologically usually very rich in comparison with the rest of the river system. The standing or slowly flowing water, and the banks are an ideal situation for lots of different plants. The rich and dense flora, in turn, makes it an excellent habitat for the fauna.

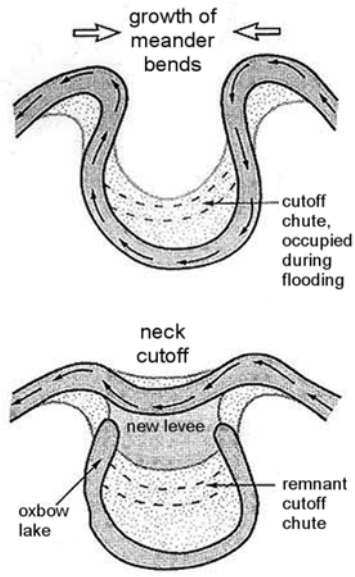

Figure 2-16, Origination of an oxbow lake (abandoned channel) and a Photograph of an oxbow lake in the river Allier

With high flow these abandoned channels are reconnected with the main channel and can be of great influence on the hydro- and morphodynamics of the river (De Kramer, 2000).

2.3.4 Sediment balance formula

Mathematically speaking morphological changes are induced by gradients in the transport capacity. The transport capacity of the flow is determined using a transport formula, of which three examples are given in section 2.2.8, 'Transport formulae'. The changes in bed morphology are than calculated according to the sediment balance:

$$(1-\varepsilon)\frac{\partial A_s}{\partial t} = \frac{\partial S}{\partial x} - q_s \qquad (2\text{-}33)$$

In which:

ε	porosity of the bed material	[-]
A_s	conveying cross-sectional area	[m^2]
S	sediment load	[$m^2 \cdot s^{-1}$]
q_s	rate of lateral sediment inflow per unit channel length	[$m^2 \cdot s^{-1}$]

The first term in equation (2-33) may be interpreted as the rate of change in channel cross-section due to sedimentation or erosion. This change is attributed to the spatial variation in sediment discharge represented by the second term, and to the lateral sediment inflow represented by the third term, of this equation. The factor (1-ε) converts the net volume of sediment used for S into bulk volume for Ab.

2.4 Vegetation

The effects of vegetation can be observed at different spatial scales. Vegetation increases the hydraulic resistance of flowing water, and consequently generates flow retardation and water set up. This results in a change in the flow pattern, and consequently, in a change in the morphological processes, that can even lead to a change of the river pattern. At the smallest scale tail bars are formed in the wake behind single trees, bushes, or woody debris. In front and alongside these tail bars the flow velocity is increased, which may result in erosion and the formation of horse-shoe shaped depressions in front of the tail bars.

Several theories on vegetation modelling have been developed, see for example Van Velzen et al. (2002). A method that is often used to account for the increased flow resistance of the bed due to the vegetation, is by increasing the Nikuradse roughness height, see equation (2-2). This method assumes a logarithmic velocity profile over the complete water depth. In reality, however, the vertical flow profile deviates from the logarithmic one. A typical velocity profile for submerged vegetation is shown in Figure 2-17. Four distinct zones can be identified in the vertical velocity profile for flow through and above submerged vegetation:

- In the first zone, near the bed, the velocity is highly influenced by the bed, and its vertical profile joins the logarithmic boundary layer profile.
- In the second zone, which corresponds to the zone inside the vegetation sufficiently away from the bed and from the top of the vegetation, the velocity is uniform.

- In the third zone, near the top of the vegetation, there is a transitional profile between the uniform velocity inside the vegetation and the logarithmic profile above it. The profile in this zone can be approximated by an exponential function.
- Finally, the fourth zone corresponds to the zone above the vegetation, where a logarithmic profile is observed.

Various studies have already shown that in the case of a vegetated bed the Nikuradse schematization exaggerates the roughness of the bed, which leads to an erroneous calculation of the bed shear stress (e.g. Baptist, 2005). Because of that it leads to errors in the morphological calculation. Baptist (2005) also proposed some methods to predict the bed shear stress and Chézy values in vegetated areas. In this thesis one of this methods is tested in a Delft3D model of the river Allier. This method is called the 'Reduction factor approach' and is explained in the remainder of this section. It should be noted that the influence of the orientation, dispersion and flexibility of the vegetation is not accounted for in the approach of Baptist (2005).

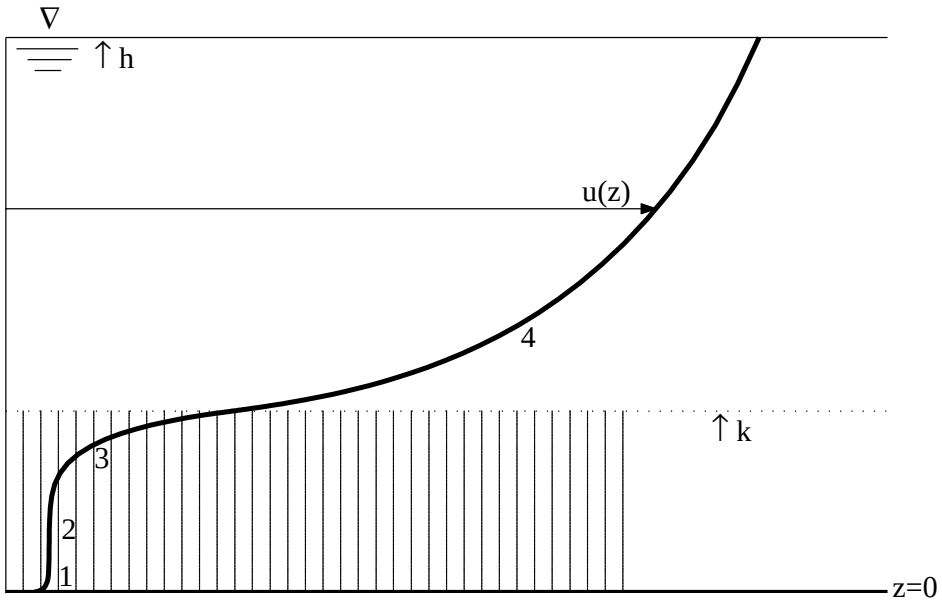

Figure 2-17, Vertical profile for horizontal velocity through and over vegetation.

Reduction factor approach

The following text is quoted from Baptist (2005, p. 47)

For uniform, steady flow in a wide rectangular channel with vegetation, part of the fluid forces are carried to the plants as a kind of body resistance force, and the energy gradient increases considerably due to the additional resistance of the vegetation. The forces on a fluid element Δx in flow through and over vegetation are given in

Figure 2-18. The force balance for flow with vegetation contains an additional plant resistance force per unit area, F_D [N·m^{-2}]. It is common to model vegetation as a group of parallel, staggered or randomly arranged rigid vertical cylinders with homogeneous properties.

The resistance force is defined as:

$$F_D(z) = \frac{1}{2}\rho \int_z^k C_D(z)\, m(z)\, D(z) \left|u(z)\right| u(z)\, dz \qquad [\text{N} \cdot \text{m}^{-2}] \qquad (2\text{-}34)$$

in which:

k	cylinder height	[m]
C_D	drag coefficient	[-]
m	cylinder density per unit area	[m^{-2}]
D	cylinder diameter	[m]
u	time-averaged horizontal flow velocity	[m/s]

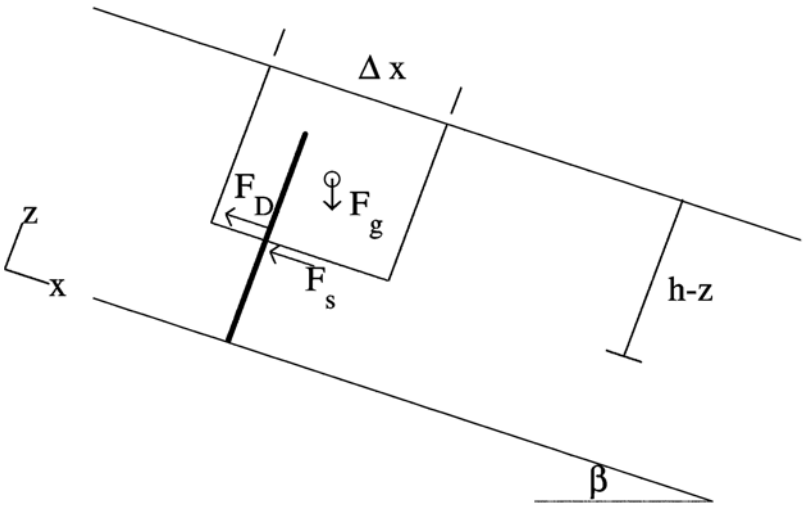

Figure 2-18, Fluid forces on a control volume, for uniform, steady flow in a wide rectangular channel with vegetation.

From now on a positive flow direction is assumed, so that F_D is a function of u^2. At the bed, z=0, the force balance for vegetated flow thus becomes:

$$\rho g h i = \tau_b + \underbrace{\frac{1}{2}\rho \int_0^k C_D(z)\, m(z)\, D(z)\, u^2\, dz}_{\text{vegetation resistance}} \qquad [\text{N} \cdot \text{m}^{-2}] \qquad (2\text{-}35)$$

bed resistance

For flow through and over vegetation, the total fluid shear stress, ρghi, equals the bed shear stress plus the additional vegetation resistance.

From this general formula of the force balance of flow, Baptist (2005) developed two different, but closely related, approaches to calculate the bed shear stress. In this Master thesis one of these formulae is used, namely the Reduction factor approach.

This bottom shear stress formula distinguishes between submerged and non-submerged vegetation. It consists of a part representing the influence of the bed and a part representing the influence of the vegetation. Figure 2-19 presents the classification of the total roughness as used throughout this thesis. In the Ph.D. thesis of Baptist the total resistance is distinguished from the bed resistance by labelling the first "*vegetated bed resistance*" and the second "*bed resistance*". Hence

the subscript *bv* (Bed Vegetated) and *b* (Bed) is used for the shear stress in the formulations presented in this chapter.

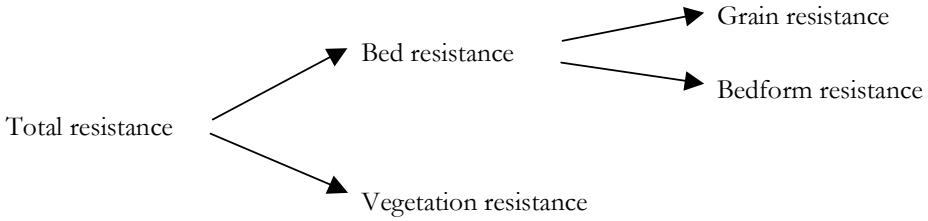

Figure 2-19, Classification of flow resistance factors.

The Reduction factor approach schematises the vertical flow profile for submerged vegetation as two non-interacting flow layers. The lower layer describes the vertical flow profile through the vegetation, which is assumed uniform over the depth, and the upper layer describes a logarithmic vertical flow profile above the vegetation. Figure 2-20 gives a definition sketch. Note that the assumption of uniform flow through vegetation only holds for relatively high vegetation density and height.

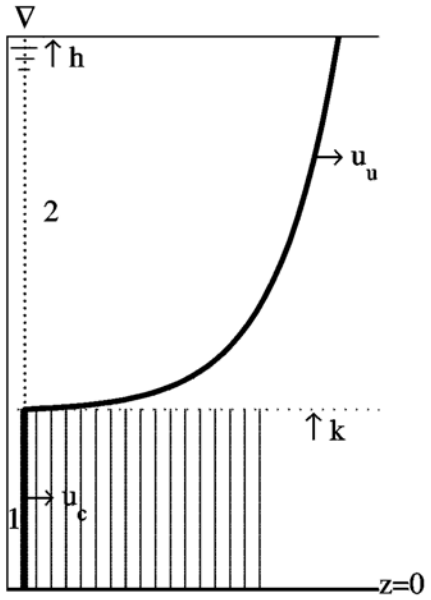

Figure 2-20, Schematised vertical flow division. Part 1 is the uniform flow part and part 2 is the logarithmic flow part (Baptist, 2005).

The Reduction factor approach leads to two different formulas. One for the case of non-submerged vegetation, the other for the case of submerged vegetation:

Non-submerged vegetation:

$$\tau_{bv,nonsub} = \frac{\rho g}{C_b^2} u_c^2 = \frac{\rho g}{C_b^2} \overline{u}^2 \qquad [\text{N m}^{-2}] \qquad (2\text{-}36)$$

Submerged vegetation:

$$\tau_{bv,sub} = f\frac{\rho g}{C_r^2}\bar{u}^2 \qquad [N \cdot m^{-2}] \qquad (2\text{-}37)$$

in which:

C_b	Chézy bed roughness	$[m^{1/2} \cdot s^{-1}]$
C_r	representative roughness of the vegetation	$[m^{1/2} \cdot s^{-1}]$
f	reduction factor for vegetated bed resistance	[-]
ū	depth averaged velocity	$[m \cdot s^{-1}]$
u_c	uniform flow velocity through the vegetation	$[m \cdot s^{-1}]$

The reduction factor, f, is given by:

$$f = \frac{1}{1+\frac{C_D m D k C_b^2}{2g}} \qquad [-] \qquad (2\text{-}38)$$

in which:

C_D	drag coefficient (= 1, in this thesis)	[-]
m	cylinder density per unit area	$[m^{-2}]$
D	cylinder diameter	[m]
k	cylinder height	[m]

Baptist (2005) elaborates different variants for the calculation of the representative roughness of vegetation. He showed that the approach by Rodríguez Uthurburu (2004) yields better results as an overall estimator of the representative roughness. This expression is derived by genetic programming and some slight adjustments to yield a more physically correct formula. This led to the following formula for the representative Chézy value for submerged vegetation:

$$C_r = \sqrt{\frac{1}{\frac{1}{C_b^2}+\frac{1}{2g}C_D m D k}} + \frac{\sqrt{g}}{\kappa}\ln\frac{h}{k} \qquad [m^{1/2} \cdot s^{-1}] \qquad (2\text{-}39)$$

in which:

κ	Von Kármán constant = 0.4	[-]
h	water depth	[m]
k	= h, in the case of non-submerged flow	[m]

This expression is very simple in its form. It consists of two parts, one is the representative roughness of the vegetated part of the water column, and the other is the representative roughness of the overlying part of the water column (Baptist, 2005). In case of vegetated flow, this representative Chézy value can be substituted for the Chézy-coefficient in formula (2-1). Figure 2-21 shows for two different vegetation types the Chézy value as a function of the water depth for both the 'conventional' Increased Nikuradse roughness height method and the Rodríguez Uthurburu (2004) method. Note for the Rodríguez Uthurbu formulation the increase of the Chézy value (decrease of roughness) when the vegetation gets submerged.

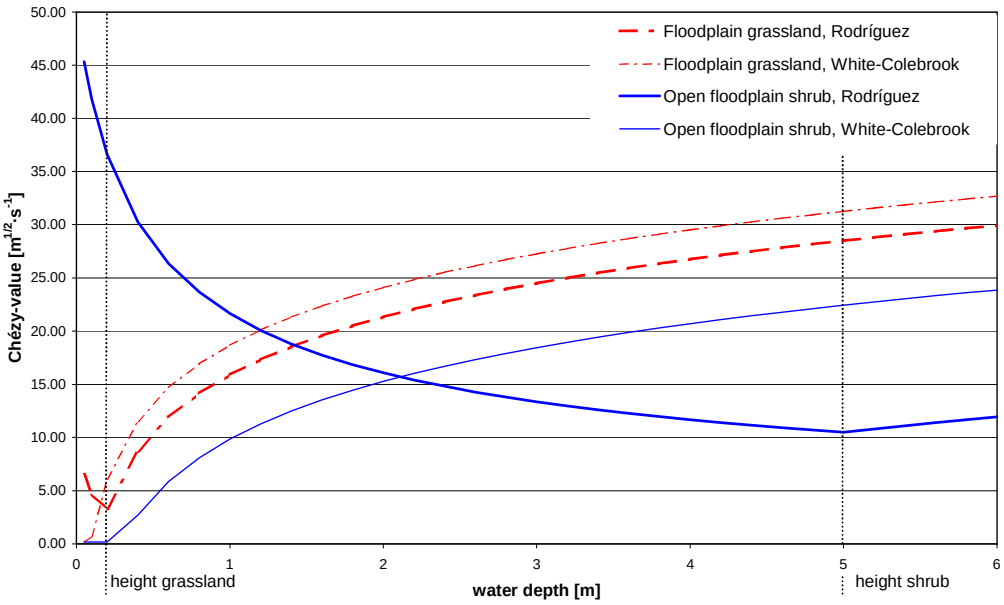

Figure 2-21, Chézy-value in a vegetated area as function of the water-depth according to the White-Colebrook formulation and the Rodríguez Uthurburu (2004) formulation for the vegetation types Floodplain grassland and Open floodplain shrub (see Table 6-3 for the used parameters).

Besides the impact on flow and transport capacity, through the bed shear stress and bed roughness, vegetation has several other aspects that are thought to have a considerable impact on the fluvial processes in rivers. Although these are not accounted for in the computational model that is studied in this thesis, they will be briefly discussed for a correct general understanding of the processes involved in reality and a clearer valuation of the model results.

Vegetation with a tight network of roots increases the resistance to erosion, which is one of the reasons why dikes are often covered with grass. Furthermore the top layer in vegetated areas is usually formed by a humus rich soil instead of a purely non-cohesive sandy or gravel soil. A first estimation of the impact of this may be modelled as a layer of cohesive sediment equal to the root depth. Another aspect is the accumulation of debris between plants. This debris may form a layer that will act as a revetment and thus decrease erosion.

3 Description of the study area: the river Allier

3.1 Introduction

The river Allier is considered as one of the last natural rivers in Western Europe. The catchment area is 12.980 km² (Agence de l'Eau Loire-Bretagne, 1991) and is nearly completely located within the province Auvergne of France. On the flanks of the Moure de la Gardille in the Massif Central at a height of 1500 m above sea level the river emerges as a mountain spring. About 410 km downstream it flows into the river Loire near Nevers at a height of 167 m. At this point the river Allier is approximately as large as the river Loire, with respect to the cross-section as well as the discharge (Wilbers, 1997).

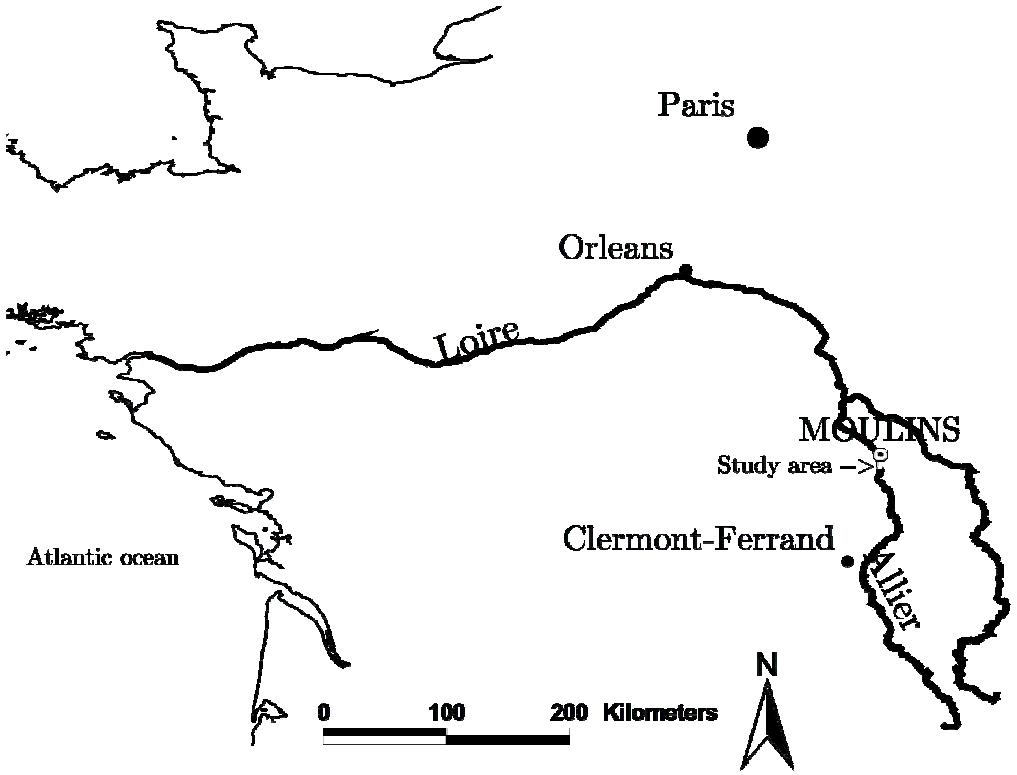

Figure 3-1, Location of the study area along the Allier (Baptist, 2005)

The study area is a meandering part of the river consisting of three meander bends located near Chateau-de-Lys, somewhere between Châtel de Neuvre, in the south, and Moulins, in the north (see Figure 3-1). The borders are located in the apex of riverbends in order to have parallel streamlines over the model-boundaries. It covers an area of approximately 6 km² and has a length of 3 km as the crow flies. The length of the main channel is approximately 5 km. The whole area is located in a nature reserve ranging from St. Loup to Moulins: Réserve Naturelle du Val d'Allier. This means, among other things, that the local farmers are not allowed to protect the riverbanks with rocks and debris. The farmers however are not particularly fond of a 'natural' river eroding their land, so in some places bank protection is still present (Van Bemmel, 2003).

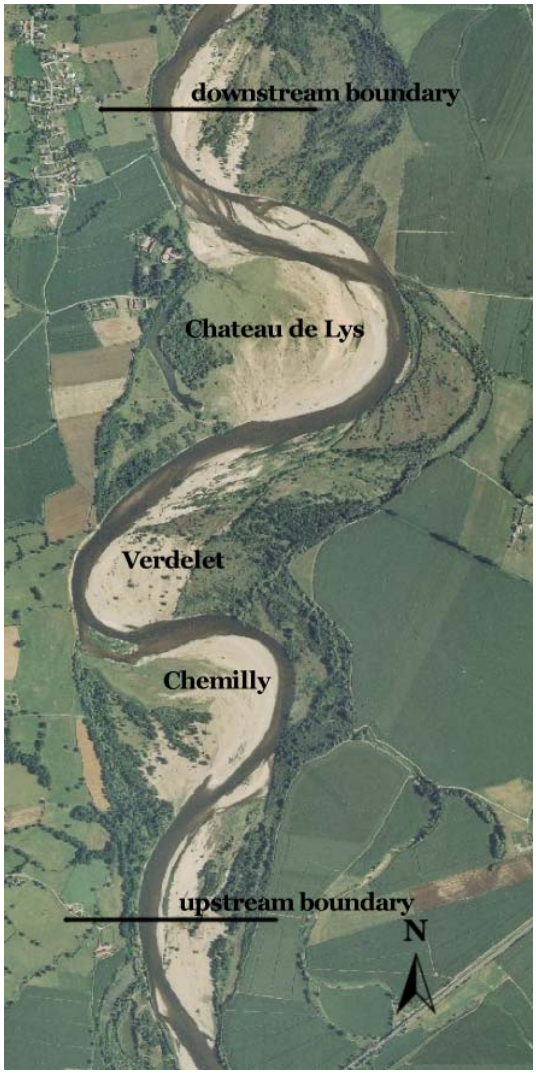

Figure 3-2, Aerial photograph of the study area made in the year 2000. Flow is from south to north.

3.2 Discharge regime

The discharge regime of the Allier is highly irregular, due to the pattern of precipitation in the upstream Massif Central and the Limagne Graben. Most rain occurs in spring, leading to high-water levels from January to May. During summer months, precipitation decreases close to zero and discharges are low (De Kramer, 2003).

Between 1968 and 2004 waterlevels are measured daily downstream and upstream of the study area by the Directions Régionales de l'Environnement (DIREN)[1]: downstream at approximately 5 km from the study area at Moulins, upstream at approximately 14 km from the

[1] DIREN is the decentralised service of the Ministry of Environment in France. The main goal is to enhance economical and social development and protection of natural resources for future generations. DIREN centre is responsible for the basin Loire-Bretagne, of which the Allier is a part. More information can be found on http://www.environnement.gouv.fr/centre/

study area at Châtel-de-Neuvre. With these waterlevels and the local Q-h relations the discharge can be determined. Because of the relative small scale of the study area in terms of rainfall-runoff and seepage it is assumed that the discharge is constant along the river reach and approximately equal to the discharge measured at Moulins (Kapinga, 2003) or Châtel-de-Neuvre. The discharge at Moulins is considered to be the most reliable because the waterlevel is measured over a weir instead of at a natural cross-section. The Q-h relation of a weir is more trustworthy because it is far easier to calibrate and it is less prone to errors because of a morphological changes in the cross-section.

Due to regulation of dams and reservoirs in the southern part of the catchment the discharge in the study area has never become less than 10.8 m^3/s. Typical peak discharges amount to 800-1200 m^3/s, lasting several days to up to 3 weeks. The maximum recorded discharge was 4700 m^3/s at Moulins (Bouchardy, 1991). The mean yearly discharge at Moulins is about 140 m^3/s. A discharge of 1000 m^3/s only happens about once every five years. A discharge of 825 m^3/s can be expected every two years. (A.W.E. Wilbers, http://globis.geog.uu.nl/users/wilbers/home.html). For the statistical distribution of maximum discharges one is referred to Appendix 1, 'Discharge analysis Moulins'.

In history, the Allier flow area and floodplains were much wider and very large discharges have occurred. In 1846, 1856 and 1866, extreme discharges in the Allier were estimated at 8000 m^3/s. It is highly unlikely that discharges of that magnitude will occur again, since the flow regime then was different and dams were absent.

3.3 Sediment characteristics

The sediment characteristics of the main channel in the study area have been studied by Wilbers (1997) and Cohen (1998). The diameter of the armoured top layer is found to be around a d_{50} of 16mm and a d_{90} of 41mm. For the bottom sediment a d_{50} of 7.7mm and a d_{90} of 34.2 mm are found. The sediment diameter varies strongly according to the location, in the horizontal as well as in the vertical plane. A field survey in the study area by Driesprong (2001) on the sediment diameter of the top layer of the main channel showed a variation of the D50 from 4.5 mm till 36.9 mm per sampling location. Concerning the point-bars, the spatial distribution is even more pronounced. Some parts close to the main channel show gravel that is almost as coarse as the sediment that is found in the main channel. But there are also some large vegetated parts with coarse sand with a D_{50} much smaller than 4.5 mm. Figure 3-3, Figure 4-4 and Figure 6-4 show that even the sediment diameter on the bare parts of the point-bar can differ widely between locations close to each other. Unfortunately no reliable sediment measurements have been collected in these areas.

Figure 3-3, Photograph of the point-bar Verdelet (front left) and point-bar Chemilly (back) (De Kramer, July 2004).

3.4 Morphology

Over a large distance the river follows the Limagne graben, where it is embedded largely in its own alluvial deposits. Within this alluvial reach originally a highly dynamic pattern was present, with in many areas braided characteristics. Mainly as a result of recent climatic change, and to some extent riverbed incision due to gravel mining during the past century, the river pattern has turned or is turning to a meandering pattern. In the current situation the transition from a meandering to a braided river takes place at the city Moulins. It is however expected that the meandering pattern will propagate further downstream in decades to come.

The meandering part of the river is gravel-dominated and has an armoured bed that has a strong influence on the morphodynamics (Kleinhans, 2000). It shows steep outer bends and gentle sloping sparsely vegetated inner bends. In years of high discharges meanders can migrate laterally with a speed of several metres to a maximum of 60 metres per year. In some cases these meander bends are cut off, in which case deserted meander bends and abandoned channels occur (see Figure 3-4).

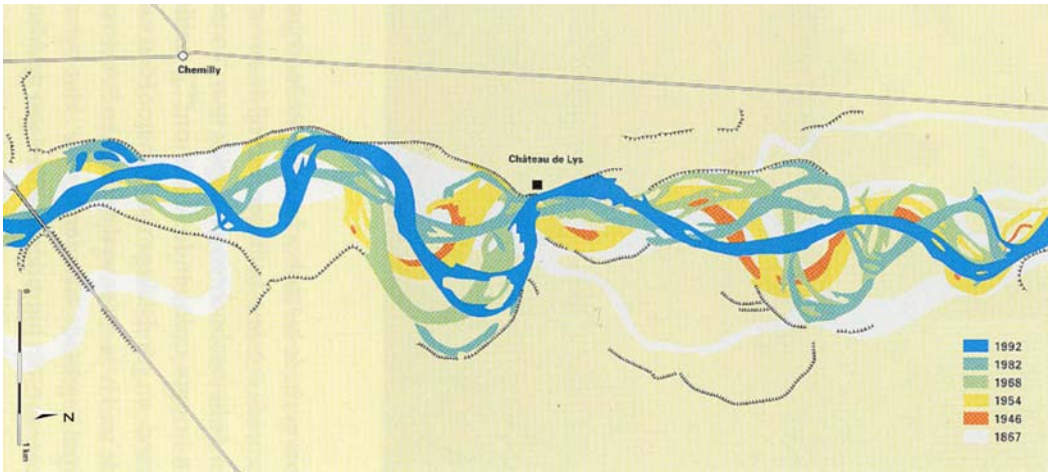

Figure 3-4, Movement of the meanderbends of the river Allier in the study area.

In the northern part of the river Allier, the river is less dynamic. It is sand-dominated and shows straight parts with islands in the main channel, active or semi-active side channels and steep walls at both sides of the channel. In this part, the river appears to have a braiding character, although it is expected that dynamics nowadays are low (Van den Berg, 2000).

3.5 Vegetation

The fluvial dynamics of the river Allier create several ecological environments that attract specific flora and fauna. Therefore the natural flora of the Allier floodplain is very rich. On the river banks, which are uncovered by water during minimum flow at the end of summer, remarkable annual plants grow, among which are found some rare and protected species. The Allier forms a migratory route for some southern plants and for some plant species that originate from plants planted in gardens (Boucherdy, 1991).

New riverine vegetation development in the Allier starts with a bare soil of freshly deposited or reworked sediment. Then some pioneer species germinate. This initial vegetation composition may develop into a mosaic landscape of different vegetation types, consisting of grassland, ruderal vegetation (herbs and weeds) and softwood forest, mainly of White willow (Salix alba) and Black poplar (Populus nigra). Whether this succession will occur depends largely upon the height of the discharges that may erode the vegetation or reset the vegetation succession.

Another factor of importance in the Allier is that of grazing. In general it can be said of the study area that the west banks are intensively grazed by cows, while at the east banks small grazers like wild deer and pigs, make little contribution to the landscape. Intensive grazing reduces the height and density of weeds. Furthermore the grazers contribute considerably to the vegetation patterns. Weeds, bushes and trees get no chance to grow because they are eaten with the grass (Van den Bosch, 2003).

Vegetation succession is a process in which different vegetation types follow up on each other when the vegetation matures. The end stage is called the climax stage (Clement, 1916). For floodplain vegetation the climax stage will be reached after more than 100 years and is characterised by hardwood forest of Oak, Ash and Elm (Baptist et al. 2002).

Peters et al. (2000) estimate that about 32% of the floodplain of the Allier between Châtel-de-Neuvre and Chemilly bears pioneer vegetation. The area of grassland and grassland with bushes and some trees is also about one third of the total area. Forests occupy the last third of the floodplain. The fast reworking of the Allier floodplain leads to relatively few hardwood forests.

4 Field survey

4.1 Introduction

The purpose of the field survey was to retrieve data to use as input for the model and data that could be used to calibrate and validate the model.

Generally speaking it can be said that the input for the model is based on the data retrieved in previous field surveys. The model results will be compared with the data from the last field survey that was carried out within the context of this master thesis. Table 4-1 lists the used data. Per data type (i) the date of measurement is stated, (ii) whether the data is used for model input or for comparison with the model output, (iii) the Section in which the data type is discussed and finally (iv) the table lists some of the reports that discuss the collection and processing of the listed data.

Table 4-1, Field survey data used in this thesis.

data type	month/year	input/output	section	report
sediment diameter	08/1998	input	3.3	Wilbers, 1997; Cohen, 1998
vegetation	08/2003	input	3.5	Van Bemmel, 2003
bathymetry	08/2003	input	4.5	Van Bemmel, 2003
discharge			3.2	DIREN
Flood Dec. 2003	12/2003	input		
vegetation	08/2004	input	4.6	
bathymetry	08/2004	output	4.2	

Each of the Sections of this chapter considers one specific data type. The Sections discuss the way in which the data is retrieved from the field as well as the processing that had to be carried out in order to make the raw data useable for model input or comparison. The field trip was carried out during 5 weeks of the months July and August in 2004. This is particularly interesting because December 2003 has known the largest flood since the start of the research on the river Allier.

It must be stated that demands on model input are different from the demands on a visual presentation. Therefore the processing of data to yield model input usually differs from the processing of data to produce tables and visualisations suitable for human interpretations.

The processing of the collected data took about two and a half month. The following programs were used:

- *Trimble geomaticss Office*: A program to write the information from the RTK-DGPS to the laptop and to translate the transferred data to a chosen geographic coordinate system. It is also used to export this data to files that can be read by ArcView.
- *ArcView*: ArcView is full-featured GIS software for visualizing, managing, creating, and analyzing geographic data. In this thesis it will be used to create maps that present the spatial distribution of the acquired data in a clear and comprehensible way.
- *Surfer*: This is a powerful contouring, gridding, and surface-mapping program. It will be used to interpolate height measurements between locations, to make 3D pictures of the area and to create files which can be used by Delft3D-QUICKIN.
- *Delft3D-QUICKIN*: This is a module of the Delft3D software package. It is used to translate the files of the software program Surfer into Digital Elevation Model files that can be used by Delft3D-FLOW. In theory Delft3D-QUICKIN can interpolate just as Surfer does, but Surfer is considered more powerful and more user friendly.
- *Delft3D-RGFGRID*: A module to generate orthogonal, curvilinear grids of variable grid size for the hydrodynamic module Delft3D-FLOW.
- *Microsoft Excel*: A general data processing tool. This program was used to generate extra data by interpolation to reduce the errors made by the program Surfer.
- *Textpad*: A text editor.

4.2 Discharge regime

The assumed discharges in the study area are based on the measurements by the Directions Régionales de l'Environnement (DIREN), see Chapter 3.2. The discharges that occurred between the bathymetry measurements of August 2003 and August 2004 are given in Appendix 1. In this period one flood occurred in December with a peak discharge of 1360 m^3/s and a return period of 25 year. In January and May of 2004 two smaller floods occurred with a peak discharge of 600 m^3/s.

4.3 Water level

Unfortunately no water level measurements during high flow were available. An attempt was made to reconstruct the water depths on the basis of flood marks, like dead wood up in the trees or abrasion scars. One of these debris spots was measured with the RTK-DGPS. The other estimates of the water depth could be reconstructed on memory and photos (see Figure 4-1). This method, however, showed to be of very little use. The main reason is that the number of flood marks is too low and concentrated in forested areas. Those forested areas are just the places where measurements with the RTK-DGPS (obstruction of satellite signals by trees) or levelling instrument (obstruction of the line of sight) are extremely difficult so one has to rely on photos which only give a very rough indication of the height of the flood mark.

Figure 4-1, Flood marks (Rink, July 2004).

4.4 Flow directions on point-bars

To estimate the flow directions on the point-bars during high flow the location and orientation of the scour holes was measured. The scour holes are probably strongly influenced by the sedimentation that occurs at the decline of the flood. This implies that the measured orientation of the scour holes does not necessarily coincide with the direction of the flow at the peak of the flood.

Rink (2005), a M.Sc. student from Utrecht University, determined the location as well as the orientation of 199 scour holes. Hereto he used the RTK-DGPS and the hand-held GPS to measure the position of the most upstream and the most downstream located points of the edge of the scour hole.

With the program ArcView, the tables containing the location and orientation of the scour holes could be easily translated to arrows on a map. Figure 4-2 shows a part of the point-bar Chateau de Lys, near the cut-off to the oxbow lake. Appendix 6 shows a map of the total study area with the measured scour holes. Appendix 7 shows the measured scour hole directions along with the modelled velocity directions in the Figures 1, 2 and 3 of 8.2.

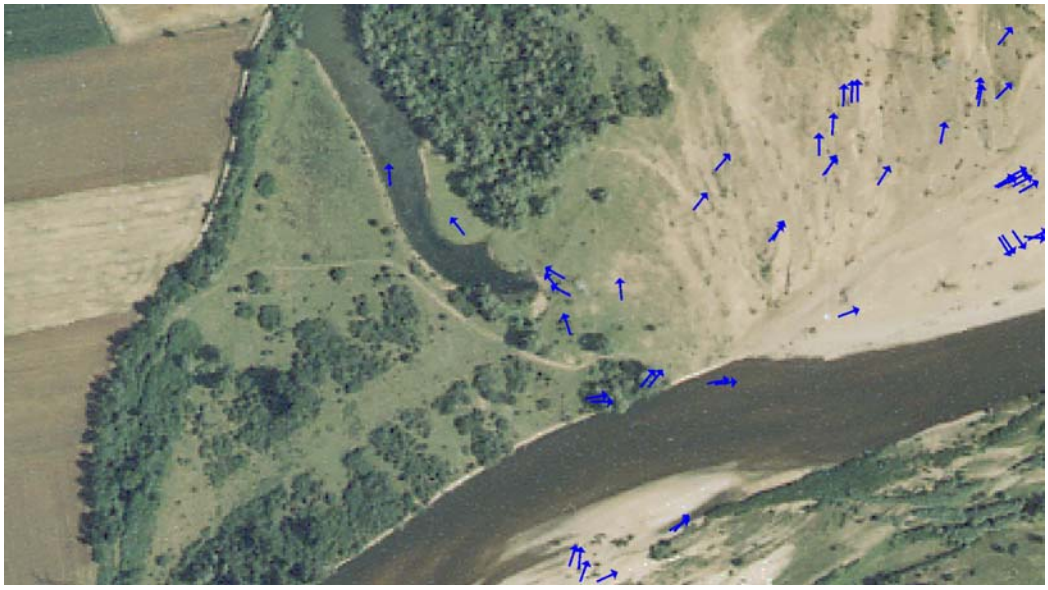

Figure 4-2, Direction of scour holes on point-bar Chateau de Lys (July 2004), overlaid on an aerial photograph of 2000.

4.5 Terrain elevation and channel depth

The bathymetry measured in 2003 was used as input for the Delft3D model. The model results were compared with the measured bathymetry of 2004. The differences and similarities led to conclusions and recommendations about the quality of the model.

Two different measuring methods were used to retrieve the morphology of the study area. The first method used the RTK-DGPS, the second method used the levelling instrument.

The first method is, with regard to accuracy, ease of use and efficiency vastly superior to the second. Nevertheless two reasons exist to use the levelling instrument instead of the RTK-DGPS. Firstly, the RTK-DGPS is sensitive to water damage. Secondly, trees tend to block the signals of the satellites. Since the RTK-DGPS uses satellites to determine its position it is not possible to measure in densely forested areas.

These forested areas however are also difficult to measure with a levelling instrument because of the difficulty to gain a free line of sight from the levelling instrument to the beacon (see Figure 4-3).

Figure 4-3, Gaining a free line of sight from the levelling instrument to the beacon.

Visual inspection

A visual inspection of the study area preceded the measurements with the RTK-DGPS or Levelling instrument. Three remarkable features were found that will be discussed briefly.

In general it can be said that the December flood of 2003 has had a very strong impact on the morphology of the study area. Numerous chutes and chute bars were found on all three point bars, especially on pointbar Chemilly, see Figure 4-4 and Figure 6-4. The width of these channels varies typically from 5 – 15 m, the depth reaches values up to 2 m, and the edges are steep, about 1:1.

The riffle between point-bar Chateau de Lys and point-bar Verdelet was strongly pronounced and covered the complete width of the main channel, see Figure 4-5. The mean water depth above this riffle was approximately 5 dm, except for a relatively small incision that eroded during the field survey. This channel had a width of approximately 5 m and a depth of 2 m in the centre. The flow velocities in this bottleneck were very high and stones with diameters of up to 20 cm have been seen to be carried away, even as some hopelessly struggling students with weights of up to 180 pound.

Another notable feature was located just downstream of this riffle. Here a channel cut-off occurred that reattached the main channel to an old abandoned channel on point-bar Chateau de Lys. Figure 4-5 to Figure 4-7 give an impression of the morphological consequences. A lot of sediment had been eroded at the location of the cut-off, it is assumed that most of this sediment was transported downstream into the abandoned channel, since large areas of heavy sedimentation have been found there.

Figure 4-4, Photograph of a chute channel on point-bar Verdelet (Rink, July 2004).

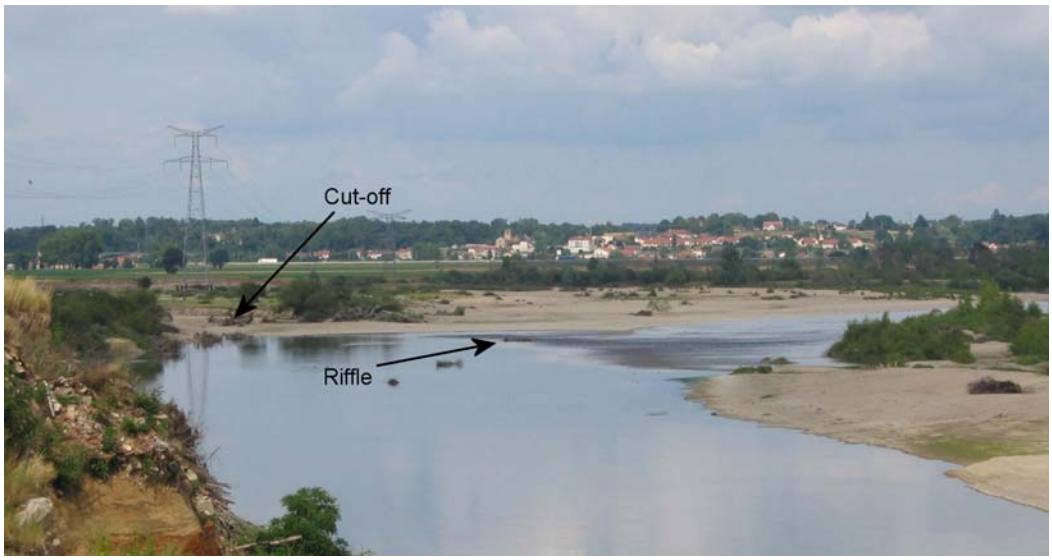

Figure 4-5, Photograph of the riffle between point-bar Verdelet and point-bar Chemilly (De Kramer, July 2004).

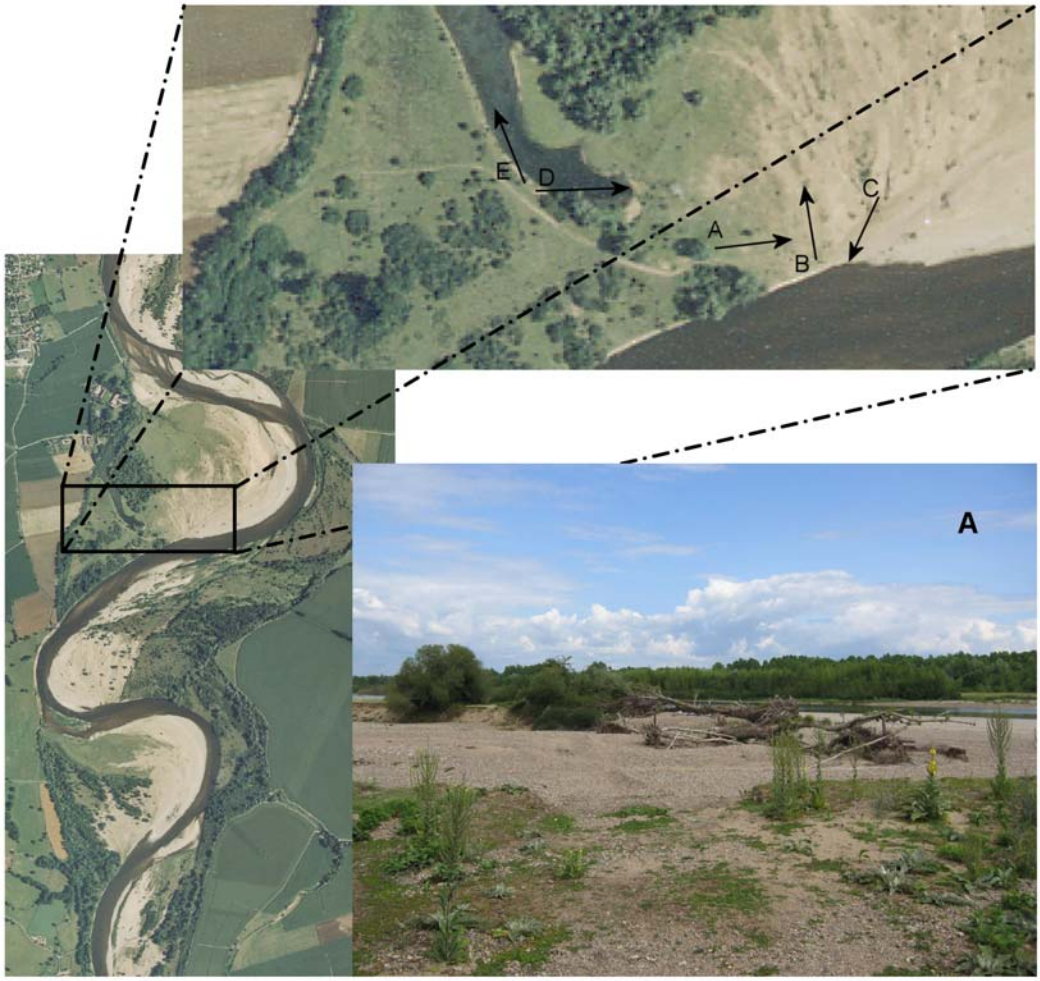

Figure 4-6, Photograph and location depicted on an aerial photograph of 2000 of the cut-off at point-bar Chateau de Lys (Baptist, July 2004).

Figure 4-7, Photographs of the cut-off at point-bar Chateau de Lys (Baptist, July 2004).

RTK-DGPS measurements

RTK-DGPS stands for Real Time Kinematic Differential Global Positioning System.

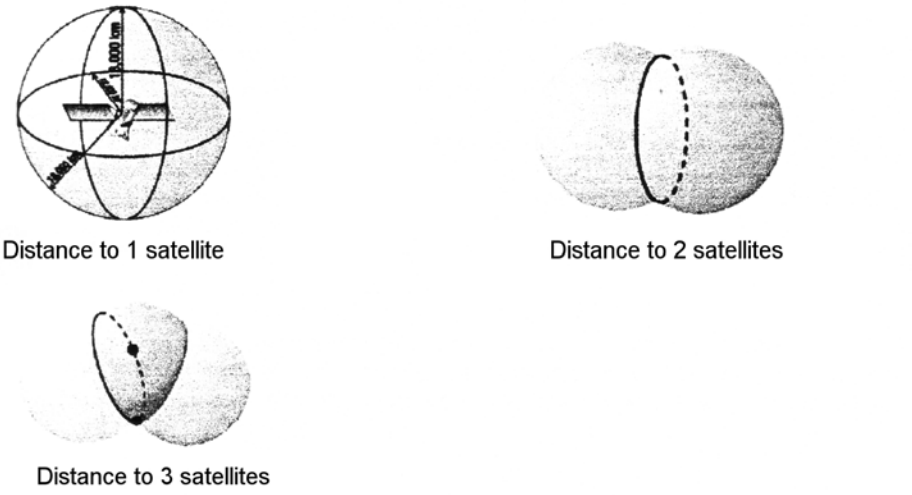

Figure 4-8, Determination of the location is possible by measuring the distance to four or more satellites.

With standard GPS the position of the receiver is determined by measuring the distance of the device to at least 4 satellites, but more satellites lead to more reliable and accurate measurements (see Figure 4-8). Usually it is possible to determine the location with just three satellites, because one of the two points will be located at an impossible position or will be moving with an impossible velocity.

The biggest difference of DGPS with standard GPS equipment is that an extra accuracy is gained by using an extra receiver. The position of this receiver is very precisely determined. The known location of this base station is compared with the location of the base station according to the measurements by the satellites. The difference between the known location and the calculated location is used as a correction on the measured positions by the rover (the other receiver). The accuracy possible with DGPS is about 1 m.

RTK-DGPS (see Figure 4-9) is even more accurate than DGPS. The extra accuracy is gained because the base station can communicate with the rover. This way the corrections can be applied instantaneous which leads to a theoretical accuracy of approximately 1 cm. In practice, however, an accuracy of about 5 cm is more likely. This is because in many cases not enough satellites can communicate with the rover and/or base station because of their position or the presence of trees. Also the measurement time needed per point increases with increasing accuracy, which renders a great accuracy time consuming. Finally the exact placement and movement of the rover can easily add up to errors of several cm. If the rover is placed on a muddy bank it is likely to sink into the bottom, if it is placed on top of a coarse gravel stone or in between some stones can easily give a height difference of 3 cm. The movement of the top of the rover, because it is not positioned vertical, can also be a source of errors up to 2 cm.

Figure 4-9, Measuring with the RTK-DGPS rover and base station (Baptist, July 2004).

Concerning this field survey the georeferenced position of the base station could be determined with the use of a levelling instrument, a compass and a georeference location with know coordinates and height (see Figure 4-3). The coordinate system that is used, is presented in Appendix , 'Parameters of measuring devices'.

Because the data of one year will be compared with other years, it is of the utmost importance the measured points do not have a constant bias between these years. To eradicate this possibility every year some points are measured scattered throughout the study area. The locations of these points are assumed to be the same over the years. For this comparison cross roads and other fixed locations are used. As base year, the year 2002 is used. This has been the first year in which the RTK-DGPS method was used to measure the bathymetry of the study area. The mean deviance between the verification points of the present year and 2002 is used as a correction on the data that is measured. Some of the verification points had to be skipped because they showed a unreliable deviance between the measurements of the year 2002 and 2004. This lead to the situation in which only three point could be used to calibrate the measurements of 2004. This is not considered to bring about significant errors in the interpretation of the measurements or models. As can be seen in Appendix the standard deviation of the used points is negligible. The standard deviation of 2.5 cm in the vertical is well within the practical accuracy of the RTK-DGPS rover. The horizontal standard deviation of 0.5 m is much lower than the grid size of 20m that is used to make the maps that are used for the calculations.

Apart from the mentioned RTK-DGPS, a laptop, a printer, and aerial photographs were used as well. The laptop was used to install the base station of the RTK-DGPS. Also, at the end of a measuring day the measured points were loaded in the program *ArcView*. This way it was

possible to determine which areas weren't measured yet and which areas should be measured in greater detail.

The printer could be used to print these maps depicting the measured points. These maps were taken into the field so the laptop could be left behind.

The aerial photographs showed to be of the greatest value to pinpoint the position in the study area and to make all sorts of notes.

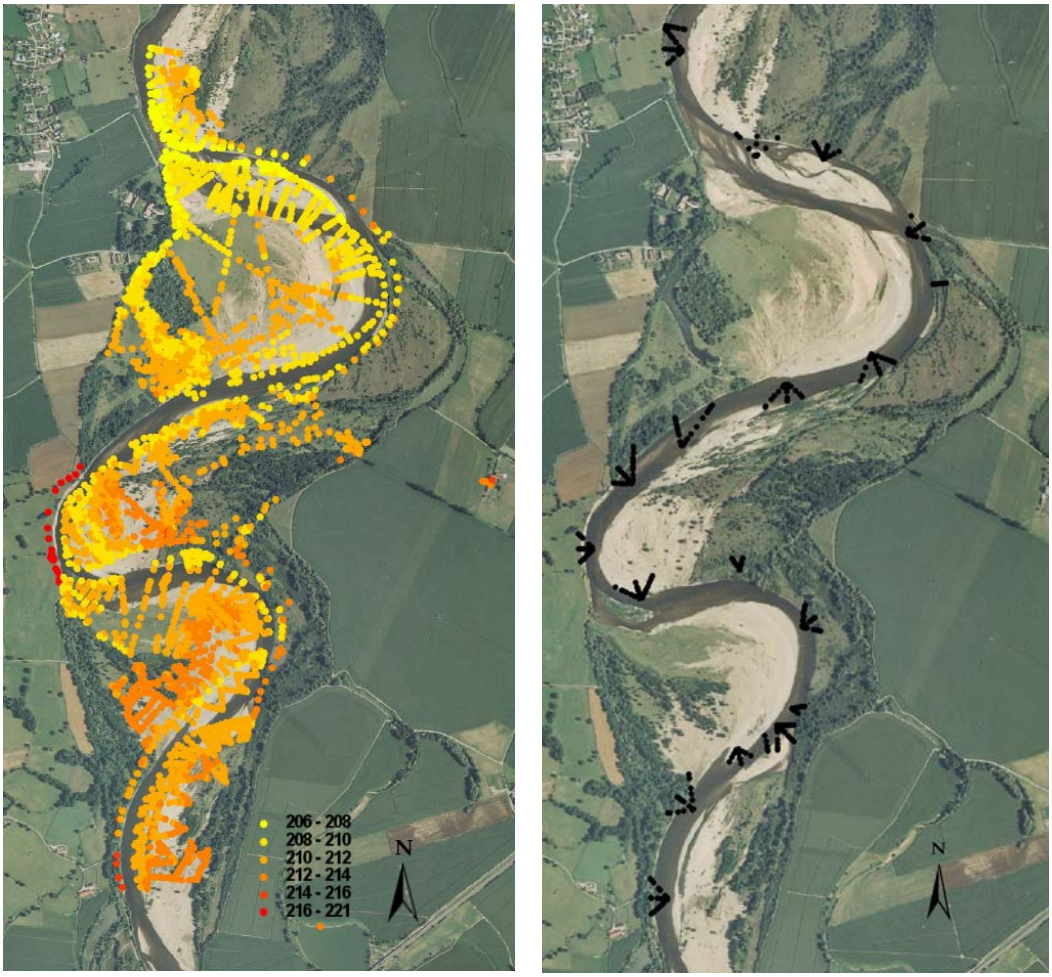

Figure 4-10, Locations measured elevation data, depicted on an aerial photograph of 2000. Left panel: Measurements by RTK-DGPS. Depicted are the z-values (depth), in French coordinate system Lambert 2 (z=0, reference level is the water level in the harbour of Marseille). Right panel: Measurements by Levelling instrument.

Approximately 5500 z_b (x, y) elevation points have been measured in the study area by RTK-DGPS (see Figure 4-10). This was done in about 15 measuring days, of which 1 day was used to install and calibrate the necessary software and equipment (particularly the base station). Except for this day it is possible to carry out the measurements alone. But for the sake of the safety and sanity of the measurer it is advisable to organise some encounters with other persons during a measuring day.

Levelling measurements

The accuracy in the vertical of levelling is about the same as the accuracy of measurements done with the RTK-DGPS. The accuracy in the horizontal plane however is much lower. Depending on the distance from the beacon to the levelling instrument the error can be up to a few metres.

With levelling the distance, height and angle of the measured points with respect to the levelling instrument is known. To know the locations of these points with respect to some arbitrary coordinate system it is necessary to know the coordinates of at least one of the measured points. Preferably the location of the levelling instrument. Within this field survey the location of the levelling instrument was measured with the RTK-DGPS.

Because the levelling method is far more labour-intensive than the RTK-DGPS method it is important to measure in accordance to an efficient measuring plan. Every levelling section consists of one measuring line perpendicular to the streaming direction, one measuring line on an angle of 45° and one on an angle of -45° with the perpendicular line. If possible two adjacent measuring sections should touch at the waterline. Figure 4-11 shows a principal sketch of this method. In this way a relatively dense measuring grid can be accomplished with a minimum effort.

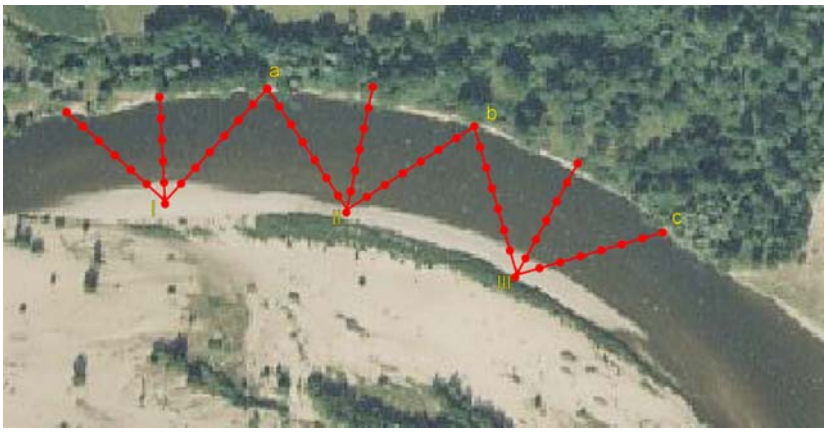

Figure 4-11, Water levelling sections. The levelling instrument is positioned in I, II and III. The dots depict the measured locations. The different levelling sections intersect at a, b and c.

Unfortunately this was not possible within the timeframe available for the field survey. Therefore it was decided to measure at least one levelling section at the apex of every meander bend and one in between every two meander bends. Apart from those sections, also some sections were measured which contained remarkable features.

A problem encountered while measuring in the streambed was the occurrence of very high flow velocities and deep pools. At some places the flow was too strong to stand still, let alone keep the beacon vertical and still. The pools reached water depths of up to 3 m. In these cases guesses were made as accurate as possible and the vertical accuracy here is assumed to be in the order of 0,5 m and the horizontal accuracy somewhere in the neighbourhood of 5 m. Which is poor with respect to levelling points measured in shallower areas with lower stream velocities and extremely poor considering the accuracy of the RTK-DGPS used on the point bars and floodplains.

Approximately 400 z_b (x, y) elevation points have been measured in the study area by levelling (see Figure 4-10). This was done in two days with two teams of 3 surveyons.

Post processing

Within the framework of this thesis it was necessary to process the data from 2003 as well as the data from 2004. Five different computer programs were used to produce the file containing the bed levels that could be used as an input file for the Delft3D model runs and to produce visual presentations of the morphology of the study area, namely: Trimble geomatics Office, ArcView, Microsoft Excel, Surfer, Delft3D-QUICKIN.

As a result of the field survey and data processing of 2003 (Van Bemmel, 2003) a file was available containing the bed level point coordinates in x, y and z. Surfer is then used to interpolate this elevation data onto a 20×20 m grid to create a Digital Elevation Model (DEM).

To construct the needed bathymetry files of 2004, the file containing the bed level point still had to be made. The xyz-file contains points from:

1. Newly measured data;
2. data from previous years in locations where zero erosion and sedimentation was assumed;
3. extra points generated by 'manual' interpolation.

(1) Every day the measured data was read into a computer using the program 'Trimble geomaticss Office'. This data was exported into comma separated text files containing the name and x, y and z-coordinates of the measured data. All these files were pasted into one csv-file.

(2) The xyz-file of the year 2003 was imported in the Software program ArcView. An aerial photograph from 2000 was placed under this xyz-file (see Figure 4-12). This way it was easy to see which points could be considered to have a constant elevation over the years. These points were extracted from the xyz-file and added to the csv-file of 2004.

(3) Although computer programs, like Surfer, are becoming evermore advanced, humans are still superior in recognizing patterns and relations. Therefore 'manual' interpolated data is added to the csv-file. The csv-file of 2004, consisting of the information gathered through step (1) and (2), was loaded into ArcView. With help of the underlying aerial photograph, points lying on the same height lines were defined. These points were for example situated on the waterline or at the edge of a steep slope. These measurements were extracted out of the csv-file and imported in the software program Microsoft Excel. Microsoft Excel was used to add data points by linear interpolation between the points extracted from the csv-file. In this way lines were produced with a very high data density, which were added to the csv-file. This method forces Surfer to 'recognize' patterns in the csv-file.

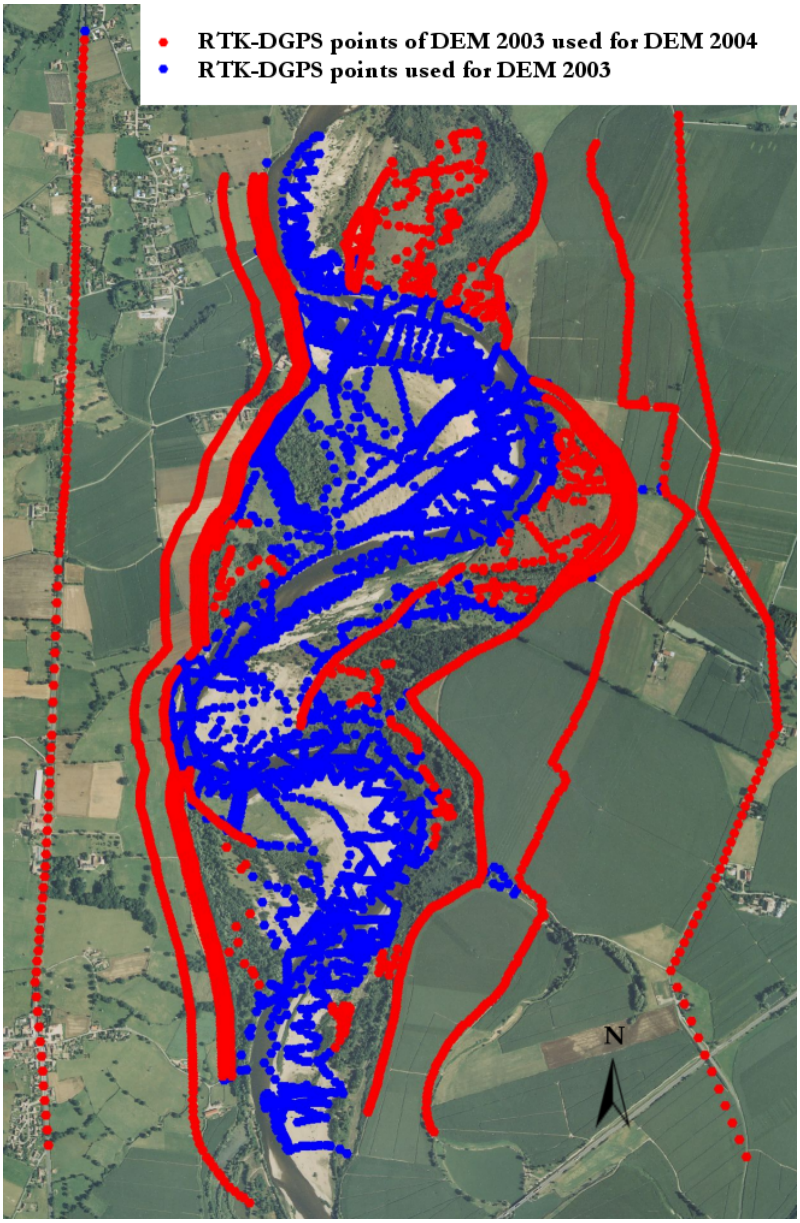

Figure 4-12, RTK-DGPS points of Digital Elevation Model of 2003 used for the Digital Elevation Model of 2004, depicted on an aerial photograph of 2000.

It is always necessary to visually check the computed results and adapt them if necessary. In this case the most disturbing errors concerned (i) the interpolation of points lying at close distance of each other, and (ii) the interpolation of the main channel.

(i) The xyz-file included points lying at a horizontal distance of less than 10 cm from each other while the height differed up to 2 m. This led to irregular lines in the interpolated depth file. In order to eliminate these errors, an option in Surfer was used that skipped all, but one point, of points closer to each other than a certain given distance.

(ii) The erroneous interpolation of the main channel was a direct result of the measurement density that was far lower in the main channel than at the point-bars and floodplains. The interpolation by Surfer resulted in a main channel level that was approximately at point bar level between two levelling sections (see Figure 4-13).

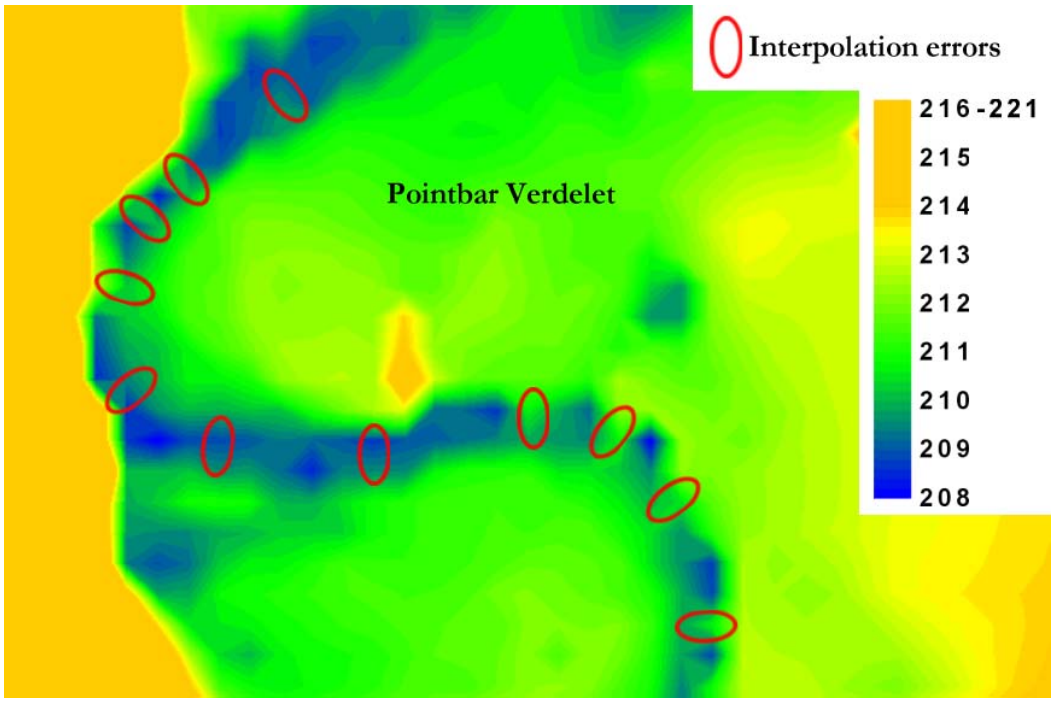

Figure 4-13, Example of interpolation errors in main channel because of low measurement density.

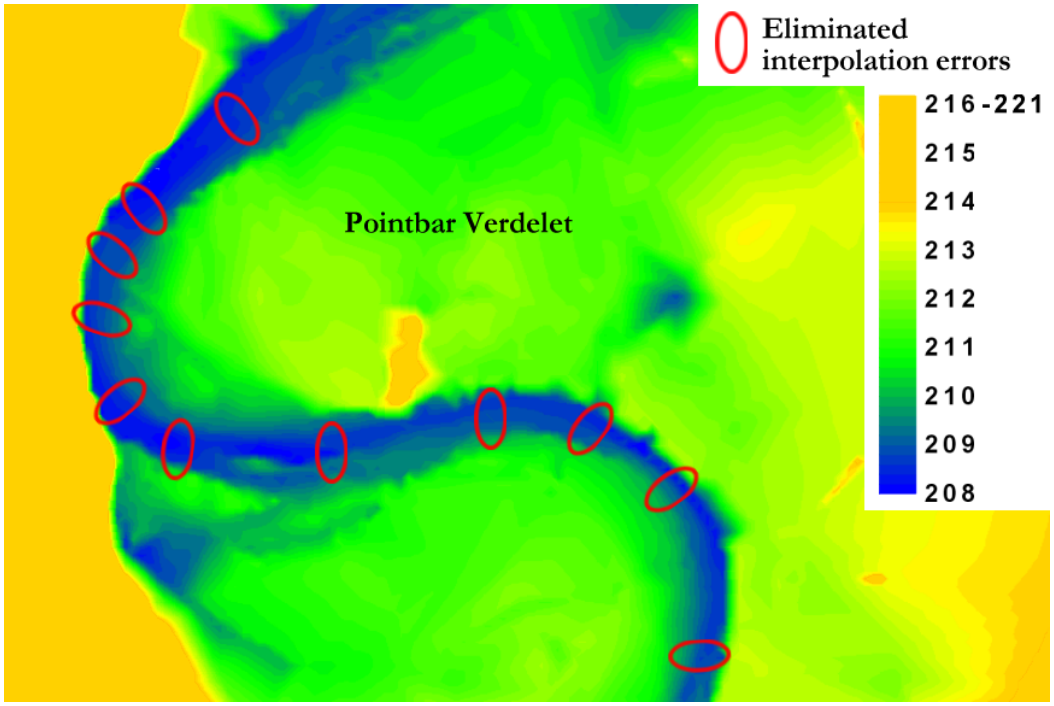

Figure 4-14, Example of eliminated interpolation errors in main channel because of low measurement density.

Generating extra data points in between the levelling sections eliminated this error. Two different methods were used to generate these points. Both methods interpolate extra points in between the measured points. The first method used Microsoft Excel and is very labour intensive. The second method uses the Delft3D-Quickin module. The results are approximately

the same, but the later method is more efficient. The first method was used because the Quickin-approach was not yet available when the first Delft3D simulations were carried out. A detailed description of both methods can be found in Appendix 3.

Another problem with the levelling data from 2003 was the absence of a measured levelling section at the downstream border. Importing the cross-section of 2004 solved this problem. It is assumed this won't yield major errors because the downstream border is fixed by the protected steep shore in the outer bend (see Figure 4-15).

Figure 4-15, Bank protection.

Surfer was also used to create visual presentations of the bathymetry. Furthermore it is capable of performing mathematical operations on the interpolated data, like volume calculations and subtracting one data set from another. This was used to generate difference files that presented the total erosion and sedimentation that occurred between August 2003 and August 2004.

The interpolated data was loaded into Delft3D-Quickin. With this program the data was translated into a dep-file that is used by Delft3D as the input bathymetry for the calculations.

Appendix 2 shows the DEM of 2003 and 2004 as they are created with the computer program Surfer. Appendix 2 also contains a figure that depicts the measured erosion and sedimentation that occurred between August 2003 and August 2004, e.g. the bathymetry of 2003 subtracted from 2004.

4.6 Vegetation distribution and vegetation characteristics

The collected data of 2004 concerning the vegetation is used to update the input files for the flood of 2003. This is possible because the vegetation on most places will not have undergone major changes between July 2003 and July 2004.

Considering the vegetation the aim of the fieldwork was to:

1. Improve the existing vegetation maps by refining the 'floodplain grassland' into 'grazed grassland' and 'natural grassland'.
2. Measure the diameter, height and density of different vegetation types to improve the schematization of the roughness of the plants for the Delft3D model.
3. Determine the location of some trees that showed to have had a considerable impact on the river morphology.

The first aim of the fieldwork could be established by marking the different types of grassland on a map.

With regard to the second point two plots of floodplain grassland (see Figure 4-16), one plot of herbaceous vegetation (see Figure 4-17), one plot of closed floodplain forest (see Figure 4-18) and one shrub (see Figure 4-19) were measured.

Figure 4-16, Floodplain grassland at the front with closed floodplain shrub at the back (July 2004).

Figure 4-17, Herbaceous vegetation at the front, closed floodplain forest at the back (July 2005).

Figure 4-18, Closed floodplain forest (July 2004)

Figure 4-19, Measured shrub (July 2004).

The area measured per vegetation plot should be large enough to give a fair estimate of the mean characteristics of the vegetation type under consideration. The location of these plots was chosen in such a way that they represent the dimensions of the corresponding vegetation types as used on the vegetation maps. However, the diversity and complexity of the vegetation in the study area is enormous (see the photos on the previous pages). Therefore, the measured vegetation can only represent the vegetation types in a crude manner. The locations of the vegetation types are given in Appendix 5, the locations of the measured vegetation plots are given in Appendix 4 along with the measured characteristics.

The floodplain grassland was measured by mowing an area of approximately 1 m^2. The cut off stalks of grass were counted and of a random set of stalks the length and diameter was measured. The number of stalks of which the length and diameter was measured, was determined through calculation of the standard deviation. If subsequent measurements did not significantly decrease the standard deviation the measurements were stopped.

Herbaceous vegetation was measured in much the same way as the grass. The considered area however, was approximately 9.0 m^2. This larger area was necessary because this vegetation type was less evenly covered.

For the forest plots an area of about 225 m^2 was measured. Only the diameter and number of stems in the plot were measured. The height of the trees is of no importance since the measured forests are not submerged during high flow.

Finally, every half meter of a selected shrub, from the roots to the top, the number of branches, their diameter and the perimeter of the whole shrub was measured.

The programs used to process the vegetation data were: ArcView with the Delft3d-GIS extension, DELFT3D-QUICKIN, Microsoft Excel and Textpad.

First of all the schematisation of the plant characteristics was determined. The available values of the different vegetation types for the Nikuradse roughness height (k_N), density (m), diameter (D) and height (k), were updated according to the measured data and gained insights. Table 4-2 shows the retrieved characteristics of the measured vegetation types. Appendix 4 shows the measurements of the different plots in detail. Table 6-3, shows the values used in the Delft3D model of this thesis.

Table 4-2, Measured vegetation types in the Allier study area and their physical properties height, k, diameter, D, density, m, and Nikuradse equivalent roughness height, k_N at 2 m water depth (modified after Baptist, 2005).

Vegetation type	Code	k (m)	D (m)	m (m^{-2})
Closed floodplain forest	GB	10	0.029	0.08
Herbaceous vegetation	R	0.61	0.002	340
Floodplain grassland	G	0.63	0.002	1721

Also the vegetation type maps were updated using the program ArcView. Appendix 5, shows the map as used in the PhD thesis of Baptist (2005), alongside the updated vegetation type map as used for the input for the Delft3D model in this thesis. The map of Baptist (2005) was updated in two ways:

- Removal of the vegetation on those locations where the main channel, as measured in August 2003, was present;
- Changing the vegetation type from floodplain grassland to grazed grassland on point bar Chateau de Lys and Chemilly.

It is assumed that the locations that silted up after the measurements of the study by Van den Bosch (2001) and before the modelled flood of December 2003, are uncovered by vegetation.

Next, the vegetation maps were translated into roughness files for Delft3D. Two distinct file types were created. The first is used for the calculations using the common Nikuradse approach. This file is like a depth file containing k_{nik} values instead of bottom levels. The second set of files is used for the calculation using the approach proposed by Baptist (2005). One file identifies the different vegetation types and their corresponding mD- (density × diameter) and k-values (height). The other file defines for every vegetated gridcell which vegetation type is present. These files were created using ArcView with the Delft3D-GIS extension and Delft3D_Quickin.

The constructed files still contained some errors concerning vegetation present in the main channel. The location of vegetation in the main channel could be found by modelling a discharge of 200 m^3/s. If the model results showed irregular peaks in the bottom shear stress this was usually due to the presence of vegetation. The program Delft3D-Quickin was used to update the k_{nik}-file. The program TextPad was used to rewrite the files for the Reduction factor approach.

Furthermore the pioneer vegetation was replaced with "no vegetation". This was done because this combination of mD and k-values could lead to Chézy-coefficients higher than the Chézy-coefficients of the unvegetated bed. And the Reduction factor approach does not apply to pioneer vegetation since it only holds under the assumption of a relatively high vegetation density and height (Baptist, 2005).

The determination of the dimensions of the shrub was done in more detail than necessary for this thesis. This data is necessary to implement the so called rod-model. The rod-model is a Delft3D application that schematizes vegetation as a certain number of vertical rods per area with a certain diameter and height (see Figure 4-20). This application, however, is only applicable in a 3D simulation and not in a 2DH simulation. The power of the available computers was not enough to make 3D calculations on the river Allier in a convenient way. The duration of one run would take about 20 days.

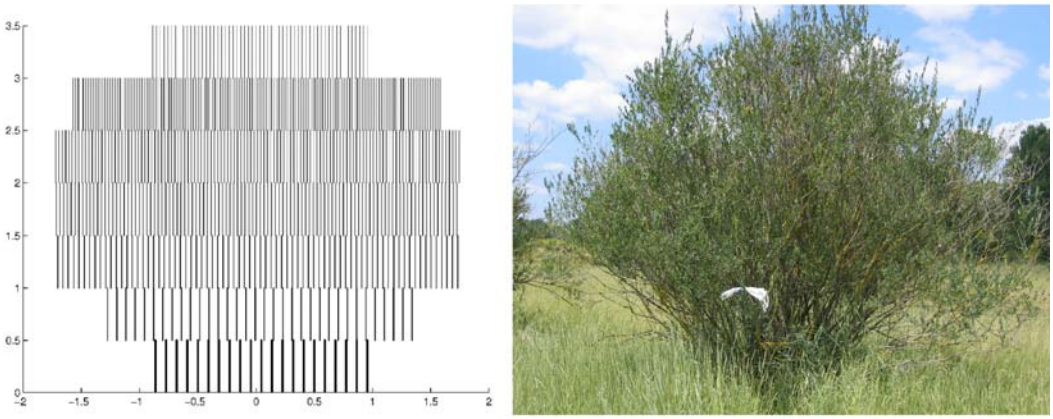

Figure 4-20, Schematisation of measured shrub into vertical rods. The number of rods shown is five times smaller than measured.

5 Discussion of the field survey results

This chapter will discuss the morphological changes the river Allier has undergone due to the flood of December 2003. First it will discuss the celerity of the cliff erosion. The other section will consist of several sediment volume calculations. With this information it is possible to establish theories on the relative importance of the different observed erosion and sedimentation processes. This information is necessary to be able to draw conclusions on the general behaviour of the constructed model.

5.1 Cliff erosion celerity

Based on the RTK-DGPS measurements of the waterline an estimation can be made of the displacement of the cliffs due to the floods that occurred between August 2003 and August 2004. Appendix 2 shows the measured waterlines alongside with the distance between those lines. Because the measurements at the waterline have an higher density and are more reliable than the measurements at the top of the cliff, the measurements at the waterline are used. The reason these measurements are more reliable is, that many of the cliffs are covered with trees that tend to block the signals of the satellites. Beside the propagation of the cliff erosion, the propagation of the sedimentation on the point-bars is given. Because of the much milder slopes these distances are far more dependent on the water level at the time of the measurement than the measurements of the cliffs. These distances should therefore be interpreted with caution. Nevertheless they are shown, because they give at least some indication of the propagation of the point bar. Furthermore the erosion and sedimentation figure, in the same appendix, shows that sedimentation has indeed taken place at the locations were the propagation of the point-bars is estimated.

Most of the measured cliff erosion can be found at point-bar Verdelet. The mean propagation of the cliff is about 30 m and varies from 10 m to even 65 m. Cliff erosion up to 25 m can be found at the upstream end of point bar Chemilly. During the field survey a lot of chute bars were observed right after this cliff. The direction of these bars was North-West, the same direction as the scour holes on that location, see Appendix 6. This suggests a flow approaching

from the upstream border point-bar almost perpendicular to the cliff of point-bar Chemilly. This flow erodes the cliff and transports the sediment onto point-bar Chemilly, where it deposits the carried sediment because the flow is severely slowed down by the forest that is located on the point-bar. The maximum measured erosion of the high cliff between point-bar Chemilly and point-bar Chateau de Lys was 15 m. Almost no cliff erosion occurred on the cliff between point-bar Verdelet and the point-bar at the downstream border. A maximum erosion of 20 m is measured, but the height of this cliff is significantly less than the height of the cliff between point-bar Chemilly and point-bar Chateau de Lys. Therefore the impact of this erosion on the sediment balance and its relative influence on the behaviour of the river Allier is of less importance.

At first sight, it is remarkable that all point-bars seem to have been extended between 20 and 40 m, independent of the cliff erosion. A closer look at the map presenting the measured erosion and sedimentation, however, gives reason to believe that the growth of a point-bar is closely linked to the erosion of the cliff at the other side of the main channel. Point-bar Chemilly has the greatest sedimentation volume, which is accompanied by the largest cliff erosion on the facing point-bar Verdelet. The smallest cliff erosion is found on the downstream point-bar, while the sedimentation at the downstream end of the point-bar Chateau de Lys is almost neglect able in comparison with the sedimentation at the downstream end of point-bar Chemilly and the sedimentation at the part of point-bar Verdelet facing the cliff between point-bar Chemilly and point-bar Chateau de Lys.

A large deviation from the 'usual' erosion and sedimentation pattern is observed in the neighbourhood of the riffle between point-bar Verdelet and point-bar Chateau de Lys. Because the riffle ends at almost the exact location where the cut-off begins, it is assumed that these two phenomena are closely related. It is not clear whether the cut-off is a result of the growth of the riffle or vice versa. The sediment balance that is discussed in the next paragraph suggests, however, that the impact of these morphological features is mostly of a local nature and the amount of sediment involved is relatively small.

5.2 Sediment volume

Appendix 2 shows the measured bathymetry of 2003, 2004, and the erosion and sedimentation that took place between August 2003 and August 2004. The total volume difference, the total sedimentation and the total erosion of different locations are given in Table 5-1, both in absolute values in m^3 and in percentages of the total study area. Appendix 2 also shows the location of the different calculated areas.

Table 5-1, Volume changes between August 2003 and August 2004 based on the field surveys carried out in July and August of 2003 and 2004.

description	total volume change		erosion		sedimentation	
	[m3]	[%]	[m3]	[%]	[m3]	[%]
total study area	-207232	100	702046	100	494815	100
main channel including cliffs	-308320	149	457512	65	149191	30
cut-off Chateau de Lys	22521	-11	28068	4	50589	10
cliff Chateau de Lys	-81976	40	95790	14	13814	3
cliff Verdelet	-136003	66	142613	20	6610	1
cliff downstream border	-52163	25	55962	8	3799	1
cliffs total	**-270142**	***130***	**294365**	***42***	**24223**	**5**
main channel excluding cliffs	**-38178**	**18**	**166120**	**24**	**127942**	**26**
point-bars	**101089**	***-49***	**247030**	**35**	**348119**	***70***

The areas printed in bold constitute together the complete study area. The summation of their total, erosion or sedimentation volumes are the same as the volumes of the total study area.

The table shows that due to the flood the study area lost about 200,000 m^3 of sediment. Which is a bit more than 2/3 of the total volume loss at the cliffs. Sedimentation is clearly dominant on the point-bars. Almost all of the sedimentation that took place in the study area occurred at the point-bars. It should be noted, however, that also a major part of the erosion in the study area occurred at the point-bars.

It is not clear whether the sediment loss out of the study area mainly originated from the cliffs, the main channel or the point-bars. It could be, for example, that most of the sediment from the cliffs is deposited in the main channel and the point-bars, while most of the sediment from the point-bars and main channel is carried out of the study area. There are, however, some indications that suggest that most of the sediment eroded on the point-bars also settles on the point-bars and that the majority of the main channel and cliff erosion surplus is carried out of the study area. If this assumption is made, about 1/3 of the total sedimentation on the point-bars can be attributed to the sediment that eroded from the cliffs and 2/3 from erosion on the point-bars themselves.

Firstly, the sediment transport in the river Allier can be characterised as bed load. The celerity of the bed transport can be estimated with the next equation:

$$c_b = \frac{b}{1-\varepsilon_p}\frac{S}{h} \qquad [m \cdot s^{-1}] \qquad (5\text{-}1)$$

in which

b	factor depending on the power of the flow velocity of used transport formula	[-]
ε_p	porosity of settled sediment	[-]
S	transport capacity in dry volume per unit width	$[m^2 \cdot s^{-1}]$
h	water depth	[m]

If the Meyer-Peter and Müller transport formula is used, the transport capacity is related to the flow velocity till the 3rd power. At high flow the maximum velocity on the point-bars is estimated at 1 m/s while the maximum velocity in the main channel is estimated at 3 m/s. If a

water depth of 1 m is assumed on the point-bars and a water depth of 4 m in the main channel, this leads to a bed celerity on the point-bars that is approximately 8 times smaller than in the main channel. Furthermore the high parts of the point-bars are probably not flooded for more than 4 days. This means that the total distance that will be covered in one flood by the sediment on the point-bars is much lower than the distance that can be covered by the sediment in the main channel. It is however not possible to estimate any absolute figures to underpin if the bed celerity on the point bars is indeed too low to be transported into the main channel. No measurements of the sediment transport capacity or flow velocity are available. And estimations concerning the bed celerity based on the simulation results are thought useless because the sediment transport capacity on the point bars is probably simulated far too low, see Section 8.5.

Secondly, the sediment balance shows that the sedimentation on the point-bars exceeds the erosion, this surplus of sediment must originate from the upstream border, the main channel or the cliffs. All of these sources have in common that the sediment must be carried through the main channel before it can be deposited on the point-bars. But since the sediment diameter of the cliffs is smallest, this sediment is most likely to be transported onto the higher parts of the point-bars where most of the measured sedimentation is found, see Appendix 2.

These assumptions should be verified by measurements in the field or at least be affirmed by convincing model behaviour. Another way to affirm or disconfirm these assumptions, is to estimate the absolute values of the bed celerity on the point-bars and the main channel. If the bed celerity in the main channel is too low to transport the sediment of the cliffs and main channel out of the model area, the sediment must have been deposited somewhere within the model area. In that case it can not be responsible for the sediment loss that is measured. If the bed celerity on the point-bars is high enough to cross the entire point-bar within the time period of 1 flood, than a major part of the eroded sediment off the point-bars was transported into the main channel instead of deposited on the point-bars.

A last remarkable aspect that can be found in Table 5-1 is the surplus of sedimentation at the cut-off at Chateau de Lys. It is possible that this difference in sedimentation and erosion must be attributed to measurement and interpolation errors. This is, however, not very likely, because the measurement density in the abandoned meander bend is quite high, both in the measurements of 2003 and of 2004. Another explanation may be that, due to the cut-off that occurred at the upstream end of this point-bar a connection with the main channel came into existence. This connection led a part of the sediment carrying flow into the abandoned channel, where the sediment transport capacity decreased because of a decrease of the flow velocity. The scour holes, see Appendix 6, indeed indicate a flow direction into the abandoned channel. It is also likely the flow velocity did decrease significantly because of the vegetation in the abandoned channel and because the stream is set up in the bottle neck between the cliff, right under Chateau de Lys, and the forest on this point-bar. Another possible explanation is that there is nothing irregular or remarkable about the sedimentation that occurred in the abandoned channel. Abandoned channels do have the tendency to silt up. It could very well be that the rate at which this takes place is significantly higher than the erosion that took place as a result of the cut-off. In this case the cut-off did not necessarily lead to extra sedimentation in the abandoned channel. The amount of sediment eroded is simply lower than the 'normal' amount of sediment deposited in the abandoned channel.

6 Modelling the river Allier

6.1 Introduction

This chapter presents the Delft3D model of the river Allier. The governing equations, the assumptions as well as the input data and other variables are explained.

As basis for the morphological model, the already available hydrodynamic Delft3D-FLOW model of the river Allier (Van den Bosch, 2003) was used. This model was updated by Baptist (2005) with the data collected by the students Van Bemmel and Van den Broek (Van Bemmel, 2003). Baptist had also altered the classification of the different vegetation types into a more standardized and applicable way. Using the bathymetry of summer 2003 as a starting point, the major flood that occurred between September 2003 and August 2004 was simulated. After which the morphological changes in the model were compared with the morphology of summer 2004. Conclusions were drawn from the difference between the model results and field measurements (residual errors).

This chapter will firstly give a general description of the computational Delft3D modelling package in Section 6.2. The following sections will describe the construction of the model of the river Allier within this package. The different aspects will be discussed in roughly the same order as given in Figure 2-1 and used in the other chapters of this thesis.

Limitations, assumptions and bottlenecks

- Within this M.Sc. thesis the impact of cliff erosion, cohesive sediment, graded sediment and armouring will not be accounted for.
- The limitation concerning the cohesive sediment is considered to be a simplification, which won't yield great erroneous results because the majority of the Allier sediment consists of coarser fractions, such as sand or gravel.
- Most of the bed material is transported as bed load (Van den Berg, 2004). Therefore the suspended load can be neglected.

- Morphological changes occur during floods, and the vegetated area adapts to the new morphology during the dry season (Tsujimoto, 1999). This assumption can be made because the river Allier has an armoured bed. Therefore the morphology is stable during low-water. During high-water the Allier has a dynamic armoured bed (Kleinhans, 2000).
- Only once each year, in July, the bathymetry is measured. So it won't be possible to distinguish between the morphological changes due to the different peak discharges of one year.
- The presence of vegetation is considered static during high flow. Thus, the displacement of vegetation by flow or the burial of vegetation by sedimentation is not taken into account.

6.2 Delft3D model description

The model is constructed with the software Delft3D-FLOW. This is a module of the Delft3D software package developed by WL | Delft Hydraulics. The FLOW module of Delft3D is a multi-dimensional (2D or 3D) hydrodynamic and transport simulation program which calculates non-steady flow and transport phenomena. It aims to model flow phenomena of which the horizontal length and time scales are significantly larger than the vertical scales (WL | Delft Hydraulics, 2003).

The numerical hydrodynamic modelling system Delft3D-FLOW solves the Navier-Stokes equations for an incompressible fluid, under the shallow water[1] and the Boussinesq[2] assumptions. The system of equations consists of the horizontal equations of motion, the continuity equation and the transport equations for conservative constituents.

The 2D depth-averaged equations used in Delft3D are given below:

Continuity equation

$$\frac{\partial \zeta}{\partial t} + \frac{\partial (hu)}{\partial x} + \frac{\partial (hv)}{\partial y} = S \qquad [\text{m} \cdot \text{s}^{-1}] \qquad (6\text{-}1)$$

In which:

ζ	water level above some horizontal plane of reference	[m]
u, v	flow velocity components	[m·s^{-1}]
S	discharge or withdrawal, evaporation, precipitation	[m·s^{-1}]

Horizontal equations of motion

$$\frac{\partial u}{\partial t} + u\frac{\partial u}{\partial x} + v\frac{\partial u}{\partial y} = -g\frac{\partial \zeta}{\partial x} - \frac{g}{C^2}\frac{u^2}{h} + HDT_x \qquad [\text{m} \cdot \text{s}^{-2}] \qquad (6\text{-}2)$$

$$\frac{\partial v}{\partial t} + u\frac{\partial v}{\partial x} + v\frac{\partial v}{\partial y} = -g\frac{\partial \zeta}{\partial y} - \frac{g}{C^2}\frac{v^2}{h} + HDT_y \qquad [\text{m} \cdot \text{s}^{-2}] \qquad (6\text{-}3)$$

[1] the vertical accelerations are small compared to the gravitational acceleration

[2] the density variations are small with respect to the water density itself

In which:

g	acceleration due to gravity	[m ·s^{2}]
C	Chézy-coefficient	[m$^{1/2}$ ·s^{-1}]
h	mean depth of flow	[m]
HDT	a horizontal diffusion term	[m ·s^{-2}]

In Delft3D-FLOW the transport of matter (and heat) is modelled by an advection-diffusion equation.

2DH transport equation, without decay process and with the source and sink terms corresponding with the erosion and sedimentation

$$\frac{\partial hc}{\partial t}+\frac{\partial huc}{\partial x}+\frac{\partial hvc}{\partial y}-h\frac{\partial}{\partial x}\left(\varepsilon_{s,x}\frac{\partial c}{\partial x}\right)-h\frac{\partial}{\partial y}\left(\varepsilon_{s,y}\frac{\partial c}{\partial y}\right)=hS \qquad [\text{kg}\cdot\text{m}^{-2}\cdot\text{s}^{-1}] \qquad (6\text{-}4)$$

In which:

c	mass concentration of sediment	[kg ·m^{-3}]
$\varepsilon_{s,x}$	eddy diffusivity of sediment in x-direction	[m^{2} ·s^{-1}]
$\varepsilon_{s,y}$	eddy diffusivity of sediment in y-direction	[m^{2} ·s^{-1}]
S	source and sink terms per unit area	[kg ·m^{-3} ·s^{-1}]

In this thesis this equation is only applied in the cases that use the Van Rijn (1984) transport formula, because that is the only formula with suspended sediment.

The secondary flow (spiral motion) is of great importance for the calculation of changes of the river bed in morphological models. In a 3D model the secondary flow is resolved on the vertical grid, but in 2D depth-averaged simulations the secondary flow has to be determined indirectly using a secondary flow model. Within Delft3D this leads to an extension to the depth-averaged shallow water equations.

For an elaborate description of the Delft3D-FLOW module, one is referred to the Delft3D-FLOW user manual (WL | Delft Hydraulics, 2003).

6.3 Computational grid and time frame

For this study a flood of 15 days was simulated, while the preceding studies by Van den Bosch (2003) and Baptist (2005) modelled a stationary flow of 858 m^{3}/s was modelled. The models by Van de Bosch (2003) and Baptist (2005) reached a steady flow situation after approximately 4 modelled hours. This means that the computation time to simulate the entire flood of 15 days would increase with a factor of approximately 90 (=15 days/4 hours), if the same grid and time-step would be used.

To reduce the computation time the 10 m rectangular grid of the former models by Van den Bosch (2003) and Baptist (2005) was enlarged to a 20m rectangular grid.`

Because of the large computation time of 3D simulations all model runs are 2DH simulations.

Although the computational scheme in Delft3D-FLOW is unconditionally stable, the numerical time step for computations should be chosen in such a way that movement of water in the model does not become unstable. The time step used was 0.1 minutes. This time step was decided upon by comparing some model runs with different time steps. A time step smaller than

0.1 minutes did not show any noticeable differences with the 0.1 minutes simulation. A first estimate of the time step was made with an option of Delft3D-QUICKPLOT that gives indicative values of the useable time step.

One is referred to the Delft3D-FLOW manual (WL | Delft Hydraulics, 2003) for more information on time step limitations.

6.4 Boundaries

6.4.1 Upstream boundary

Hydraulic boundary

The flood of December 2003, with a peak discharge of 1360 m^3/s, is modelled. This flood has a return period of 25 years (see Appendix 1). The measured discharges were used as upstream inflow. It was assumed that no morphological changes occur at a discharge of less than 200 m^3/s. Therefore only that part of the flood was modelled that had a discharge of more than 200 m^3/s. The two other smaller floods that occurred between the bathymetry measurements of 2003 and 2004 (see Chapter 4.2) have not been simulated, since it is assumed that the major part of the morphological changes took place during the highest flood. The next graphs (see Figure 6-1) show the measured discharge of this flood together with the input used with the MORFAC scale factor of 8, note the timescale. Appendix , 'Parameters of Delft3D model' contains tables that depict the used data.

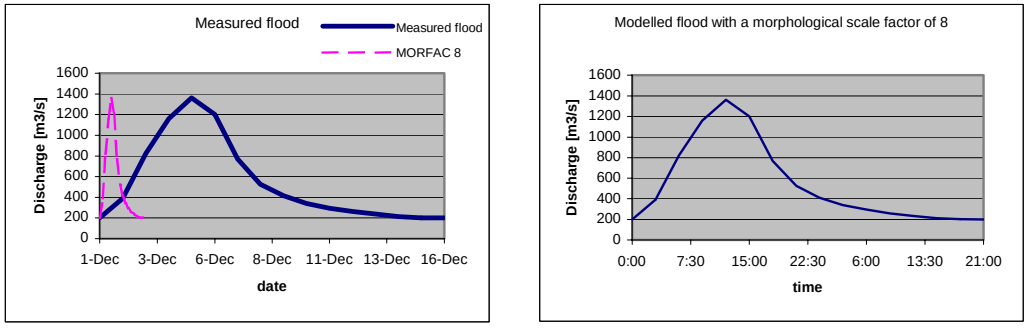

Figure 6-1, Measured flood and modelled flood as input at upstream boundary.

Because of an unfortunate mistake with the construction of the discharge file for Delft3D, the discharges of Châtel-de-Neuvre were used instead of the discharges measured at Moulins, which are considered more reliable (see Chapter 3.2). This yields however no significant errors for this thesis.

Morphologic boundary

The bed load transport vector at open boundaries is set perpendicular to the boundary and equal in magnitude to the component in this direction at the adjacent internal water level point.

6.4.2 Downstream boundary

Hydraulic boundary

In this study an adapted version of the Q-h relation by Van den Bosch (2003) is used for the downstream boundary, whose Q-h relation was in turn based on research done by Kapinga (2003).

Figure 6-2 shows both the Q-h relation of Van den Bosch (2003) and the adapted Q-h relation used in this thesis. Appendix 9 contains the corresponding tables. An explanation about the way in which was decided upon the adaptations can be found in Section 7.3.1.

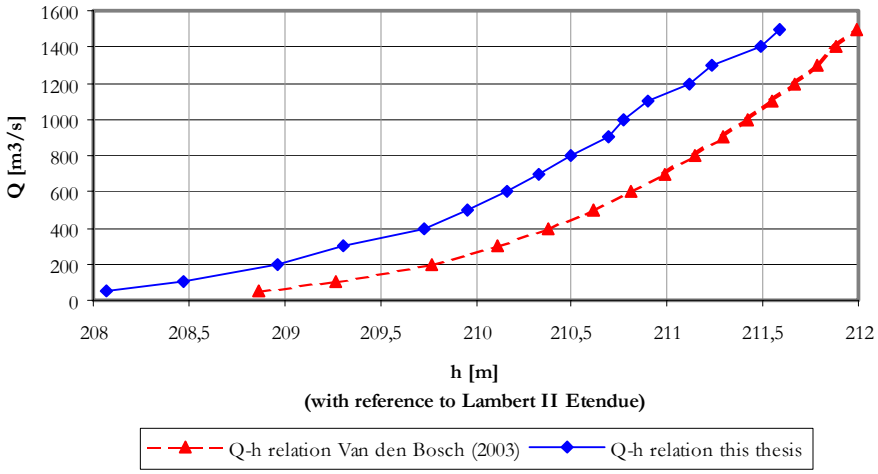

Figure 6-2, Q-h relations of different studies on the river Allier.

6.5 Bed roughness

Delft3D recalculates the used roughness values into Chézy friction coefficients. The Nikuradse-values are translated into Chézy-values using the White-Colebrook formula, see equation (2-2), the Manning-values are translated using the Manning formula, see equation (6-5).

$$C = \frac{1}{n} R^{1/6} \qquad [m^{1/2} \cdot s^{-1}] \qquad (6\text{-}5)$$

Thus the only implication of using Nikuradse-values instead of Chézy-coefficients is that the bed roughness decreases with increasing water depth if Nikuradse or Manning values are used, while the roughness is independent of the water depth if Chézy coefficients are used. From the White-Colebrook formula it can be seen that in the situation of $k_n > 12 \cdot h$, extremely low, sometimes even negative[1] values can be found. This can happen, for example, in the case of high trees with small water depths.

[1] In Delft3D this problem is 'solved' by using $C = 18 \log\left(1 + \frac{12R}{k_N}\right)$.

The bed induced roughness was simulated using three different coefficients (for 2DH) of Delft3D, namely: Chézy-coefficient, Manning roughness factor and the Nikuradse roughness height. In all cases the bed roughness was considered uniform over the whole area. Table 6-1 presents the chosen values. The Nikuradse and Manning values were calculated with a water depth of 2 m and a Chézy coefficient based on experience with the models of Baptist (2005).

Table 6-1, Bed induced roughness values with a waterdepth of 2m.

formulation		value	
Chézy	C	50	$[m^{1/2}/s]$
Nikuradse	k_n	0.04	[m]
Manning	n	0.026	$[s/m^{1/3}]$

6.6 Topography

Two different depth files were used as input for the model. One file corresponded with the actual situation before the flood of December 2003. The other file was adjusted in an effort to simulate the effects of the cut-off at point-bar Chateau de Lys. Hereto the bed level in the depth file was lowered at the cut-off location (see Appendix 2, 'Topography study area').

6.7 Sediment transport

6.7.1 Sediment diameter

In the model, the sediment is considered uniform over the whole area, d_{50} = 8 mm and d_{90} = 35 mm. Unfortunately it is not (yet) possible to define several bed load sediment fractions in Delft3D-FLOW in combination with the used Reduction factor approach vegetation module. The following sediment diameters are used in the sensitivity analysis.

Table 6-2, Sediment diameters used in the simulations.

Name	D50 [mm]	D90 [mm]	Comments
top layer	16	41	armored bed (Wilbers, 1997 and Cohen, 1998)
subsoil	8	35	armored bed (Wilbers, 1997 and Cohen, 1998)
point bar sand	1	1.5	fine material found on some places on the point bars

6.7.2 Transport formula

In this thesis three different transport formulas have been implemented:

- Meyer-Peter and Müller formula (1948);
- Engelund-Hansen formula (1967);
- Van Rijn (1984).

Since all these formulas are at least in part empirical, the applicability of the different formulas tends to differ widely from case to case. The three formulas were used to determine which formula is most appropriate for the studied part of the river Allier.

Delft3D simulates the sediment either as bed load or as suspended load. In the case of a total load transport formula (e.g. Engelund and Hansen) the sediment is modelled as bed load. Only the simulations using the Van Rijn transport formula include both the suspended and the bed load transport. In this case both the suspended and the bedload fraction consist of the same diameter.

6.7.3 Morphological scale factor

One of the complications inherent in carrying out morphological projections on the basis of hydrodynamic flows is that morphological developments take place on a time scale several times larger than typical flow changes. One technique for approaching this problem is to use a "morphological time scale factor" (MORFAC) whereby the speed of the changes in the morphology is scaled up. This method to scale up the morphological changes is used to reduce calculation times. The MORFAC is increased to the rate at which the morphological changes begin to have a significant impact on the hydrodynamic flows.

The implementation of the morphological time scale factor is achieved by simply multiplying the erosion and deposition by the MORFAC-factor, at each computational time-step. This allows accelerated bed-level changes to be incorporated dynamically into the hydrodynamic flow calculations.

Within this thesis a MORFAC of 8 showed to be possible. Thus the modelled flood of 15 actual days could be reduced to a flood of 2700 model hours (1.875 days).

6.7.4 Non-erodable layer

The steep cliff at the downstream border is modelled as a non-erodable layer. This is because this bank is very heavily protected with heavy debris deposited by the local farmers (see Figure 4-15).

6.8 Vegetation

The modelling of the influence of vegetation on the fluvial processes knows some difficult problems. The height, density and diameter of the vegetation stems are necessary input parameters for many different predictors of the roughness of the vegetation. This data is very labour-intensive to obtain (see Chapter 4.6, 'Vegetation distribution and vegetation characteristics'). Another aspect that has shown to be of some importance is the orientation and dispersion of the vegetation (Van Velzen et al., 1999). It is not possible to assign a single computational grid cell to every single tree or bush. Therefore the orientation of the vegetation with respect to the flow is lost if the vegetation characteristics are averaged over the whole grid cell (see Figure 6-3). The same study showed, however, that this averaging method yields reliable results. Therefore it is assumed that the orientation and dispersion of the vegetation can be neglected on scales smaller than the used grid-size (20m).

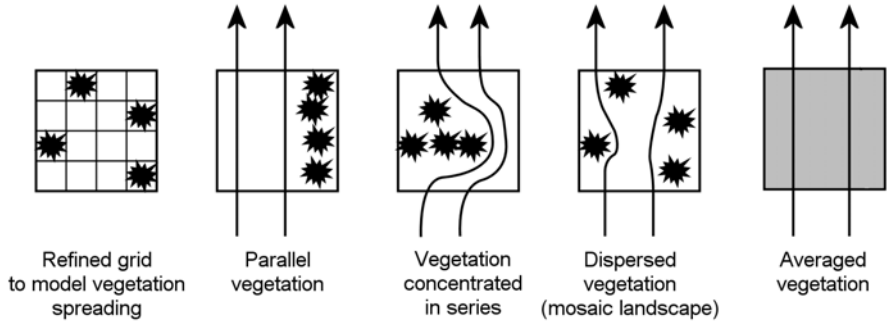

Figure 6-3, Grid refinement to account for the spatial arrangement of the vegetation. Flow in an area with parallel, concentrated and dispersed vegetation.

Another problem that arises because of the coarse grid is the influence of single trees. As shown in Figure 6-4 the impact of isolated trees can be enormous. This unpredictable behaviour is completely eradicated in computer simulations, because the computational grid is too coarse to account for these phenomena's.

The flexibility of vegetation gives rise to even other complex behaviour. Grass and weeds have the tendency to lie down when submerged by flowing water, thus reducing the height and roughness of the vegetation. The movement of bushes, small trees and branches will probably have significant influence on the energy dissipation and thus on the energy gradient, the flow and the morphodynamics.

Figure 6-4, Impact of trees on the morphodynamics of the river Allier (Maronier, July 2004).

6.8.1 Vegetation models

To simulate the influence of the vegetation on flow and morphodynamics two different models were used to calculate the roughness and the bottom shear stress:

- Increased Nikuradse (1933) roughness height;
- Reduction factor approach (Baptist, 2005).

The Nikuradse method uses an Increased Nikuradse (1933) roughness height to simulate the vegetation, k_n is taken more or less equal to the height of the vegetation. Thus the k_n value depends on the vegetation that is present (see Table 6-3). This method is used as a base case that is compared with the Reduction factor approach.

In comparison with the Nikuradse schematization the Reduction factor approach calculates a different value of the total roughness, the bed roughness and the bed shear stress (see Chapter 2.4). The formulation of the Reduction factor approach for the bed shear stress has been slightly adapted by Jagers (see Appendix 10) to be implemented in Delft3D. The big advantage is that both, the submerged and non-submerged formulations for total shear stress (bed + vegetation) can be written as:

$$\tau_{bv} = \frac{\rho g}{C_b'^2}\bar{u}^2 \qquad [\mathrm{N \cdot m^2}] \qquad (6\text{-}6)$$

in which:

C'_b effective Chézy-based roughness $[\mathrm{m^{1/2} \cdot s^{-1}}]$

In the case of non-submerged vegetation C'_b equals C_b and $\bar{u}$ equals u_c. For submerged vegetation the equations for C'_b is:

$$C_b' = C_b + \frac{\sqrt{g}}{\kappa}\sqrt{1+\frac{C_D m D k C_b^2}{2g}}\ln\left(\frac{h}{k}\right) \qquad (6\text{-}7)$$

Which gives us C'$_b$ directly in terms of the vegetation characteristics and the bed roughness C$_b$.

It should be noted that Delft3D does not use the bed shear stress to calculate the water movement or sediment transport. It is an output variable that is a function of the depth-averaged velocity, the bed roughness and a factor to account for the influence of the vegetation characteristics.

For the calculation of the water movement the total roughness, C$_r$ is used, as given by equation (2-39). For the calculation of the sediment transport capacity, C'$_b$ is applied, as given by equation (6-7). The value of this roughness parameter is higher than C$_r$, and thus the flow resistance is lower. In this way the major errors of the Increased Nikuradse roughness height method are avoided. Being a wrong assumption of the vertical flow profile and a too high Nikuradse-roughness length leading to a too high bed shear stress.

In case of an Increased Nikuradse roughness height, to account for the vegetation resistance, the resulting C would become much too low (and the resistance to high), leading to erroneous results.

6.8.2 Vegetation parameters

The height, k, diameter, D, density, m, and Nikuradse equivalent roughness height, k$_N$ at 2 m water depth of the different vegetation types are depicted in table Table 6-3. The distribution of the vegetation types is shown in Appendix 5.

Table 6-3, Vegetation types in the Allier study area and their physical properties height, k, diameter, D, density, m, and Nikuradse equivalent roughness height, k$_N$ at 2 m water depth (modified after Baptist, 2005).

Vegetation type	Code	k (m)	D (m)	m (m^{-2})	k$_N$ (m)
Production forest	CB	10	0.042	2	6.5
Closed floodplain forest	GB	10	0.042	1.2	4.6
Open floodplain forest	OB	10	0.042	0.4	1.8
Closed floodplain shrub	GS	5	0.01	10.2	7.3
Open floodplain shrub	OS	5	0.01	3.4	3.4
Herbaceous vegetation	R	0.5	0.005	400	2.3
Floodplain grassland	G	0.2	0.003	3000	1.1
Production grassland	CG	0.1	0.003	4000	0.8
Grazed grassland	MG	0.2	0.0015	3000	0.83
Pioneer vegetation	P	0.1	0.003	50	0.15
Bare	K	-	-	-	0.04

6.9 Remaining parameters

This Section sums up the parameters that have not yet been mentioned.

6.9.1 Eddy viscosity and diffusivity

The horizontal eddy viscosity and diffusivity were determined with the following rule of thumb:

$$0.1\times\left(0.1\times\text{grid length}\right)\times\left(0.1\times\text{average velocity}\right) \tag{6-8}$$

With a grid length of 20 m and an average velocity of approximately 2 m/s this leads to an eddy viscosity and diffusivity of 0.04 m^2/s.

6.9.2 Spiral motion

In a 3D model the secondary flow (spiral motion) is resolved on the vertical grid, but in 2D depth-averaged simulations the secondary flow has to be determined indirectly using a secondary flow model.

The following factors are necessary input for the secondary flow model used in this thesis.

Table 6-4, Parameters for the inclusion of secondary flow.

Betac	0.5
Equili	#N#
Espir	1.0

Betac: Fraction of the shear stress due to secondary flow taken into account in the momentum equation (Betac=0 means no inclusion).

Equili: The secondary flow may be computed from a local equilibrium approach (Equili=#Y#) or from an advection/diffusion equation (Equili=#N#).

Espir: The factor with which the spiral intensity is multiplied. This factor only influences the morphodynamic part of the calculations. It is not used for the hydrodynamics.

6.9.3 Bed slope effect

Within Delft3D one can choose from two different methods to adjust the bed-load transport for bed-slope effects. The Bagnold (1966) and the Koch & Flokstra (1980) approach. The Bagnold method has two factors that can be set, 'Alfabs' and 'Alfabn'. These are multiplication factors for the transport of sediment. The first is for a bed slope in the same direction as the flow velocity in the bottom layer. The second for a bed slope normal to the flow velocity in the bottom layer.

In this thesis both the formulation of Bagnold and of Koch & Flokstra have been used. Usually the formulation by Koch & Flokstra is most applicable to rivers. The factors used in the Bagnold equation however could be used to eradicate some of the unrealistic model results. Therefore some model runs used the Bagnold formulation.

The following table presents the values used for the different parameters of the two formulations.

Table 6-5, Parameters for the inclusion of the bed slope effect.

	Koch & Flokstra	**Bagnold**
Alfabs	-	1
Alfabn	-	1, 10 or 20
Ashld	1.6	-
Bshld	0.5	-

Alfabs: Factor used in Bagnold formulation. Longitudinal bed gradient factor for bed load transport.

Alfabn: Factor used in Bagnold formulation. Transversal bed gradient factor for bed load transport.

Ashld: Factor used in the Koch & Flokstra formulation. Often the value is estimated with the formula $9\times\left(\frac{D}{h}\right)^{0.3}$. This parameter can also be used as a calibration parameter.

Bshld: Is a power in the formula of Koch & Flokstra.

7 Sensitivity analysis

7.1 Introduction

The construction of a good model consists of the model set up, sensitivity analysis, calibration and validation. Calibration inhibits those activities to obtain a previously determined degree of similarity between model and measurements in the field by the (systematic) change of uncertain factors (often parameters), followed by analysis of the residual errors. The validation is defined by the comparison of model output with an independent (i.e. not yet used in calibration) set of measuring data in order to determine whether the model is 'good' (or whether the concept is good, whether the model is able to reproduce the past with the required accuracy and whether the model is suitable to answer all the questions). After the calibration and validation, several scenarios can be simulated and studied. Within this M.Sc. thesis this was not possible. The water levels and flow velocities during high flow are unknown but are necessary to calibrate the model. To validate the model independent sets of measuring data must be available and at the moment not enough years of data are available to create these sets. And the general behaviour of the model showed too large residual errors to render the simulation and comparison of different scenarios useful. Therefore the sensitivity analysis is not followed with sections on the calibration, validation and scenarios of the model, but concluded with a section in which the global behaviour of the model is discussed. In this way recommendations can be made with respect to further research, but first the variables on which the models behaviour was specifically tested, are presented. In the subsequent sections the sensitivity analysis is discussed. The investigated aspects are organised according to Figure 2-1.

Flow

- Q-h relation downstream border;
- spiral motion;
- bed roughness coefficient;
- bed roughness magnitude.

Sediment transport

- Sediment transport formulae;
- sediment diameter;
- bed slope effect;
- erosion of dry cells.

River morphology

- Non-erodable layers;
- Cut-off at point-bar Chateau de Lys.

Vegetation

- Vegetation model;
- vegetation density and vegetation diameter;
- individual trees.

The sensitivity analysis is carried out on formulae, measurable parameters and calibration parameters. Different formulae were investigated for three variables: total roughness, bed shear stress and sediment transport. The first two are discussed in the Section 'Vegetation model', the last one is discussed in the Section 'Sediment transport formulae'. Another formula that was investigated, was the Q-h relation. Six parameters that can be measured directly in the field were considered: the sediment diameter, non-erodable layers, the cut-off at point-bar Chateau de Lys, the location of individual trees, the vegetation density and the vegetation diameter. For the bed roughness different coefficients have been developed (see Chapter 2.2 and 6.5). In theory these coefficients can be calculated with formula using actual physical parameters, like grain size, and variables, like water depth. In the field of practical river engineering, however, the bed roughness is often used as a calibration parameter. In this thesis the bed roughness magnitude and the used coefficient were also considered calibration parameters. Three other calibration parameters are: spiral motion, bed slope effect and the erosion of dry cells. These parameters have no direct physical meaning but are used in Delft3D to calibrate different dependent variables in the model.

All graphs and maps referred to in this chapter can be found in Appendix 7. The figures are labelled with the same names as the corresponding sections. The label also contains two numbers. The last number indicates the number of pages in the appendix that belong to the section, the first number indicates the serial number of the figure within this section. The maps and graphs that are created on basis of the field survey measurements and the simulation that is used as the base case, are given under the Figures of section 7.7.

7.2 Investigated dependent variables

To evaluate the performance of the model five dependent variables were used in particular:

- Flow velocity;
- flow direction;
- water level;
- bed shear stress;
- morphology.

The first four parameters concern the hydrodynamic behaviour of the model, while the last one has to do with the morphological performance.

It should be noted that none of the mentioned parameters has been measured during high flow. The magnitude and direction of the different quantities is based on assumptions and expert knowledge and is not known in absolute quantitative terms. Therefore the performance of the model will be judged by the general physical behaviour, instead of quantitative correctness at specific locations. What this means for every single dependent variable will be explained in the following Sections.

7.2.1 Flow velocity

The low flow situation is simulated by a constant discharge over the upstream border of 50 m^3/s. This is the lowest flow condition for which the Q-h relation of the downstream border is calibrated. At this discharge the depth averaged flow velocity can be assumed to reach maximum values of 2 m/s. This approximation is based on research done by Neessen (2000) and Driesprong (2001) who measured local depth averaged velocities of up to 1.7 m/s during a discharge of approximately 30 m^3/s. Both of the discharges remain within the low waterbed. Therefore the width of the channel may be considered equal in both cases. In the equilibrium state the discharge is roughly proportional to the third power of the stream velocity, because of:

$$h = \frac{u^2}{C^2 i} \quad \text{(Chézy, see Equation (2-1))} \qquad [m]$$

and

$$h = \frac{Q}{bu} \quad \text{(continuity equation)} \qquad [m]$$

which leads to:

$$u^3 = \frac{C^2 i}{b} Q \qquad [m^3 \cdot s^{-3}] \qquad (7\text{-}1)$$

which leads to:

$$\frac{u_1^{\,3}}{u_2^{\,3}} = \frac{Q_1}{Q_2} \qquad [-] \qquad (7\text{-}2)$$

This means that the maximum depth averaged flow velocity during low flow (50 m^3/s) can be approximated by $(50/30)^{1/3} \cdot 1{,}7 = 2{,}0$ m/s.

The flow velocities during high flow have not been measured. The following assumptions are made concerning the flow velocities: in the main channel it can reach up to 3 m/s, on the bare parts of the point bar it does not exceed 2 m/s and in the vegetated parts it stays below 1 m/s. These values are based on rough predictions using the Chézy formula (2-1); see Table 7-1. The Chézy value of the bare parts of the point bars is taken equal to the bed roughness coefficient in the main channel. The Chézy value of the vegetated parts is approximated by using the White-Colebrook formula (2-2) and a k_n value based on the dominant vegetation ($k_n \approx 3.5$ m). The water depth is estimated by field observations and model results. The energy gradient (i), is calculated by subtracting the measured height of the waterline at low flow downstream from the one upstream. The flow length is taken somewhere in between the length of the low waterbed and the length in a straight line from the upstream border to the downstream border.

Table 7-1, estimation of maximum velocities during high discharges in the river Allier.

	C [$m^{1/2}$ s^{-1}]	**h** [m]	**i** [-]	**U** [m s^{-1}]
main channel	*50*	*5*	*8 ·10⁻⁴*	3
unvegetated point bar	*50*	*2.5*	*8 ·10⁻⁴*	2
vegetated point bar	*20*	*2*	*8 ·10⁻⁴*	1

The highest velocities will be at the outer bends near steep slopes. Especially if the main channel is narrow. The lowest flow velocities will be on the point-bars in densely vegetated areas. At low flow the lowest flow velocities will be at the inner bends of those parts of the river where the flow-conveying cross-sectional area is large.

Regarding the variation of the flow velocities at the floodplain, the highest local flow velocities of the point-bar are likely to occur at the upstream part of the point-bar. At this point the water flows from the main channel onto the floodplain. The coarsest sediment can be found here, and the deepest scour holes are also positioned at the upstream part of the point-bar. Calculations confirm this theory (Kapinga, 2003, p. 90).

7.2.2 Flow direction

A fair estimate of the flow direction on the point-bars during high flow has been made using scour holes (see Section 4.4). Appendix 6 presents an aerial photograph of the study area on which the direction and location of the scour holes is projected.

7.2.3 Water depth

The water depth should not overtop the cliffs located on the west of the study area because no signs of flooding, as a result of the flood of December 2003, were found there. The maximum simulated water depth on the point bars should be about 2.5 m, since this is the maximum observed height of a flood mark on the point bars.

7.2.4 Bed shear stress

A physical convincing range for the bed shear stress was not formulated. Sedimentation or erosion is expected if the model computes a strong change of the bed shear stress over a relatively short distance. If the measured topography shows no such morphological changes the computed bed shear stress gradient is highly questionable.

7.2.5 River topography

The topography of the study area is the only variable that has been measured. Therefore the bathymetry of August 2003 and August 2004 are quite precisely known. For a gravel dominated river with a armoured bed, most of the morphological changes occur during high discharges. Between August 2003 and August 2004, three floods have occurred in the river Allier. It is assumed that the influence of the two smaller floods on the morphodynamics can be neglected with respect to the influence of the larger flood of December 2003. Because of this assumption the bathymetry of August 2004 can be considered almost the same as the bathymetry right after the flood of December 2003. Therefore the measured bathymetry of 2004 is compared with the bathymetry as calculated by the model after the flood of 2003.

It is not possible to validate the morphological changes during high flow since no measurements were done during this period.

7.3 Flow

7.3.1 Q-h relation at the downstream boundary

As stated in Section 6.4.2, the Q-h relation used by Van den Bosch (2003) was adapted to yield a physically more convincing water depth, flow velocity magnitude and flow velocity distribution. This analysis was carried out for a discharge of 50 m^3/s and for every 100 m^3/s more, ranging from 100 m^3/s till 1500 m^3/s. Every discharge step was run with the corresponding downstream water level of the Q-h relation of Van den Bosch (2003), a run with a water level of 0.5 m below, and at last a run with a water level of 1.0 m below the Van den Bosch (2003) water level. For every discharge and Q-h relation, maps were created presenting the flow velocity and maps presenting the water depth. Appendix 7 contains a page with a map for all three Q-h relations at a discharge of 1000 m^3/s.

Considering the requirements for a physically convincing flow velocity and water depth a decision was made on the most reliable downstream water level for every modelled discharge. Which Q-h relation was considered physically convincing, was decided upon using the flow velocity and water depth. The absolute velocity was compared with the estimated values according to Section 7.1. Furthermore, the Q-h relation was tested on the agreement of velocities and water depths between the down stream end of the model and the rest of the model. Based on these simulations a new Q-h relation was constructed. The resulting Q-h relation is given in Figure 6-2, of Section 6.4.2, and in Appendix 7. Appendix 7 also contains a map presenting the

flow velocity at a discharge of 50 m^3/s of both the Q-h relation of Van den Bosch (2003) and the newly constructed Q-h relation. Although the original Van den Bosch (2003) Q-h relation yields a slightly better maximum velocity, the simulated velocity and depth distribution is worse.

The maps that were created to construct a more reliable Q-h relation also showed that the influence of the downstream border does not reach much further upstream than the apex of the meander around point-bar Chateau de Lys, see Appendix 7, 'Q-h relationship at the downstream boundary', 1/3, 2/3 and 3/3. This area, however, already covers approximately 25% of the total study area. It is therefore strongly advised to construct a more reliable Q-h relation based on field measurements.

7.3.2 Spiral motion

The influence of the spiral flow calculated by Delft3D is studied by enlarging the secondary flow intensity. To that end, simulations were run with a spiral intensity (Espir) of 0, 1, 5 and 10.

None of these showed any significant improvements. The simulation with Espir = 10 even showed highly unlikely behaviour with the core of the channel erosion bouncing from one side of the channel to the other. Both the simulations with a spiral flow intensity above 1 show instability lines of erosion and sedimentation. Especially at the boundaries and point-bar Verdelet. See Figure 1/2 of this section and Figure 1/10 of Section 8.5.

Next, the grid size was refined to 10 m, see Figure 2/2. This simulation led to a flow velocity distribution of which the core was more concentrated towards the outer banks. Also the sedimentation on the point-bars increased. On the other hand, the erosion of the main channel also increased. Nevertheless it can be said that a refinement of the grid-size from 20 to 10 m, has a strong and positive impact on the flow distribution over the width of the channel.

It is thought very important to simulate the behaviour of the spiral motion in a correct way. As explained in section 2.3 the secondary flow is of great importance in formation of the point-bars and the erosion of the outer banks. That the secondary flow seems to be underestimated in the models could be one of the reasons why the modelled morphological changes on the point-bar are also underestimated.

7.3.3 Bed roughness coefficient

It was not possible to determine which bed roughness formulation performs best in the Allier case. The differences in model outcomes were too small.

It showed that the Manning formulation and the White-Colebrook formulation differ less from each other than from the approach with a constant Chézy coefficient. This can be easily explained with the following graph (see Figure 7-1), that shows the impact of the water depth on the Chézy value calculated by Delft3D and used for its computations. It shows that both formulations yield approximately the same Chézy values for all waterdepths, while the Chézy method uses a Chézy value of 50 $m^{1/2} \cdot s^{-1}$ independent of the waterdepth.

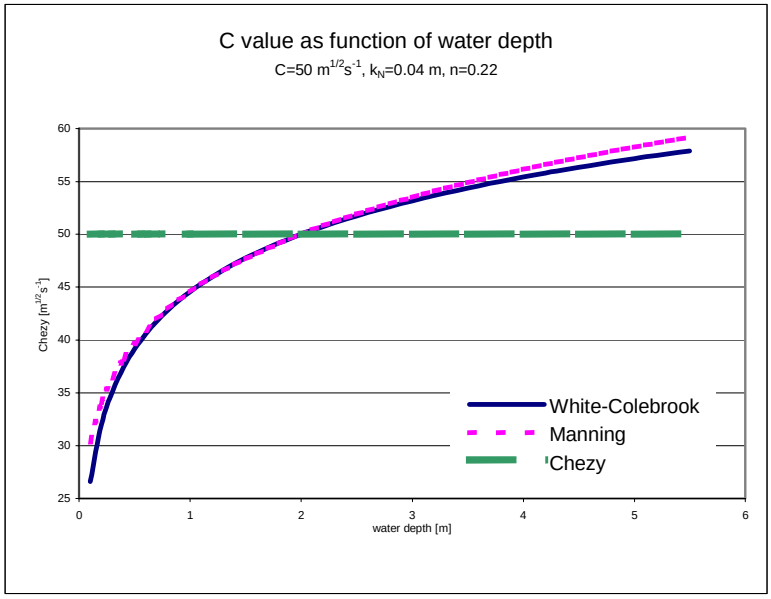

Figure 7-1, C value as a function of the water depth. At the reference water depth of 2m all roughness formulations yield the same Chézy roughness value.

Both depth-dependent roughness formulations show a little less incision of the main channel.

Since none of the formulations yields significantly better results, a constant Chézy coefficient will be used in the remainder of this thesis. This is done for the sake of clarity, because the Reduction factor approach (Baptist, 2005) also uses a bed roughness coefficient that is independent of the total water depth, while the use of the Manning or the White-Colebrook roughness formulation leads to roughness coefficients that are dependent of the water depth.

7.3.4 Bed roughness magnitude

The Chézy equation (2-1) makes clear that the roughness of the flow carrying channel and the flow velocity are strongly related. The maps show indeed that the bed roughness magnitude has a considerable impact on the maximum velocities, see Figure 3/4. Another effect that can be seen is that an increase of the bed roughness leads to a reduction of the erosion in the main channel and also a reduction of the sedimentation on the point bars, Figure 1/4 and Figure 2/4. This is most likely due to the fact that no sediment is carried out of the main channel onto the point bars, see also Section 7.5.1. The graphs depicting the measured and modelled bathymetry, see Figure 1/4 and Figure 2/4, also show some locations with remarkable differences between the simulation with a Chézy-coefficient of 50 $m^{1/2} \cdot s^{-1}$ and the simulation with a Chézy-coefficient of 35 $m^{1/2} \cdot s^{-1}$. Generally speaking it can be said that the simulation with the lower Chézy-value shows the best results. As well with respect to the maximum velocities as with respect to the morphodynamics, see also Section 7.7.

It is remarkable that the simulation with a Chézy-coefficient of 60 $m^{1/2} \cdot s^{-1}$ and the simulation with a Chézy-coefficient of 35 $m^{1/2} \cdot s^{-1}$ predict less erosion of the main channel and less sedimentation on the point-bars. The differences, however, are much less pronounced in the case of C=60 $m^{1/2} \cdot s^{-1}$ than in the case of C=35 $m^{1/2} \cdot s^{-1}$. This becomes especially clear from the

bathymetry graphs, in which no significant differences between the simulation with a Chézy of 50 $m^{1/2} \cdot s^{-1}$ and the simulation with a Chézy of 60 $m^{1/2} \cdot s^{-1}$ are found.

The Chézy-coefficient of 35 $m^{1/2} \cdot s^{-1}$ yields, in general, the best results, lower maximum velocities and also less erosion of the main channel. Nevertheless the proposed value of 50 is used, for two reasons. The lower Chézy value brings less sediment on the point bars, while the sedimentation is already far too low with a Chézy value of 50 $m^{1/2} \cdot s^{-1}$. Also the Chézy value of 50 $m^{1/2} \cdot s^{-1}$ is considered to be physically more realistic than the extremely rough Chézy value of 35 $m^{1/2} \cdot s^{-1}$. Nevertheless it is advised to find a more accurate Chézy-coefficient for the study area as soon as a better performing model, with respect to channel erosion and point-bar sedimentation, is constructed.

7.4 Sediment transport

7.4.1 Sediment diameter

The impact of three different sediment diameters was studied. This was done by setting up three simulations in which the diameter of the sediment fraction was changed. The fractions used are given Table 6-2.

The impact of the sediment diameter on the simulated morphological behaviour of the river Allier turns out to be very large. Also the field survey showed major difference in the diameter of the sediment deposited in the vegetated areas and the diameter of the sediment on the bare point-bars and especially the main-channel. The modelling of several sediment fractions should therefore be enhanced. At the moment, it is not possible in Delft3D to simulate a spatial variation of the sediment fractions and the simulations in which different fractions were incorporated yielded instabilities that have not been solved. Further perfection of the sediment fractions calculations in Delft3D, however, will not solve the simulation problems. Even with a very fine sediment fraction the morphologic activity on the point bars is too low, whereas the simulation with the armoured bed fraction still predicts too much erosion of the main channel.

7.4.2 Sediment transport formula

As stated in Section 2.2.8, three different sediment transport formulae were examined. The different formulae showed to have a significant impact on the simulated erosion and sedimentation patterns, see Figure 1/1. All three presented, however, the same errors as described in Section 7.7. Therefore it was not possible to give a well-founded advice for using one or the other formula.

Expert knowledge and the scope of the different formulae (see Section 2.2.8) suggest that the Meyer-Peter and Müller formula is most applicable to the river Allier.

As with the bed roughness magnitude, it is highly advisable to reinvestigate the performance of the sediment transport formulae, as soon as a more reliable model is constructed.

7.4.3 Bed slope effect

By using the method by Bagnold (1966) and increasing the factor Alfabn it was possible to decrease the erosion of the main channel and also decrease the sedimentation on the banks, see Figure 1/1. Because of the increased Alfabn the sediment transport down the slopes and into the main channel is increased. Because of this effect the possibility was studied to simulate the cliff erosion by increasing the ALFABN factor. This method, however, showed to be unsuitable to simulate cliff erosion, since cliff erosion usually occurs at the outer bend, whereas this factor increases the erosion of slopes independent of its location.

To eradicate the main channel erosion the Alfabn factor had to be increased to at least 10. This factor was thought too large to make any physical sense, for the following reasons. Firstly, this factor leads to an unnatural flattening of the slopes. Secondly, by enlarging the 'downhill' component of the sediment transport it frustrates the impact of the secondary flow, which transports sediment from the outer bend to the inner bend, i.e. 'uphill'. Thirdly, the way in which the erosion of the lower bed is prevented is purely artificial. There is a range of phenomena that can explain why the erosion of the main channel does not occur in reality. The supply of sediment by cliff erosion, the availability of coarser gravel at the bed, lower flow velocities, more sediment supply from upstream. It is highly unlikely that the erosion of the main channel is solely nullified by sediment rolling from the slopes.

Since the Koch&Flokstra (1980) method was developed for river bends and the Bagnold (1966) was not suitable to eradicate the erosion of the main channel, the Koch&Flokstra method was used in the other simulations, although the Bagnold simulation with an Alfabn of 10 showed less erosion of the main channel.

7.4.4 Cliff erosion

In an effort to simulate cliff erosion the ThetSD-scheme was examined. This method was developed for the case of erosion near a dry beach or bank. The standard scheme will not allow erosion of dry cells adjacent to wet eroding cells, even when a steep scour hole would develop right next to the beach. The ThetSD-factor governs the fraction of the erosional volume of the wet cell that is assigned (evenly) to the adjacent dry cells; if ThetSD equals zero, the standard scheme is used; if ThetSD equals 1, all erosion that would occur in the wet cell is assigned to the adjacent dry cells.

Steep cliff erosion is, however, a completely different process than the process simulated with the ThetSD-scheme. The scheme makes erosion of cliffs possible, but only for a few centimetres instead of the complete height of the cliff. This continuing slow erosion from the top of the cliffs, when they're still dry, is not the same process as steep cliff erosion. Cliff erosion occurs as a result of the undercutting of the cliff due to the erosion by the water. When the cliff becomes too steep it collapses at once into the river over its complete height. Because of this difference it was not possible to simulate cliff erosion with the ThetSD scheme.

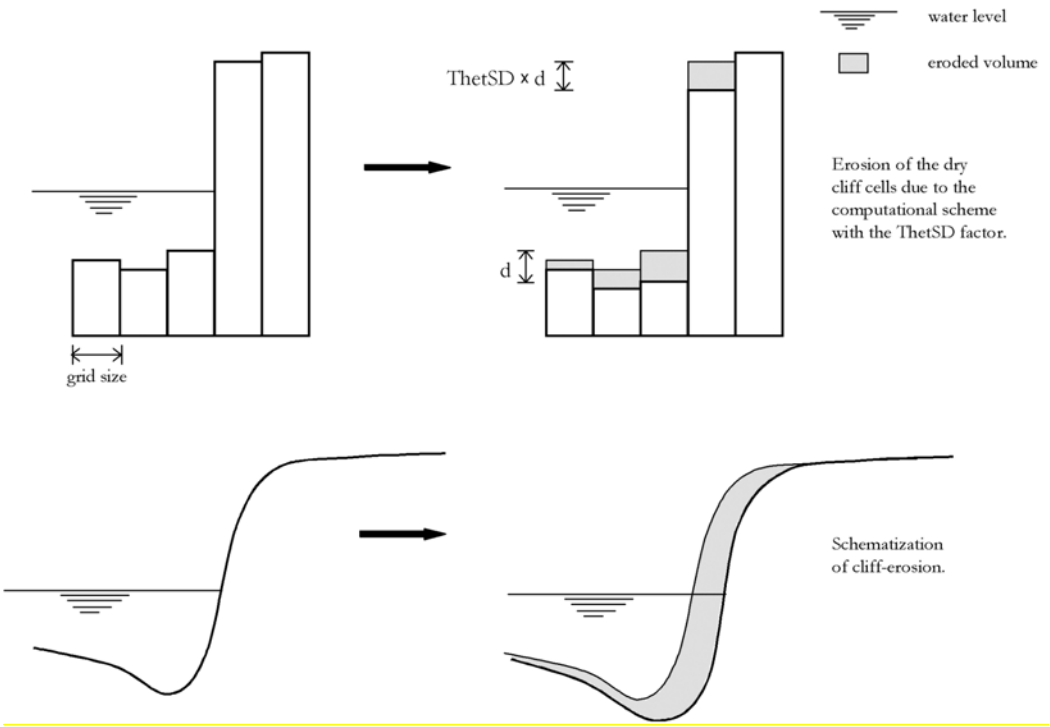

Figure 7-2, Schematical presentation of the difference between cliff-erosion and the erosion simulated by the ThetSD-scheme.

No significant changes can be found between the different simulations. This is mostly due to the fact that, because of the coarse sediment, the flow velocities have to be quite high to cause erosion. These high velocities are only reached if the water depth is large enough. In such situations, however, the adjacent cells are likely to be flooded as well, whence the ThetSD-facility cannot be used.

Because the ThetSD-scheme is thought unfit for the simulation of cliff erosion and because the variation of the ThetSD-factor yields no significant changes in the model results, the ThetSD-factor is set to zero in the other simulations.

7.5 River morphology

7.5.1 Non-erodable main channel bed

The simulations tend to overrate the main channel erosion, see 8.5. To study the influence of this on the other sedimentation and erosion processes, several runs were done with a fixed main channel bed. Figure 1/1 clearly shows that the simulation with the fixed main channel bed predicts considerably less sedimentation on the banks of the main channel. Also the sedimentation on the point-bars slightly decreased, but this difference can be considered negligible. From these results it was concluded that in the simulations the major part of the sediment deposited on the banks originated from the eroding main channel.

7.5.2 Cut-off at point-bar Chateau de Lys

In an effort to simulate the impact of the cut-off at Chateau de Lys, the bed level in the model input was lowered at the location of the cut-off. Simulations with this lowered bed, however, showed no significant changes and no extra flow through or sedimentation in the old meander bend could be found.

7.6 Vegetation

7.6.1 Vegetation model

Figure 1/2 shows the total erosion and sedimentation that was simulated for both the Increased Nikuradse roughness height simulation and the Reduction factor approach simulation. The differences between these two simulations are remarkably small. Especially if these are compared with the large differences in the simulated bed shear stress, see Figure 2/2. Possible reasons for this lack in difference will be discussed in Section 8.5.

Concerning the bed shear stress it can be stated that the Increased Nikuradse roughness height approach yields physical unconvincing results. The bed shear stress at the vegetated parts of the point bars is higher than the bed shear stress in the main channel, while the low flow velocity and vegetation on the point bars should lead to lower bed shear stresses instead of higher. The results of the Reduction factor approach yield far better results concerning the vegetated areas. The bed shear stresses in the main channel, however, are probably overestimated in both simulations. This assumption is confirmed by the fact that the simulations yield to much erosion of the main channel. The maximum bed shears stress of 310 $N \cdot m^{-2}$ in the Nikuradse approach is far too high and is the result of some instabilities at the down stream border. On most locations the bed shear stress stays well below 36 $N \cdot m^{-2}$.

7.6.2 Vegetation density and vegetation diameter

Concerning the vegetation a sensitivity analyses was carried out to discern whether the density (m) and diameter (D) of the vegetation (the product of m×D is called the 'mD-factor') is of great importance to the morphological behaviour of the river Allier. Thus a decision can be made whether further investigation of the vegetation density or diameter is advisable.

Measurements showed that the mD-factor can easily show a deviation 20% within the same vegetation type. See Appendix 4, where the density, height and diameter of two spots of floodplain grassland, measured on the same point-bar, already show a difference of 20% in the mD-factor. Therefore three model runs with different mD-factors have been compared with each other. The first model run used the mD-factors as estimated by Baptist (2005), the next used an mD-factor that was decreased with 20% for all vegetation types, the last run had the mD-factor increased with 20% for all vegetation types.

The differences between the simulated morphological changes turned out to be insignificant. It is expected, however, that the changes will increase if the model would better approximate the high morphological activity on the point bars.

Aside from simulations with an increased or decreased mD-factor, a simulation without any vegetation has been run. Figure 1/2 shows the cumulative erosion and sedimentation of this simulation alongside the simulation with the normal mD-factor. It is clear that the presence of vegetation has a very strong influence on the simulated morphodynamics. As can be seen in Figure 2/2, the flow velocity in the non-vegetated simulation is far higher on the point bars than in the vegetated simulation. This is probably the main reason for the higher morphological activity on the point-bars in the non-vegetated simulation. This higher velocity can easily be explained by the influence the vegetation has on the total roughness. According to Chézy the velocity is linear proportional to the Chézy-coefficient, see equation (2-1). In non-vegetated areas this value is taken equal to 50 $m^{1/2}/s$. For the hydrodynamic calculations in vegetated areas the Chézy-coefficient is calculated according to Rodríguez Uthurburu, see equation (2-39). Figure 2-21 shows that with a water depth of 1 m the Chézy-value of almost all the vegetation types is already twice as low as the Chézy value of a non-vegetated area. With increasing water depth, this difference even increases. If one assumes a maximum water depth on the point-bars of 3 m, another remarkable aspect can be noted. The Chézy-coefficients of all of the vegetation types are relatively close to each other compared to the Chézy-coefficient of 50 $m^{1/2} \cdot s^{-1}$ of non-vegetated areas. An exception to this rule is the pioneer vegetation type, but this one is simulated as non-vegetated or bare vegetation, because the assumptions made for the Reduction factor approach don't hold for pioneer vegetation.

From these observations it can be concluded that it is of major importance whether a certain area is vegetated or not. Of less importance is the exact density, diameter and height of the vegetation.

7.6.3 Individual trees

The influence of individual trees on the morphodynamics was also studied. Trees that showed to have had an important contribution to the morphological changes were simulated as very rough grid cells. The Reduction factor approach used an mD-factor of 20 m^{-1} and a k-value (height) of 10 m. Obviously this mD-factor is physical impossible. It could, for example, be represented by 5 trees per square meter with a diameter of 4 meter and a height of 10 m, or herbaceous vegetation with a diameter of 5 mm and a density of 4000 stems per square meter instead of the measured 400 stems. The Increased Nikuradse roughness height approach used a k_N-value of 10 m. This should be represented by grains with a diameter of 10 m, also highly unlikely. However, to get a first impression of the possibilities to simulate the impact of individual features, like uprooted trees, it is thought to suffice.

The model results, see Appendix 7, show that some of the extra trees have a very strong influence on the local morphology but almost no influence on the global behaviour. The tree on point-bar Verdelet, for example, splits the simulated channel cut-off on point-bar Verdelet in two smaller channels. But, the changes on the downstream point-bars Chateau de Lys and the downstream point-bar are already negligible. Furthermore the impact on the total volume of sediment that left the model area is also negligible, see Table 7-2. This supports the hypothesis that these kind of hard individual features only have a local effect. So it depends on the objective

of the model, simulate local or global behaviour, whether it is necessary to incorporate these individual hard features in the model.

Table 7-2, Calculated erosion and sedimentation volumes of a simulation without individual trees compared with a simulation with individual trees.

simulation	**extra sedimentation [m³]**	**extra erosion [m³]**	**total difference [m³]**
no trees added compared with trees added	76357	75449	908

7.7 Summary of the sensitivity analysis

This section presents in Table 7-2 which variables and parameters of the sensitivity analysis showed to have the strongest influence on the different investigated dependent variables. It should be noted that this table should be read with the necessary caution and can only be understood correctly if the corresponding Sections of the sensitivity analysis are understood.

Table 7-3, Results of the sensitivity analysis.
++ strong significant influence, + significant influence,+/- minor influence, - insignificant influence

	Flow velocity	Flow direction	Water level	Bed shear stress	River topography	
Flow						
Q-h relation	++	-	++	+	+	impact from downstream border till the apex of Chateau de Lys
Spiral motion	-	-	-	-	-	probably due to difficulty in modelling 3D processes in a 2DH model
Bed roughness coefficient	+	-	-	+	+	
Bed roughness magnitude	++	-	+/-	+	+	
Sediment transport						
Sediment diameter	-	-	-	-	++	especially for a coarser bed material
Sediment transport formula	-	-	-	-	++	
Bed slope effect	-	-	-	-	+	
Cliff erosion	-	-	-	-	-	
River morphology						
Non-erodable main channel	-	-	-	-	++	
Cut-off at point-bar Chateau de Lys	-	-	-	-	-	
Vegetation						
Vegetation model	-	-	-	++	-/+	
Vegetation density and magnitude	-	-	-	-/+	+	
no-vegetation	+	+	+	++	++	
Individual trees	+	+	-	+	+	local, global the impact is negligible

8 Discussion on the behaviour of the model

This Section will discuss the performance of the model. For the demands put on the dependant variables by which the model is evaluated, one is referred to Section 7.2.

8.1 Flow velocity

The simulated depth averaged flow velocities are probably a bit too large in the main channel. Figure 3/3 of Section 7.3.1 shows that at low flow the velocities are a little too large compared with the measurements. The flow velocities at maximum discharge are probably also a bit too high, see Figure 1/1. The simulated velocity in the main channel surpasses the estimated maximum velocity of 3 m/s in almost the entire channel. The velocities on the vegetated parts of the point-bars are seldom larger than 0.5 m/s. This is considerably lower than the estimated maximum depth averaged velocity of 1 m/s.

Although the model predicts a bit too high velocities in the main channel and too low velocities in the vegetated areas, the results are quite acceptable. If a Chézy-coefficient of 35 $m^{1/2} \cdot s^{-1}$ is used instead of C = 50 $m^{1/2} \cdot s^{-1}$ the simulated high velocities in the main channel can even be reduced to more reliable magnitudes without significantly decreasing the velocities in the vegetated areas, see Figure 3/4 of Section 7.3.4.

Comparison of the map by Driesprong (2001) with the model results shows that the modelled velocity distribution over the width of the channel differs strongly from the measured velocity distribution. Especially in the part before the island the measured maximum velocity is located closer to the outer banks. This is probably due to an erroneous calculation of the secondary flow. See also Section 8.5.1.

8.2 Flow direction

In general it can be said that the direction of flow as indicated by the scour holes shows a satisfactory agreement with the modelled flow direction at peak discharge. Some places, however, show scour holes with a direction almost perpendicular to the low waterbed.

Some of the locations are indicated with circles. It is assumed that these scour holes were formed during the waning of the flood. The water flows back from the point-bar into the low waterbed along the path with the steepest energy descent. If the waterlevel in the low waterbed drops fast enough and some obstacles on the point-bar confine the flow, it is possible that water flowing from the point-bar reaches velocities high enough to create scour holes. This process is not simulated by the Delft3D model during the decline of the flood. This is probably due to the local circumstances necessary to produce scour holes of this kind. These cannot be reproduced on a 20 m grid.

Some other locations are indicated with squares. These scour holes are directed away from the low waterbed and thus cannot have been created by the same process as the scour holes indicated by circles. It suggests that the Delft3D model is not capable of simulating the strong curves in the flow that occur in the river Allier. An aspect that will be further investigated in Section 8.5.

8.3 Water depth

The water depths simulated on the point-bars reach values up to 2.5 m. This is quite close to the observed maximum height of the flood marks. The majority of the simulated water depths on the point-bars at high flow is around 1 m. This seems to be reasonable, but since no good estimations or measurements of the water depths during high flow are available, it is not possible to say something conclusive about the accuracy of the simulation results.

The sensitivity analysis showed that the possibilities to calibrate the water depth are very limited. The only parameters that had any significant influence were the bed roughness magnitude and the presence of vegetation, see Figure 1/1. The only parameter of these two that can be used as a calibration parameter is the bed roughness magnitude and its influence on the water depth is limited. The Q-h relation of the down-stream border had a strong impact on the water depth. But the influence of this variable is limited to the downstream end of the model area.

8.4 Bed shear stress

No physical reliable range of the bed shear stress was determined. Because changes in the bed shear stress are likely to lead to erosion or sedimentation this dependent variable is discussed in the section about the river morphology, Section 8.5

8.5 River morphology

It turned out to be impossible to construct a model that matched the measured data in a satisfying manner. Appendix 7 Figure 1/10 of Section 8.5 shows a typical modelled bathymetry after the modelled flood alongside the measured bathymetry of August 2004. The most remarkable simulated morphological features are:

- Almost no morphological activity on the point-bars, especially in the vegetated areas;
- movement of sediment banks over the bare parts of the point-bars;
- strong erosion of the main channel and growth of 'levees' on both sides of the main channel;
- no erosion of the cliffs;
- growth of a riffle between point-bar Verdelet and point-bar Chateau de Lys;
- growth of strong channel cut-offs on point-bar Chemilly and point-bar Chateau de Lys.

8.5.1 Point-bars

The simulation maps of Figure 2/10 and 3/10 shows almost no sedimentation or erosion between the vegetation and little morphological changes on the bare parts of the point-bar. The measured map, on the other hand, shows major sedimentation on the point bars. Several explanations can be given for this lack of morphological activity.

One of the causes of this deviation probably is that in the model the sediment carried out of the riverbed onto the point bars settles already on the slopes, see Section 8.5.3. Therefore no sediment is actually available to settle on the point bars. This phenomena can not, however, be the only cause, because there is not only a lack of sedimentation on the point-bars, but also a lack of erosion.

Probably the lack of spiral flow plays an important role in the simulated errors on the point-bars and main channels. In reality the spiral flow is responsible for the typical build up of a meandering river. The secondary flow carries sediment from the outer bend to the inner bend. The simulations do not show this very important feature of a meandering river.

Although the morphological errors on the point-bars are concentrated between the vegetation, it is unlikely that these errors can be ascribed to a flaw in the used vegetation model. As can be seen in Figure 1/2 of Section 6.8.1 both models, the Increased Nikuradse roughness height and the Reduction factor approach, show the same errors. Most remarkable is that the Reduction factor approach does not perform any better than the Increased Nikuradse roughness height approach. An explanation for this lack in difference can be found in the way the used transport formula reacts to decreasing water depth and depth averaged velocities. The Engelund and Hansen transport formula, for instance does produce major morphological activity on the vegetated point-bars if the Increased Nikuradse roughness height method is used, see Figure 5/10 of this section and Figure 1/1 of Section 7.4.2.

Two major differences between the Van Rijn (1984) and the Meyer-Peter and Müller (1948) formula on the one hand and the Engelund and Hansen (1967) formula on the other can be noted. Both of these differences may be responsible for the lack of difference between the Increased Nikuradse roughness height approach and the Reduction factor approach.

From Appendix 11 the following set of relations for the equilibrium state can be found for between the vegetation:

For the Engelund and Hansen (1967) transport formula:

$$\frac{s_{e1}}{s_{e0}} = \left(\frac{C_1}{C_o} \right)^{1/3} \tag{8-1}$$

for the Meyer-Peter and Müller transport formula:

$$\frac{s_{e1}}{s_{e0}} = \left(\frac{C_1}{C_0} \right)^{5/4} \tag{8-2}$$

for the Van Rijn (1984) transport formula:

$$\begin{cases} \dfrac{s_{e1}}{s_{e0}} = \left(\dfrac{C_1}{C_0} \right)^{2.8} & \text{for } T < 3.0 \\ \dfrac{s_{e1}}{s_{e0}} = \left(\dfrac{C_1}{C_0} \right)^{2} & \text{for } T \geq 3.0 \end{cases} \tag{8-3}$$

in which:

s_{e0}	equilibrium sediment transport capacity per unit width before the vegetation
s_{e1}	equilibrium sediment transport capacity per unit width within the vegetation
C_0	Chézy-coefficient within the vegetation
C_1	Chézy-coefficient before the vegetation

So with a decrease of C (increase of roughness), both the Van Rijn (1984) and the Meyer-Peter and Müller (1948) transport formulae predict less erosion, while the Engelun-Hansen (1967) transport formula predicts more erosion. The theory is, that the problem with the Increased Nikuradse roughness height is that it overestimates the resistance of the bed, thus leading to too high bed shear stresses and thus to too high sediment transport capacities. But, from these formula follows that an overestimation of the roughness (too low Chézy-coefficient) only leads to higher sediment transport capacities if the Engelund and Hansen transport formula is used. The two other transport formula predict a decrease of the transport capacity. Of course it should be noted that these equations only hold for the equilibrium state, which never actually occurs at high flow, but it is very likely that the simulated situation will tend towards this behaviour.

The other explanation is found in the critical value for sediment transport below which no erosion occurs. The following equations are retrieved from the Delft3D manual (2003). First the Meyer-Peter and Müller (1948) transport formula will be presented. In this formulation transport only occurs if:

$$\mu\theta > \theta_{cr} \tag{8-4}$$

in which:

$$\theta = \left(\frac{q}{C} \right)^2 \frac{1}{\Delta D_{50}} \quad [-] \tag{8-5}$$

$$\mu = \min\left(\left(\frac{C}{C_{g,90}}\right)^{1.5}, 1.0\right) \quad [-] \quad (8\text{-}6)$$

$$C_{g,90} = 18\log_{10}\left(\frac{12h}{D_{90}}\right) \quad [m^{1/2}\cdot s^{-1}] \quad (8\text{-}7)$$

θ	Shields mobility parameter	[-]
μ	ripple factor according to Meyer-Peter and Müller	[-]
θ_{cr}	critical mobility parameter (=0.047)	[-]
q	magnitude of flow velocity	[m·s^{-1}]
$C_{g,90}$	grain related Chézy-coefficient according to Meyer-Peter and Müller	[m$^{1/2}$·s^{-1}]

According to Van Rijn (1984) transport only occurs if:

$$\mu_c \tau_{bc} > \tau_{bcr} \quad [N\cdot m^{-2}] \quad (8\text{-}8)$$

in which:

$$\tau_{bc} = \frac{1}{8}\rho_w f_{cb} q^2 \quad [N\cdot m^{-2}] \quad (8\text{-}9)$$

$$f_{cb} = \frac{0.24}{\left[\log_{10}\left(\frac{12h}{\xi_c}\right)\right]^2} \quad [-] \quad (8\text{-}10)$$

$$\mu_c = \left(\frac{18\log_{10}\left(\frac{12h}{\xi_c}\right)}{C'}\right)^2 \quad [-] \quad (8\text{-}11)$$

$$C' = 18\log_{10}\left(\frac{12h}{3D_{90}}\right) \quad [m^{1/2}\cdot s^{-1}] \quad (8\text{-}12)$$

$$\tau_{bcr} = \rho_w \Delta g D_{50} \theta_{cr} \quad [N\cdot m^{-2}] \quad (8\text{-}13)$$

$\mu_c \tau_{bc}$	effective shear stress	[N·m^{-2}]
τ_{bcr}	critical bed shear stress according to Shields	[N·m^{-2}]
ξ_c	reference level (bed-load layer thickness) or roughness height	[m]
C’	grain related Chézy-coefficient according to Van Rijn	[m$^{1/2}$·s^{-1}]
θ	Shields parameter (see Figure 2-9)	[-]

Table 8-1 presents some dominant values on the point-bars if the Increased Nikuradse roughness height method is used. The water depth and flow velocity are varied, but for all the other parameters that value is chosen that is applicable to the study area and at the same time makes the chance of surpassing the critical transport value most likely. But even if these values are substituted in the above mentioned relations, the corresponding critical values are not

reached. Which means no sediment transport is calculated on the point bars. The table also shows that for the Meyer-Peter and Müller (1948) transport formula a smaller sediment diameter may be expected to lead to sediment transport on the point-bars. If this sediment diameter is used in combination with the Increased Nikuradse roughness height method, than the simulations indeed predict sediment transport on the point-bars, see Figure 8/10. But if the Reduction factor approach is used, still no erosion occurs. This is explained as follows. The Reduction factor approach uses the bed roughness instead of the total roughness to calculate the sediment transport. Hence the Chézy coefficient is higher, which leads the transport formulae again very close to the critical value.

Concerning the Van Rijn (1984) sediment transport formulation, the situation is different. Although the critical shear stress estimated in Table 8-1 is not surpassed, morphological activity is simulated on the point-bars if sediment with a D_{50} of 8 mm and a D_{90} of 300 mm is used, see Figure 9/10. This sediment fraction distribution is highly unlikely to occur in reality, but the resulting simulations did show remarkable results. If the Van Rijn (1984) sediment transport formula is used the simulations show significantly more erosion on the point-bars if the Reduction factor approach is used than if the Increased Nikuradse roughness height approach is used. The reason can be found in Appendix 11 from equation 1.29. This equation shows that for the equilibrium state the transport capacity is not directly related to the roughness. Only through the impact of the total roughness on the velocity the sediment transport capacity is influenced. Around the dominant waterdepth (1.5 m) on the point-bars, the total roughness according to White-Colebrook is usually a bit higher than the total roughness according to Rodríguez Uthurburu, see Figure 2-21. The first formulation is used in the Increased Nikuradse roughness height approach, the second is used in the Reduction factor approach. Therefore it can be expected that the simulated velocities, and thus transport capacities, are a bit higher if the Reduction factor approach is used instead of the Increased Nikuradse roughness height approach, see Figure 10/10.

Table 8-1, Rough estimations of the critical values for sediment transport.

					remarks
Δ	1.6	1.6	1.6	1.6	
g	9.81	9.81	9.81	9.81	
D50	8	1	1	8	
D90	35	1.5	1.5	300	
q	0.7	0.7	0.7	0.7	
h	1.5	1.5	1.5	1.5	
k_N	7.6	7.6	-*	7.6	-* a fixed Chézy coefficient is used
C	9.5	9.5	50	9.5	calculated with the White-Colebrook formula
Meyer-Peter					**critical value surpassed**
θ_{cr}	0.047	0.047	0.047	0.047	
$\mu\theta$	0.036	0.158	0.069	0.036	
Van Rijn					**critical value surpassed**
τ_{bcr}	37.7	4.71	4.71	37.7	calculated with shields parameter of 0.03
$\mu_c \tau_{bc}$	2.95	1.13	1.13	8.68	

8.5.2 Movement of sediment on the bare parts of the point-bars

The maps of Figure 6/10 and the graphs of Figure 7/10 show the movement of sediment across the point-bars. This bed movement is a process that is expected to occur in reality. But, as with the growth of the cut-off channels, this simulated behaviour is expected but is simulated to pronounced.

8.5.3 Main channel

Whereas the model predicts far too little activity on the point-bars, it predicts too much activity in the main channel. Here the model predicts large erosion, up to 4 m. The field observations, however, account only for a shifting of the main channel in downstream direction, but not for the river incising itself into the bottom. As the modelled river cuts itself into the bottom, the slopes of the main channel are increased in steepness. So in general the river narrows and gets deeper, see Figure 4/10. This is obviously not a process that occurs in reality.

A first reason for this behaviour is probably the absence of cliff-erosion in the simulations. This lack of cliff-erosion has a negative impact on the main channel erosion in two ways. The first is that in the simulation no sediment from the cliffs is fed to the main channel. Thus sediment from the cliffs that may be deposited in the main channel in reality, is not available in the simulation. The second reason can be explained as follows. As stated in Section 8.1 the flow velocities in the main channel are simulated quite well, probably even a bit too high. In nature the resulting sediment transport capacity is 'used' to erode the cliffs. In the simulations the computed

flow does have a large sediment transport capacity at high flow, but it can not be used to erode the cliffs. Instead it erodes the bottom of the main channel. This explanation is supported by the fact that at the cliff where almost no cliff-erosion has occurred in reality, the depth of erosion of the main channel is simulated reasonably accurate. See Figure 2/4 cross-section A of Section 7.3.4. Whereas the simulated erosion of the main-channel is exaggerated at the cliff where large cliff erosion has occurred, see Figure 2/4 cross-section C around point 700 m of Section 7.3.4. The lack of cliff erosion may also lead to erosion because the feeding of sediment to the main channel from the cliffs of the main-channel because the sediment that erodes from the cliffs in reality , however, can not explain all of the erosion of the main channel. As can be seen in Figure 2/4 cross-section C around point 200 m of Section 7.3.4 and Figure 4/10 of this section. Both Figures show deep main channel erosion on a location where no cliff is situated or cliff erosion is measured.

Another reason can be found in the sediment diameter. Figure 1/2 of Section 7.4.1 shows that the enlargement of the sediment greatly reduces the erosion of the main channel. The sediment diameter used in this simulation is actually measured on several locations in the main channel, so at least a part of the too large erosion of the main channel can be attributed to the used sediment diameter. But Figure 1/2 of Section 7.4.1 also shows that even with the coarse sediment fraction the erosion of the main channel is too large.

Aside from the strong erosion of the main channel, strong sedimentation on the banks of the main channel can be seen in the simulations. As stated in Section 8.5.1, the sediment transport capacity on the point-bars is much lower than in the main-channel. Therefore the sediment carried from the eroding main channel onto the point-bars is deposited almost immediately. So, as with the problems in the vegetated areas of the point-bars, a partial solution to eradicate this error is probably the use of graded sediment in the model.

8.5.4 Cliff erosion

As can be seen from several figures, for example Figure 2/2 of Section 7.6.3, the model does not reproduce any cliff erosion. The current Delft3D model does not contain any appropriate methods to simulate steep cliff erosion (see Section 7.4.4). Moreover, a grid size of 20 m is too large to simulate the cliff erosion in the river Allier. The cliff erosion as a result of the simulated flood is mostly between 5 and 15 m, which is less than one grid size. Only at some places cliff erosion of up to 60 m occurs, which would cover only three grid cells, see Appendix 2.

8.5.5 Riffle

The strongly pronounced riffle between point-bar Verdelet to point-bar Chateau de Lys is a feature that is also predicted by the model. But the location in the model is about 200 m downstream of the actual location. The way in which the model simulates the formation of this riffle is probably not the same process as usual in nature (see Chapter 2.3.2). Appendix 7, Figure 6/10 shows a number of simulation figures that clearly show that the water leaving the bend around point-bar Verdelet does not follow the strong curve of the low waterbed, but goes straight on and cuts itself into point-bar Chateau de Lys. For this particular riffle it may very well be that this is the same process as the one responsible in reality for the formation of the riffle.

This riffle was far more pronounced than any other riffle found in the river Allier, which suggests that it was formed in an unusual way. Furthermore, very strong erosion was found during low flow across this riffle, while riffles usually are relatively stable features in a meandering river.

8.5.6 Channel cut-off and chutes

The model does not simulate the strong curves of the watermovement that seem to have occurred in the river Allier during the flood of December 2003. A clear example of this can be seen in the deviance of the direction of the scour holes and chutes on the upstream part of the point-bar Chemilly and the simulated flow direction, see Figure 1/3 from Section 8.2. Another example is the inability of the model to generate a flow into the abandoned channel on point-bar Chateau de Lys, even if a connection between this channel and the main channel is made in the bathymetry input file, see Section 7.5.2. A last clear example can be seen in the long straight reaches of erosion that occur on point bar Verdelet and point bar Chateau de Lys. In reality the water also tends to too cross the point-bars at high flow, creating channel cut-offs and chute channels. But the simulated channel cut-offs are far more pronounced and located further on the point-bars than the shortcut channels that were observed in the field survey.

The model does not simulate the growth of chute channels. But to model these phenomena at least the grid should be refined, because the width of these chutes does not surpass 20 m, which is the size of just one grid cell. This problem is especially clear at the simulated tree on point-bar Verdelet. Cross-section A and B of Figure 1/2 of Section 7.6.3 show that the placement of the 'tree' in the model leads to the erosion of a channel that is not measured in the field. The field observations did show, however, some major chute-channels around this location. Because of the coarse grid and maybe also a too low measurement density, these chutes are not reproduced in the elevation map.

8.5.7 Sediment volume

Another residual error can be found in the sediment volume calculations. The next table shows the eroded and deposited sediment volumes of the total area of both the simulation and the measured situation. The total measured volume loss in the study area is about 7 times larger than the simulated volume loss. The majority of this difference can be attributed to the differences in the cliffs. While the measured data shows a sediment loss of $270 \cdot 10^3$ m^3 the simulation even shows a, though minimal, sediment surplus. The measured sediment surplus on the point-bars is approximately 2 times larger than the simulated surplus, while the simulated sediment loss in the main channel is about 2 times larger than the measured sediment loss. These two observations underpin the observations made in the previous sections that the erosion of the main channel is overestimated, the erosion of the cliffs is absent and that the sedimentation of the point-bars is underestimated by the simulations.

Table 8-2, Measured sediment volumes compared with simulated sediment volumes.

	description	total volume change		erosion		sedimentation	
		[m3]	[%]	[m3]	[%]	[m3]	[%]
simulated	cliffs total	4,251	14	*17,344*	7	21,594	10
	main channel excluding cliffs	-76,896	249	175,198	69	98,302	44
	point-bars	41,704	-135	62,923	25	104,627	47
	total	*-30,942*	*100*	*252,474*	*100*	*221,532*	*100*
measured	cliffs total	-270,142	130	*294,365*	42	24,223	5
	main channel excluding cliffs	-38,178	18	166,120	24	127,942	26
	point-bars	101,089	-49	247,030	35	348,119	70
	total	*-207,232*	*100*	*702,046*	*100*	*494,815*	*100*

Except for the erroneous calculation of the erosion and sedimentation processes an erroneous calculation of the sediment load over the upstream boundary may be, partly, responsible for the volume differences between the measured situation and the simulation.

9 Conclusions and recommendations

The conclusions and recommendations are presented in two parts. The first concerns the field survey and data processing, the second the modelling with Delft3D.

9.1 Field survey

The construction of the Digital Elevation Model (DEM) is based on two different kinds of measurements. For the floodplains, point-bars and other dry areas, the RTK-DGPS was used. The bathymetry of the main channel is determined with a Levelling Instrument. The accuracy and measurement density of the first is much greater than of the latter. This leads to errors in the DEM that have a severe negative impact on the simulation results. Therefore, at least 50% more elevation points should be measured in the main channel than is done in previous years.

Another point of interest is the lack of data in wooded areas. The measurements of these locations yield problems because:

- The measurements with the RTK-DGPS are hindered by trees that block the satellite signals.
- The measurements with the Levelling Instrument are hindered because the trees block the line of sight from the Levelling instrument to the beacon.

Correctly describing the terrain elevation of the wooded areas in the model is considered to have a strong impact on the model results and it is therefore advisable to increase the measuring density of these areas. However, the measurement density on the bare point-bars and in the main channel should remain larger than in the other areas, because most of the morphological activity occurs on these bare plains.

In this field survey the precision of the RTK-DGPS was set to 2 cm. To reach a certain accuracy the receiver has to remain steady for some time, this time increases with increasing precision. Therefore the time needed to acquire the measurements would reduce if the precision would be reduced to 5 cm. This accuracy is considered enough, because the interpolation of the measured points on the 20m grid will easily ad up to errors of a few centimetres.

Only three measured points were available to project the elevation points of the survey of 2004 on the elevation points of the survey of 2002. Although this doesn't seem to lead to significant errors it is advisable to acquire the calibration points with more accuracy. This would increase the reliability of the comparison between the different years and especially the created cumulative erosion and sedimentation maps.

It was not possible to calibrate and validate the hydrodynamic model. Some trust in the hydraulic behaviour was gained by defining reliable ranges of the flow direction, flow velocity and water depth. The methods used to define these ranges are too coarse to yield data suitable for calibrating the model. The morphological behaviour can be calibrated with the DEM, but this is highly questionable and difficult because the driving force behind the morphological behaviour, the flow, cannot be calibrated. Therefore water level and flow velocity measurements are necessary, especially during high flow.

The accuracy of the Q-h relation of the downstream boundary is highly questionable. Although the influence of the downstream border does not reach farther upstream than the apex of point-bar Chateau de Lys, it is advised to calibrate the Q-h relation with water level measurements. This is because the complete study area consists of only three point-bars and the unreliability of the Q-h relation renders the downstream end of the model almost completely useless.

The sediment diameter depends on the location in the study area and the local vegetation. Nevertheless no reliable sediment characteristics are available for any location but the main channel. The spatial distribution observed during the field survey and the model simulations suggest that the sediment diameter is of great importance in the biogeomorphological behaviour of the river Allier. It is therefore considered of great importance to retrieve sediment characteristics of the point-bars. It is of less importance to refine the measurements in the main channel. This is because the accuracy of the available data is already high in comparison with other parameters which are of equal or even more importance to the model's behaviour, e.g. the water level, the bathymetry of the main channel or the sediment on the point-bars.

The volume calculations showed that between July 2003 and July 2004 about 200,000 m^3 of sediment left the study area. A total of 270,000 m^3 eroded from the cliffs, of which the maximum measured propagation was 60 m. 100,000 m^3 of sediment was added to the point-bars

The simulations, which modelled the vegetation as vertical stiff rods, showed no significant differences with a deviation of 20% in the mD-factor (m=rods per m^2, D=diameter of the rods). It is therefore unnecessary to refine the current mD measurements of vegetation types of which the m and D is measured on two or more spots. However, some vegetation types remain still unmeasured. Also the model output showed that the presence of vegetation had a strong impact on the hydro- and morphodynamics. Therefore it is important to accurately know which parts of the study area are vegetated and which parts are bare. Two M.Sc. students of the University of Utrecht have reinvestigated the spatial arrangement of the vegetation types in the study area. In future model studies this new map should be used to replace the vegetation map of 2002.

9.2 Model

This section discusses the most important aspects of the model's behaviour. First it some brief remarks are made on the assumptions. Then the sensitivity analysis is covered. And after that, the general behaviour of the model is discussed. This section closes with some recommendations for further study.

Assumptions

The following assumptions that have been made are indeed considered of minor importance:

1. *Cohesion of sediment between vegetation due to root structure.* Due to the fact that the simulated erosion in vegetated areas is, as yet, far too low, it seems to be of minor importance to study the increase of the cohesion of the sediment due to catchment by roots.
2. *Armour layer.* The armour layer in the river Allier strongly influences the characteristics of this river. For the modelling of the river Allier it is yet of less importance. The armour layer is very thin (1 or 2 times the grain size) and completely disturbed during high flow. The amount of armour layer sediment in the total amount of transported sediment during a major flood event is thus negligible. The major changes in the morphology occur during the floods, after which some minor changes and the restoration of the armoured layer occur during mean and low flow. The armoured layer fixes the main channels morphology. This means almost no morphological changes occur in between two floods. As long as the simulations are not capable of predicting the major morphological changes that occur during those floods, it is thought unnecessary to investigate the influence and the building up of the armoured layer.
3. *Morphologic upstream boundary.* The standard scheme used by Delft3D to predict the sediment transport over the upstream boundary seems to be satisfactory since no unreasonable erosion or sedimentation occurs just downstream of this boundary. Except from the model wide erosion of the main channel and sedimentation on the river banks.

Sensitivity analysis

A sensitivity analysis made it possible to distinguish between variables of major and minor influence on the morphological behaviour of the model. It should, however, be noted that if the model's behaviour becomes more accurate, some of the conclusions of the sensitivity analysis should be re-examined.

The examined parameters that showed to have a significant influence on the morphological behaviour are:

1. *Transport formula.*
2. *Sediment fraction.* Especially the simulation with a coarse sediment fraction (D_{50}=16 mm, D_{90}=41 mm) showed strong morphological differences with the simulations that used the regular fraction (D_{50}=8 mm, D_{90}=35 mm).
3. *Single very rough grid cells.* These rough grid cells were introduced to simulate the impact of single features, like uprooted trees. The impact is strong but only of a local nature.
4. *Chézy-coefficient.* Especially if a value was taken that was lower than the standard Chézy-coefficient of 50 $m^{1/2} \cdot s^{-1}$.

5. *Downstream boundary*. Although the influence of the Q-h relation does not reach very far upstream, the impact within its influence reach is very strong.
6. *Grid size*. The 20m grid showed to be rather coarse, especially if one is also interested in local behaviour. Most of the important morphological features in the river Allier cannot be projected properly on the 20 m grid. Chute channels are mostly 15m wide, cliff erosion reaches up to 60m at max, the width of the main channel is about 70m and some of the vegetated areas that showed to have a significant impact on the flow and morphodynamics are less than 20 m in width. Decreasing the grid size of the model to 10m already improved the prediction of the velocity distribution due to secondary flow.

Model behaviour

Features that were predicted in a more or less correct way:

1. The flow direction on the point-bars.
2. The field survey showed strong shortcut channels on the point-bars. The model also shows the appearance of these shortcuts. The simulated shortcuts are, however, to deeply cut into the point-bars and reach too far and to straight onto the point-bars.
3. The influence of a row of trees on point-bar Chemilly and one tree on point-bar Verdelet.
4. The simulation shows the movement of sand over the point-bars. This seems to resemble the movement of chute-bars in an adequate way, but the simulated height of these moving sediment banks is too large.
5. The appearance of a strong pronounced riffle between point-bar Verdelet and point-bar Chateau de Lys. However, the riffle in the simulations appears about 200 m too far downstream.

Some of the model errors that showed in all simulations:

1. Too much erosion of the low waterbed.
2. Too much sedimentation on the banks forming natural levees on both sides of the river.
3. Not enough morphological on the point-bars, especially in the vegetated parts.
4. No cliff erosion.
5. Unconvincing secondary flow, probably one of the reasons for the lack of sediment transported to the point-bars.
6. No sediment transport into the abandoned channel on point-bar Chateau de Lys, not even when a break through from the main channel to this abandoned channel was forced by artificially lowering the DEM between these two channels.
7. Too strongly pronounced cut off channels on the point-bars Verdelet and Chateau de Lys.
8. Not enough sediment is transported out of the model area.

Concerning the vegetation models the following can be said. The Reduction factor approach seems to simulate more reliable bed shear stresses than the Increased Nikuradse roughness height method. With respect to the sediment transport capacity the effect of the Reduction factor approach is relatively small if the Van Rijn (1984) transport formula is used. If the Engelund and Hansen (1967) or the Meyer-Peter and Müller (1948) transport formula is used, the differences between the Increased Nikuradse roughness height approach and the Reduction factor approach are much larger. Furthermore, only if the Engelund and Hansen sediment transport formula is used it is likely too large sediment transport capacities are simulated if the roughness is overestimated. Both of the other transport formula simulate too low sediment transport capacities instead of too large. Whether the Increased Nikuradse roughness height method

overestimates or underestimates the roughness depends on the vegetation type and water depth. But due to the residual errors in the simulation runs, it was not possible to say anything conclussive about the correctness of the Reduction factor approach (Baptist, 2005) concerning the sediment transport capacity. But the much more physical convincing simulated bed shear stresses and more accurate physics underlying this theory, indicate strongly that the Reduction factor approach is superior to the Increased Nikuradse roughness height method.

Recommendations

All the simulations used only one sediment fraction. The field survey showed however a major difference in the diameter of the sediment deposited in the vegetated areas and the diameter of the sediment on the bare point-bars and especially the main-channel. Also the model showed that the impact of the chosen sediment diameter on the morphodynamics, was considerable. It is therefore important to account for several sediment fractions when simulating the river Allier.

None of the methods tried to simulate cliff erosion showed to be successful. The incapability of the model to correctly simulate the cliff erosion is thought to strongly influence many of the other residual errors of the model. Because the channel cannot migrate in a downstream direction, but does have the transport capacity to erode, it cuts itself into the bottom. Because no collapse of sediment into the river occurs the main channel is not fed with extra sediment. This leads to a deeper erosion of the main channel and to less sediment transport onto the point-bars. While the model does not simulate this cliff erosion, this is most likely the reason for the vast difference in sediment balance between the modelled situation and the measured situation. Because of the major influence cliff erosion seems to have on the morphological behaviour of the river Allier, it is strongly advised to investigate the modelling of this feature. Furthermore a finer grid-size is probably necessary because most of the cliff erosion does not reach farther than 30 m, and this 30 m contains a major volume of sediment because of the height of the cliffs.

The last feature that is thought responsible for the errors is the secondary flow. In reality this flow is of major influence on the formation of the typical features of a natural meandering river. The simulations however do not show any of the secondary flow induced morphodynamics, for example the build up of a point-bar on the inside of a river bend. Therefore it is strongly advised to study if the erroneous calculation of the morphodynamics in ad 2DH simulation is indeed partly due to a wrong calculation of the secondary flow. If this is the case a 3D study should be carried out or the secondary flow formulations used in the 2DH model of Delft3D should be enhanced.

Literature

Agence de l'Eau Loire-Bretagne 1991, Overview of Allier discharge measuring stations and discharge characteristics (in French).

Bagnold R.A. 1966. 'An Approach to the Sediment Transport Problem from General Physics'. *U.S. Geological Survey Professional Paper* 422-1, Washington.

Baptist, M.J., W.E. Penning, H. Duel, A.J.M. Smits, G.W. Geerling, J.S.L. van Alphen 2002. 'Assessment of cyclic floodplain rejuvenation on flood levels in the Rhine River'. *River Research and Applications*, John Wiley & Sons, Ltd.

Baptist, M.J. 2005. *Modelling floodplain biogeomorphology*. Ph.D. thesis, Delft University of Technology, ISBN 90-407-2582-9

Bemmel, E. van, M. van den Broek 2003. *Stage Allier, 30 juli 2003 - 29 Augustus 2003*. Delft: Delft University of Technology.

Berg, J. van den, J. de Kramer, M. Kleinhans, A. Wilbers 2000. 'De Allier als morfologisch voorbeeld voor de Grensmaas, Deel I: Vergelijkbaarheid en rivierpatroon'. *Natuurhistorisch Maandblad*, no. 7 jaargang 89, p.118-122.

Berg, J.H. van den, T. Balyuk 2004. *Interaction of vegetation and morphodynamics in pointbars of the Lower Volga (Russia) and the Allier (France)*. Centre for Geo-ecological Research.

Bosch, L. van den 2002. *Biogeomorphology in the Allier, research plan*. Delft: Delft University of Technology.

Bosch, L. van den 2003. *Influence of vegetation on flow and morphology in the river Allier, France*. MSc. Thesis. Delft: Delft University of Technology.

Bouchardy, C. 1991. *L'Allier. Rivières et vallées de France*. Privat, Toulouse.

Brown, C.B. 1950. 'Sediment Transportation'. In: H. Rouse (Ed.) *Engineering Hydraulics*, chapt. XII, John Wiley, New York, pp. 769-857.

Chang, H.H. 1988. *Fluvial Processes in river engineering*. San Diego State University: John Wiley & Sons.

Clements, F.E. 1916. *Plant succession: an analysis of the development of vegetation*. Carnegie Institution of Washington, Washington, United States, Publication/Institution of Washington, no. 242.

Cohen, K. 1998. *Spatial variability of gravel bed pavements in the Allier*. Vakgroep Fysische Geografie, Faculteit Ruimtelijke Wetenschappen, Universiteit Utrecht.

Dietrich W.E., Smith, J.D., and Dunne, T. 1979. 'Flow and Sediment Transport in a Sand Bedded Meander'. *Journal of Geology*, 87, pp. 305-315.

Driesprong, A. 2001. *Boundary Shear Stress and Hydraulic Roughness in the Allier River*. Utrecht: Utrecht University.

Einstein, H.A. 1950. 'The bed-load function for sediment transportation in open channel flow'. *Tech. Bull.* US Dep. of Agr., Washington, D.C., no. 1026.

Engelund, F. and E. Hansen 1967. *A monograph on sediment transport in alluvial streams*. Copenhagen: Teknisk Forlag.

Jansen, P.Ph., ed. 1994. *Principles of River Engineering, the non-tidal alluvial river*. Delft: Delftse Uitgevers Maatschappij.

Kapinga, S. 2003. *Scour around large wooden debris, determination of flow velocities during floods by studying local scour holes in the river Allier*. Delft: Delft University of Technology.

Kennedy, J.F., N.H. Brooks 1963. 'Laboratory Study of Alluvial Streams at Constant Discharge'. *Proceedings, Federal Interagnecy Sedimentation Conference, Miscellaneous Publication* No. 970, Agricultural Research Service, pp. 320-330.

Kirkby, M. 1990. 'The landscape viewed through models'. *Zeitschrift fur Geomorphologie*, Suppl.-Bd. 79, 63-81.

Kleinhans, M., J. van den Berg, A. Wilbers, J. de Kramer 2000. 'De Allier als morfologisch voorbeeld voor de Grensmaas, Deel III: Sedimenttransport en afpleistering'. *Natuurhistorisch Maandblad*, no. 9 jaargang 89, p.202-207.

Koch, F.G. and C. Flokstra 1980. 'Bed level computations for curved alluvial channels,' *Proc. XIX Congress of the IAHR*, Vol. 2, New Delhi, India, p. 357.

Kramer, J. de, A. Wilbers, J. van den Berg, M. Kleinhans 2000. 'De Allier als morfologisch voorbeeld voor de Grensmaas, Deel II: Oevererosie en meandermigratie'. *Natuurhistorisch Maandblad*, no. 8 jaargang 89, p.189-198.

Kramer, J. de 2003. *Riverine vegetation development, Observations on interactions between vegetation growth and succession, hudrodynamics and morphodynamics in the Lower Volga, Russia and Allier, France*. Utrecht: Utrecht University.

Meyer-Peter, E. and Müller, R. 1948. 'Formulas for bed load transport'. *IAHR, Proc. 2nd Congr.*, Stockholm, Vol. 2, Paper 2, pp. 39-64.

Neessen, C.A.J. 2000. *Three-dimensional flow patterns in the river Allier*. Utrecht: Utrecht University.

Nikuradse, J. 1933. 'Stromungsgesetz in rauhren rohren'. *vdi-forschungsheft* 361.
(English translation: 'Laws of flow in rough pipes'. *Technical report, NACA Technical Memo 1292*. National Advisory Commission for Aeronautics, Washington, DC., 1950)

Peters, B., K. van Looy, G. Kurstjens 2000. 'Pioniervegetaties langs grindrivieren: de Allier en de Grensmaas'. *Natuurhistorisch Maandblad*, no 7 jaargang 89, p. 123-136.

Rijn, L.C. van 1984, 'Sediment transport, part I: Bed load transport'. *Journal of Hydraulic Engineering ASCE*, Vol.11D, pp. 1431-1456.

Rijn, L.C. van 1990. *Principles of fluid flow and surface waves in rivers, estuaries, seas and oceans*. Aqua Publications, Amsterdam.

Rijn, L.C. van 1993. *Principles of sediment transport in rivers, estuaries and coastal seas*. Aqua Publications, Amsterdam.

Shields, A. 1936. 'Anwendung der Aehnlichkeits-Mechanik und der Turbulenzforschung auf die Geschiebewegung'. *Preussische versuchsanstalt für Wasserbau und Schiffbau*. Berlin, Heft 26.

Simons, D.B. and Richardson, E.V. 1961. 'Forms of bed roughness in alluvial channels'. *Proc. ASCE*, 87, HY 3, paper 2816, 87-105.

Terwindt, J.H.J. & Berg, J.H. van den 1997. *Riviermorfologie, deel 1: tekst*. Faculteit Ruimtelijke Wetenschappen Utrecht.

Tsujimoto, T. 1999, 'Fluvial processes in streams with vegetation'. *IAHR, Jour. Hydraul. Res.*, Vol.4, No.6, pp.789-803.

Rodríguez Uthurburu, J. 2004. *Evaluation of physically based and evolutionary data mining approaches for modelling resistance due to vegetation in sobek 1d-2d.* M.sc. thesis hh485, Unesco IHE, Delft.

Vanoni, V.A., N.H. Brooks, N.H. 1957. *Laboratory studies of the roughness and suspended load of alluvial streams.* Calif.Inst.Technol.Sedim.Lab.,Pasadena, Report no. E 68, Publ.no. 149.

Velzen, E.H. van, Jesse, P., Cornelissen, P., Coops, H. 2002. *Stromingsweerstand vegetatie in uiterwaarden, deel I handboek versie 1.0, RIZA werkdocument 2002.*140x, RIZA in opdracht van Rijkswaterstaat, Directie Oost Nederland.

Viles, H.A. 1988. *Biogemorphology*. Oxford: Basil Blackwell Ltd.

WL|Delft hydraulics 2003. *User Manual Delft3D-FLOW*. Delft, WL|Delft hydraulics, 2003.

Wilbers, A. 1997, *De Allier, een rivier met twee patronen.* Utrecht: Utrecht University.

Software

ArcView GIS 3.2a. 2000. Environmental Systems Research Institute. Inc.

Delft3D-Flow 3.05. WL|Delft Hydraulics

Delft3D-Quickin 4.11.02.00. WL|Delft Hydraulics

Delft3D-Quickplot 2.07.00. WL|Delft Hydraulics

Jasc Paint Shop Pro 8.00. Corel

Matlab 7.0.0.19920 (R14). 2004. The mathworks, Inc.

Microsoft Excel 2000. 1999. Microsoft Corporation.

Microsoft Word 2000. 1999. Microsoft Corporation.

Surfer 7.00. 1999. Golden Software, Inc.

Textpad 4.4.1. 2001. Helios Software Solutions.

Trimble geomaticss Office. 1.60. 2002 Trimble Navigation Limited.

Appendix 1

Discharge analysis Moulins

TUDelft

Appendix 2

Topography study area

Appendix 3

Interpolation of the main channel

TUDelft

Appendix 4

Vegetation characteristics

TUDelft

Appendix 5

Vegetation map

Appendix 6

Location and direction of scour holes

TUDelft

Appendix 7

Results of Allier model

TU Delft

Appendix 8

Parameters of measuring devices

TUDelft

Appendix 9

Parameters of Delft3D model

TUDelft

Appendix 10

Rewriting of the Reduction factor approach for the Delft3D simulations, by Jagers

TUDelft

Appendix 11

Equilibrium state analysis of transport formula by Baptist